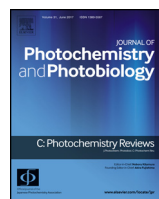




Contents lists available at ScienceDirect

Journal of Photochemistry and Photobiology C: Photochemistry Reviews

journal homepage: www.elsevier.com/locate/jphotochemrev



Review

Inorganic semiconductors-graphene composites in photo(electro)catalysis: Synthetic strategies, interaction mechanisms and applications



Lütfiye Yıldız Ozer^a, Corrado Garlisi^a, Habeebllah Oladipo^a, Mario Pagliaro^b, Saad Asadullah Sharief^c, Ahmed Yusuf^a, Saif Almheiri^c, Giovanni Palmisano^{a,*}

^a Department of Chemical Engineering, Khalifa University of Science and Technology, Masdar Institute, Masdar City, PO BOX 54224, Abu Dhabi, United Arab Emirates

^b Istituto per lo Studio dei Materiali Nanostrutturati, CNR, via U. La Malfa 153, 90146 Palermo, Italy

^c Department of Mechanical Engineering, Khalifa University of Science and Technology, Masdar Institute, Masdar City, PO BOX 54224, Abu Dhabi, United Arab Emirates

ARTICLE INFO

Article history:

Received 6 March 2017

Received in revised form 7 June 2017

Accepted 12 June 2017

Available online 15 June 2017

Keywords:

Photocatalysis

Photoelectrocatalysis

Inorganic semiconductors

Graphene

Composites

ABSTRACT

The remarkable physicochemical properties of graphene (GR) and derivatives can be leveraged in the photocatalytic activity of GR-semiconductor photocatalysts. The hitherto state of knowledge on the role of GR in these composite materials is insufficient and leaves many questions unanswered, thus it is imperative to fully understand the interaction mechanisms between GR and inorganic semiconductors. Detailed study and optimization of the features related to the interface are still very much sought to efficiently design photocatalysts targeting their eventual commercialization. This review shows that photocatalytic activity of such composites depends not only on high GR electron mobility and charge transfer, but also on the properties of the interface (such as interface morphology, size, crystal phases and facet, dimensionality of composites, etc.). Focusing on the last advancements in this field, this review analyses the challenges involved in the synthetic strategies of GR-semiconductor photo(electro)catalysts in various applications including pollutant degradation, organic synthesis, hydrogen evolution and photoreduction of carbon dioxide (CO₂). Mechanism of interaction between GR and semiconductors are thoroughly discussed by examining the proposed mechanism in the diverse areas where the composite materials are employed in photo(electro)catalytic processes. In addition, various synthetic and characterization technique available hitherto are presented, since they are pivotal to the understanding of the composites properties (such as morphology, crystal phases and exposed facets, degree of crystallinity, dimensionality etc.), and even to shed more light on interaction mechanisms of the photocatalyst constituents. As a future outlook, it is envisaged that research will not only focus on optimizing GR electrical and chemical properties, yet in the synthesis of GR-semiconductor photocatalysts attention needs also be placed on the properties of the resulting composites, using suitable synthetic methods and proper characterizations to assess their performance.

© 2017 Elsevier B.V. All rights reserved.

Contents

1. Introduction	133
2. Synthetic techniques	134
3. Dimensionality of composites	136
3.1. Two-dimensional structures	136
3.2. Three-dimensional structure	136
4. Chemical doping effect	137

* Corresponding author.

E-mail address: gpalmisano@masdar.ac.ae (G. Palmisano).

5. Characterization strategies	139
6. Cooperative mechanism at graphene-inorganic semiconductor interface	142
7. Applications	144
7.1. Pollutants degradation	144
7.2. H ₂ production by H ₂ O and H ₂ S splitting	148
7.3. Organic synthesis	152
7.4. CO ₂ reduction	155
8. Conclusions and future outlook	158
Acknowledgements	159
References	159



Lütfiye Yıldız Ozer received her B.S in Biology (2008) and her M.S. in Biotechnology from Middle East Technical University (METU) (2011), Turkey. She worked as a research engineer under the supervision of Drs. Lina F. Yousef, Ahmed F. Yousef and currently of Dr. Giovanni Palmisano at the Masdar Institute (Khalifa University of Science and Technology) of Abu Dhabi (UAE). Her research interests mainly include the synthesis of reduced graphene oxide, the development and characterization of nitrogen doped TiO₂/graphene composites for hydrogen production from H₂S splitting, and decontamination of greywater.



Ahmed Yusuf received BS in Chemical Engineering from Obafemi Awolowo University, Nigeria in 2012, and Masters in chemical engineering from Masdar Institute, UAE in 2016 with research thesis titled "techno-economic evaluation of CO₂ utilization for Soda ash production using NaOH solution". He is currently a PhD student of Masdar Institute (Khalifa University of Science and Technology) under the supervision of Professor Giovanni Palmisano working on kinetic modelling of photocatalytic microreactor for water treatment applications and H₂S splitting.



Corrado Garlisi is currently pursuing Doctoral Degree at Khalifa University of Science and Technology, Abu Dhabi (UAE). He earned his Master's Degree in Chemical Engineering from University of Palermo, Italy. Prior to joining Khalifa University of Science and Technology, he worked at ENEA (Italian National Agency for New Technologies, Energy and Sustainable Economic Development). His current research work focuses on the fabrication and characterization of semiconductor thin films for solar light activated glass.



Saif Almheiri received his B.S. degree from the University of Arizona and M.S. and PhD degrees from the University of Miami, all in Mechanical Engineering. In 2014, he was a Visiting Assistant Professor at the Electrochemical Energy Laboratory at the Massachusetts Institute of Technology (MIT), where he worked on energy storage solutions. His research interests include energy storage, fuel cells for stationary and mobile applications, hydrogen production and synthesis of graphene and its applications.



Habeebullah Oladipo received a B.S. in Chemical Engineering from Obafemi Awolowo University, Nigeria in 2011 and M.S. in Chemical Engineering from King Fahd University, Saudi-Arabia in 2016. He is presently a PhD student at Masdar Institute (Khalifa University of Science and Technology) under the supervision of Professor Giovanni Palmisano. His research interests include synthesis of nanostructured materials for clean fuel production and pollutant degradation.



Giovanni Palmisano is assistant professor of chemical engineering at the Masdar Institute (Khalifa University of Science and Technology) of Abu Dhabi (UAE). Giovanni's research activities have been developed in Italy, Spain and UAE and concern photo-catalytic processes for organic chemistry, hydrogen production, water and air remediation, self-cleaning coatings, and hybrid photovoltaics. From 2009–2012, he was administrator, chief engineer and safety manager at Hedera Engineering Srl – an Italian company operating in the field of solar energy plants. From 2008–2013 he has held free-lance consulting activity for private companies and Italian municipalities. He has co-authored ca. 80 journals papers and he has to his record six patents, six books and six invited book chapters.



Mario Pagliaro is a chemistry and energy scholar based at Italy's Research Council in Palermo where he leads a research Group focusing on nanotechnology, solar energy and the bioeconomy. In recognition of his "significant contributions to the chemical sciences" in 2014 he was designed Fellow of the Royal Society of Chemistry. The achievements of his Group's research developed in co-operation with leading researchers based in 20 countries include numerous important advances reported in over 180 research papers and several book chapters. He ranks amongst Italy's most cited scientists in nanotechnology and materials chemistry.



Saad Asadullah Sharief holds a Bachelor of technology (2012) from Jawaharlal Nehru technological University (India) and a Master of Science degree in Chemical Engineering (2015) from Masdar Institute. Following graduation, he joined the Electrochemistry Lab of Masdar Institute as a Research Engineer, where his work focused on electrochemical synthesis of graphene. His research interests mainly include large scale production of graphene, application of graphene in the realm of sensors-biosensors in particular and electrically conductive polymers.

1. Introduction

Rising concerns about global pollution and climate change due to ever increasing consumption of non-renewable, fossil hydrocarbons as fuels and chemical feedstocks [1] has made the development of green technologies for the production of goods [2] and the abatement of pollutants [3] the core of contemporary chemical research. Photocatalysis applied both to the degradation of organic and inorganic pollutants in water [4,5] and air [6,7], as well as to photoreduction of CO₂ [8,9], and hydrogen evolution [10–12], has emerged as a most promising method in our common path to sustainability.

Heterogeneous photocatalysis based on the utilization of semiconductors such as TiO₂ [13–17], CuO [18,19], ZnO [20,21], and Fe₂O₃ [22–24] to produce highly reactive radical species able to trigger oxidative reactions, as well as conduction band (CB) electrons promoting reduction conversions, presents many advantages, including low operation cost and no production of secondary hazardous metabolites. The open challenges before photocatalytic

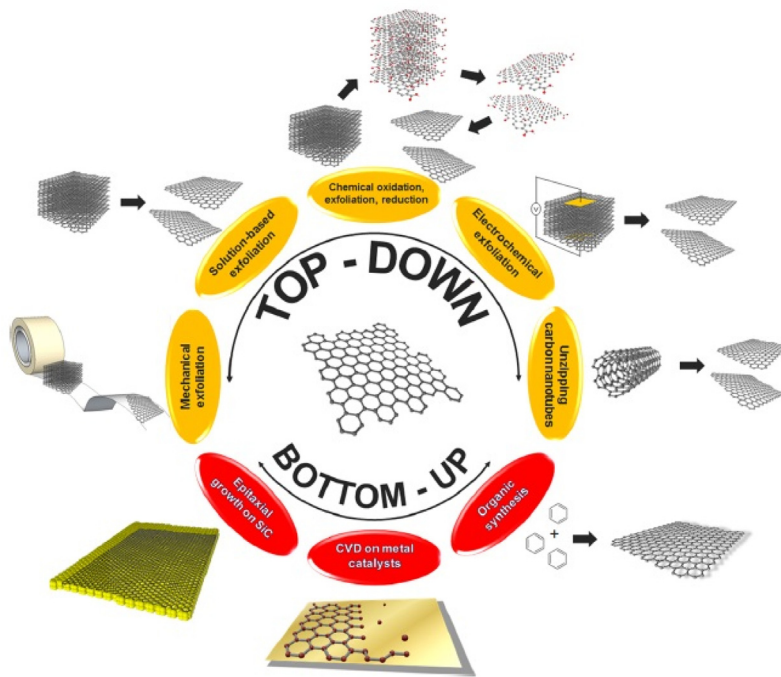


Fig. 1. Routes for the synthesis of GR. Reprinted with permission from Ref. [39]. Copyright 2014 American Chemical Society.

processes become economically feasible for large scale industrial applications include the need to enhance efficiency under solar radiation, and to mitigate recombination of photogenerated electrons and holes. Several strategies have been developed including doping with metal and non-metal species, coupling with other semiconductors, and sensitization with organic chromophores [5,25–31], which have not all yet resulted in practical applications.

The discovery of GR [32], a 2D form allotrope of carbon and zero band gap semiconductor [32] exhibiting extraordinary electron mobility (10^6 m s^{-1}), excellent large surface area ($2630 \text{ m}^2 \text{ g}^{-1}$) responsible for improved interfacial contact with other species [33], and high chemical stability and mechanical resistance [34–36], might soon solve many of the practical problems encountered in photocatalysis [37], especially now that economically feasible synthetic routes to GR are becoming available [38].

GR has different physicochemical features depending on the synthesis technique used for its preparation: bottom-up, where the smallest building blocks of the material are assembled together to obtain a high quality GR [28,39–41] and top-down by breaking down graphite into the desired material by chemical or physical processes (Fig. 1) [42–46]. The latter approach opened up the possibility of massive production when solution-based chemistry was discovered [47].

Early applications of GR in photocatalysis mostly relied on reduced graphene oxide (RGO) [45,48], rather than on GR, obtained via thermal [49], chemical [46], and electrochemical [39], reduction of graphene oxide (GO) synthesized by modified Hummer methods [42,50]. The presence of covalently bonded oxygenated groups (including hydroxyl, epoxy, carboxyl etc.) in the GO structure offered anchoring points for the binding of semiconductors. Structural defects and abundance of oxygen bearing groups in the GO structure, however, impact on electrical properties by interrupting the conductive delocalized π -conjugation and also induce a tendency to aggregate with a final detrimental effect not only on specific surface area, but also on electronic properties [37,47,51–53].

In general, GR-semiconductor composites form photocatalysts showing enhanced activity toward pollutants abatement, photore-

duction of CO_2 and photocatalytic hydrogen evolution, thanks to i) the suppressed recombination of photogenerated electrons and holes, ii) extended absorption range of light wavelengths, and iii) better adsorption of reactants [54–57]. Furthermore, these characteristics can be tuned and optimized working on many factors including tunable layer number, edge morphology, crystallinity degree, type and extent of defects, size effect and exposed crystal facets [37,58–65].

In this account, we address the challenges and opportunities in the production of second generation GR-semiconductor composites. Recent advances in the synthesis and photo(electro)catalytic applications, and in the understanding of the interaction mechanisms among different moieties in the resulting nanostructures are discussed and put in context with the aim to provide guidelines in the development of new composites capable of meeting productivity, stability and cost requirements needed for practical application in the emerging solar [66] and bio-based [67] economy. Throughout the described applications, a special consideration is given to the ability of GR to provide a platform to attract and convey electrons, promote (photo)adsorption of reacting substrates, and enlarge the absorption range of semiconductors towards the visible region [37,56,68].

2. Synthetic techniques

In the fabrication of GR semiconductor composites, GR behaves either as compositing component of inorganic semiconductors, or as a substrate where the semiconductors are grown/supported. A number of methods do exist allowing for the fabrication of GR-semiconductors composites with diverse morphology, size, dimensionality and interfacial domains [69], all affecting the efficiency of the photocatalytic processes. However, all the synthetic techniques producing GR conjugated composites can be categorized into: *in situ* crystallization and *ex-situ* hybridization [70].

In situ crystallization, which is the most common method, is based on the direct and homogenous growth of nanomaterials (such as nanoparticles, nanowires, nanorods, nanotubes or

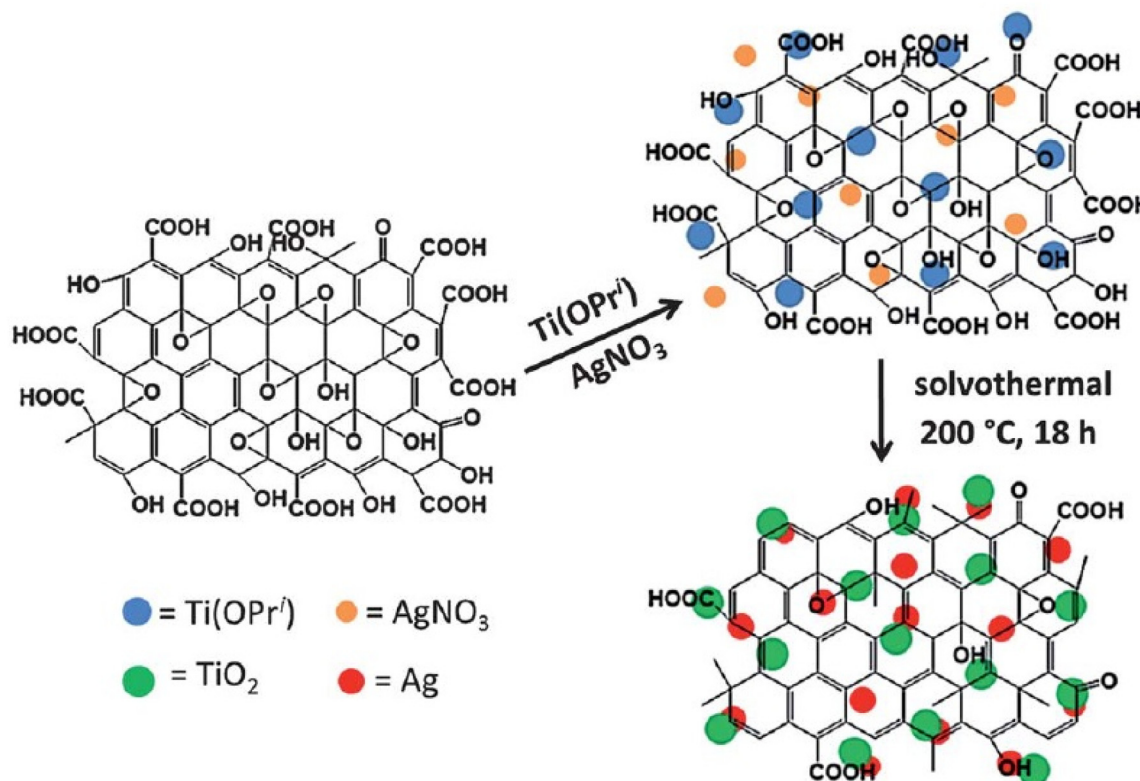
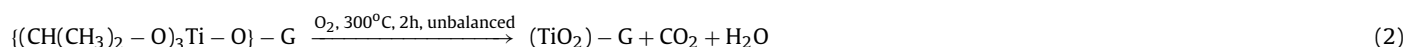
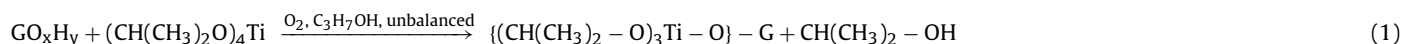


Fig. 2. Fabrication of Ag-TiO₂-RGO ternary nanocomposite photocatalyst. Reprinted with permission from Ref. [84]. Copyright 2013 Royal Society of Chemistry.

nanofilms) on the surface of a GR precursor, mainly GO or RGO [70]. In situ crystallization is based on mixing GO or RGO and the soluble precursors of the inorganic semiconductors in a solvent, following a chemical, thermal, optical or ultrasonic treatment of the mixture to finally anchor the inorganic catalysts on the surface of GR. The oxygen sites of GO act as nucleation points for the adjustment of size, morphology and crystallinity of the nanoparticles and enable the efficient interfacial contact of nanomaterials on GO/RGO surface to improve the efficiency of electron transfer. In situ methods including sol-gel method, hydrothermal/solvothermal treatment, and microwave-assisted deposition have been exploited to fabricate GR based composites through a one-step growth or by a multi-step reaction procedure.

Sol-gel method, a wet chemical approach, is based on phase transition from a precursor, a colloidal liquid, into a solid gel through a series of hydrolysis and polycondensation reactions. Its key advantage is the effective anchoring of the catalyst at the $-\text{OH}$ groups of GO/RGO by chemical bonding. The precursors used in the preparation of GR-semiconductor composites are mostly metal alkoxides, metal chlorides, and organometallic compounds. As an example, in the fabrication of TiO₂-RGO or GO composite photocatalysts via a sol-gel method, the precursors used were titanium tetraisopropoxide (TTIP) [71–73], titanium butoxide (TBOT) [26,74–77], and titanium tetrachloride (TiCl₄) [78], which resulted in different structures of TiO₂ depending on the experimental conditions applied. From TTIP the following steps produced a composite catalyst:



Final drying and annealing at temperatures typically above 300 °C resulted in semiconductor photocatalysts, whose crystallinity and photocatalytic activity were strongly affected by the

final heat treatment. Studies on the structural integrity of GR-inorganic semiconductor composites have been conducted by Chun et al. [79], who found out that a high temperature up to 400 °C in the final treatment enhances the photocatalytic activity of TiO₂-3% (w/w) GO without significantly affecting its structural features.

Hydrothermal/solvothermal method is widely used for the fabrication of composite photocatalysts, based on crystallization of catalysts on GO sheets with the simultaneous reduction of GO at high temperature and pressure. It can take place with or without reductants starting from an aqueous/alcoholic solution [80–83].

Sher Shah et al. [84] synthesized Ag-TiO₂-RGO, a ternary nanocomposite photocatalyst, by dispersing TTIP in N,N dimethylformamide (DMF) and ethylene glycol (EG) containing silver nitrate and RGO to reduce silver nitrate to silver and mitigate the agglomeration of RGO nanosheets upon treatment at 200 °C for 18 h, as illustrated in Fig. 2. The resulting Ag and TiO₂ nanoparticles were evenly distributed on RGO sheets without agglomeration of RGO. During the fabrication of GR-semiconductor photocatalysts, Liu et al. [85] targeted different exposed facets of TiO₂, namely {101}, {100}, and {001}, to be grown on GR through a hydrothermal reaction by capping anions at 180 °C for 24 h. After a thorough structural and physicochemical analysis, they reported that directionality on the facet growth also affected the photocatalytic activity by changing the bonding structure of GR and TiO₂, and thus the interfacial charge transfer rates.

Microwave-assisted synthesis is a fast and low temperature method of producing GR-inorganic semiconductors composites

compared to other *in situ* procedures. This technique enables to induce nucleation and growth of small and homogenous particles on GR [86]. UV microwave-assisted technique was used during the fabrication of OH-TiO₂/RGO by UV irradiation of their precursors, i.e. TBOT and GO, and treating them through microwaves [59]. The results indicated that surface hydroxylation on RGO/TiO₂ catalyst enabled extension of visible light absorption up to about 600 nm with a color shift to yellow, at the same time reducing crystal sizes, inducing surface defects such as Ti³⁺ states and oxygen vacancies, thereby enhancing charge transfer with a lower recombination rate.

All reviewed studies on *in situ* synthesis suggest that GO is the most used precursor of GR because of its high degree of hydrophilic functional groups that allows for water processability. TiO₂ and CdS also seem to have made the forefront of inorganic semiconductors that are mostly composited with GR. TiO₂-GR composites seem to be commonplace because of TiO₂ availability, nontoxicity and economic favorability. TiO₂ precursors used include TTIP, TBOT and TiCl₄; with the choice of precursor and synthetic method being dependent on the structures and morphology of the required composites. Among the *in situ* methods, microwave-assisted synthesis is fast compared to sol-gel and hydrothermal. However, hydrothermal treatment seems to be the most widely used because GO is fairly reduced to RGO, thus yielding a better photocatalytic activity of the resulting composite materials.

Ex-situ hybridization is based on mixing nanomaterials with a defined structure and composition with GR precursors, aiming to anchor the inorganic particles to oxygen moieties existing at the surface of GO or RGO via covalent or noncovalent interaction [70]. For instance, coating GO sheets on a Nb-doped TiO₂ (TNO) thin film resulted in a transparent conducting oxide (TCO) layer fabricated by a self-assembly technique, and being indium free, low cost and enhancing charge transport. According to the photocatalytic activity measurement, GO on TNO films exhibit an improved photocatalytic efficiency on degradation of methylene blue (MB) [55].

In self-assembly technique, the distribution of nanomaterial on GR is random. For this reason, to maximize unique properties of GR, the surface modification of either GR or the inorganic semiconductors is necessary to improve their ability to process solvent, and to increase the spatial interaction between GR and the catalysts [54]. Xiao et al. [87] constructed 2% RGO/SiO₂ hollow microsphere composites via ultrasound-assisted interfacial self-assembling of negatively charged GO sheets on positively charged SiO₂ modified with poly(diallyldimethylammonium) chloride (PDDA). Sonication enabled the composite to disperse in the aqueous solution thus preventing aggregation. The following solvothermal treatment resulted in a further reduction of GO and better interfacial contact between SiO₂ and RGO.

Another approach involves the aerosol assisted self-assembly method, which is simple, low cost and easy to scale up, allowing to achieve a charge transfer between TiO₂ and RGO sheets and to foster interfacial contact between TiO₂ and RGO compared to the electrostatic assembly approach [88].

From the perspective of synthesizing composites with robust interfacial contact between inorganic catalysts and GR, the *ex-situ* synthesis method is often less efficient than *in situ*. The stronger interfacial interactions can be attributed to the generation of chemical bonds which tends to foster the effective separation of electron-hole pairs with an efficient electron transfer and the narrowing of optical band gaps. Conversely, we want to highlight that the advantage of *ex-situ* method is to the control of the morphology of the materials into ordered and monodisperse structures by pre-selection of semiconductors with desirable morphology. In the course of *ex-situ* preparations, the shape, size and morphology of the used semiconductors in the composites are nearly the same as the initial ones. A fair comparison of the photoactivity of the com-

posites with respect to inorganic semiconductors is then feasible, without any concern on the morphological structure influence.

3. Dimensionality of composites

Besides doping/codoping techniques to modulate the carrier separation and transfer of GR-semiconductor, several studies indicated that the photocatalytic performance of GR-semiconductor composites are also improved by tuning surface area, mass transfer kinetics and local assembly environment, since these parameters have a synergistic effect on the whole photocatalytic reactions.

We can differentiate among quantum dots, which are zero-dimensional (0D), nanoribbons, nanotubes, nanowires and nanorods, belonging to the one-dimensional (1D) category, single-atom thick material like sheets being two-dimensional (2D) and, finally, nanospheres and nanocones, which are among the 3D morphologies. Dimensionality can explain the atomic assembly of the materials and also affect their properties to a significant degree. The same component can exhibit a very different photocatalytic activity when existing in different shapes, due to a different charge mobility and reduced recombination resulting in a prolonged charge life and shorter transfer paths.

3.1. Two-dimensional structures

The dimensionality of each component of a composite and the increased interfacial contact area are able to enhance the electron transfer thus result in a better photocatalytic activity. Coupling of lower dimensional structures and GR such as in 0D/2D, 1D/2D and 2D/2D heterostructures, is an effective way for boosting the global photocatalytic performance [89].

In 0D/2D and 1D/2D composites, nanoparticles, nanorods, nanowires or nanotubes have been coupled with GR through *in situ* growth methods or *ex-situ* assembly. However, 2D/2D heterostructures have better interfacial contact areas due to the more efficient face-to-face contact, which enhances the photocatalytic performance by increasing the electron transfer and separation of photogenerated electron-hole pair compared to 0D/2D, where inorganic semiconductors are dispersed on 2D GR sheets, either homogeneously or wrapped inside nanosheets, and also compared to 1D/2D configurations, where a line-to-line interaction occurs as shown in Fig. 3 [89]. A 2D/2D arrangement has been described for instance by Luan et al. [90], who indicated that the usage of 2D TiO₂ nanosheets in the fabrication of GR-modified semiconductor catalysts has advantages, serving as a hosting material to load guest functional nanomaterials, providing a large interaction area between catalyst and organic pollutant.

As reported by Bera et al. [91], GR/CdS nanosheets composite (2D/2D) enhances the photocatalytic activity in the degradation of MB of about 4 times, compared to GR/CdS nanorod (2D/1D), which in turn shows ca. 3.4 times greater activity than GR/CdS nanoparticles (2D/0D), fabricated by hydrothermal treatment. This study highlights how increasing dimensionality results in a better photocatalytic activity.

3.2. Three-dimensional structure

GR, with its unique 2D structure, can be used as the building block for the self-assembly of 3D functional materials. Due to the strong interaction among GR sheets, it is hard to dissolve GR in most solvents. However, in a gel medium, it can be well dispersed thanks to the covalent π-π stacking interactions with a gelator peptide [92]. Moreover, when synthesized by Hummer method, GO is soluble in water yielding a homogenous liquid which is beneficial for the 3D self-assembly procedures, producing organogels, aerogels, and hydrogels.

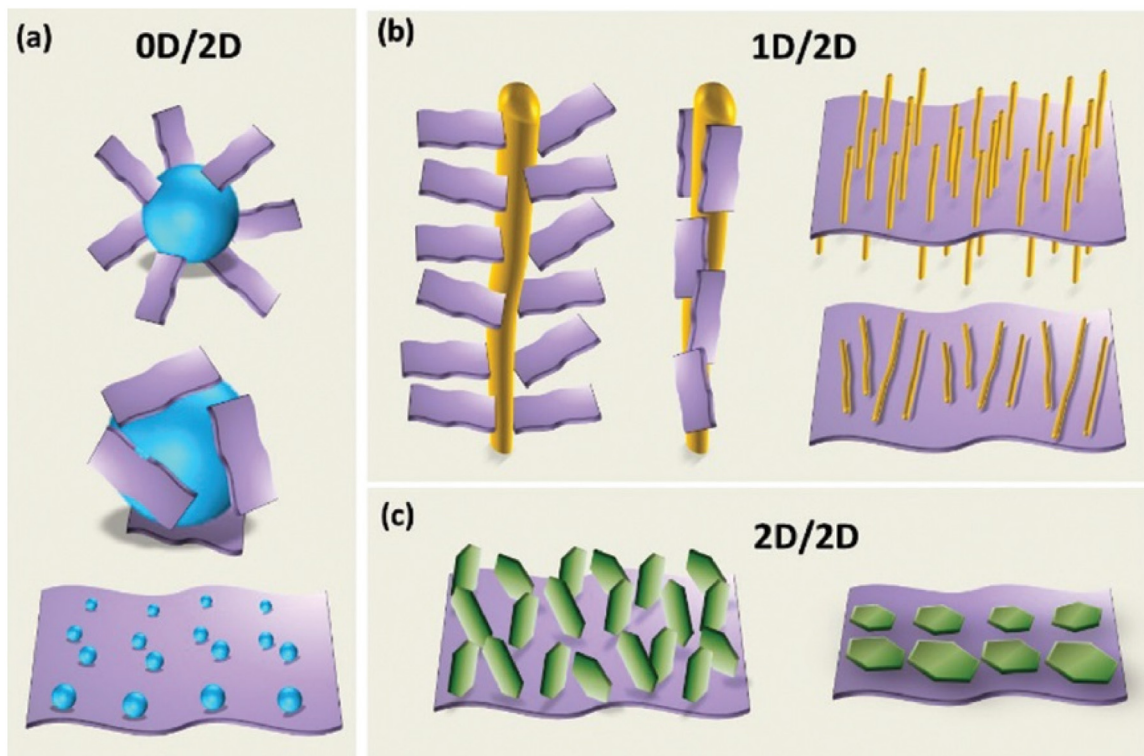


Fig. 3. GR based composites with different dimensionality and interfacial contacts. Reprinted with permission from Ref. [89]. Copyright 2016 Royal Society of Chemistry.

The 3D structures obtained, for instance, in porous films, aerogels, and scaffolds, allow GR to enhance specific surface area, charge carrier transfer and conductivity, and to inhibit aggregation, by means of combination of 3D porous structure and the peculiar properties of GR, namely high surface area, high conductivity and electron mobility.

Among the several 3D structures of GR which have been reported, GR hydrogels/aerogels have attracted widespread attention due to (i) the porous structure providing an ideal support to fabricate photocatalytic semiconductors, (ii) the shapes, volumes and densities adaptability, allowing for high adsorption ability, and (iii) the affordable and convenient recycling of the photocatalysts due to the prompt separation from the reaction media. As an example, a study focused on construction of 3D porous aerogel constituted by GR sheets and Bi_2WO_6 nanosheets, indicated that the bi-component photocatalyst achieved higher degradation of rhodamine B (RhB) compared to bare Bi_2WO_6 , due to a 60% higher specific surface area and higher adsorption of RhB compared to bare Bi_2WO_6 sheets [93]. GO/polymer hybrid microspheres were fabricated by getting 2D GO sheets wrapped on the surface of polymer microspheres and assembled into 3D structures [94]. The wrinkled surface of the photocatalyst increased the specific surface area and allowed the particles to grow on 3D structures by providing effective sites [95]. The photocatalytic activity of $\text{TiO}_2/\text{RGO}/\text{polymer}$ composites on the degradation of RhB under visible light was about 96% in 30 min, much better compared to TiO_2 Degussa P25, owing to the good crystallinity and the small size of anatase TiO_2 particles, the unique electrical conductivity of GR, and the interactions between TiO_2 and RGO in this complex composite.

As a final remark on 3D assembled composites, GR functionalized by melamine resin monomer (MRGO), assembled with CdS, was reported to give an enhanced separation efficiency of photo-generated electrons by means of multidimensional transport pathways compared to CdS-RGO sheets (Fig. 4) [96]. Furthermore,

hydroxyl end groups of melamine resin monomers were found to inhibit restacking of MRGO in the composite CdS-MRGO.

4. Chemical doping effect

Many efforts have been directed towards exploiting the superior physicochemical properties of GR by compositing with catalysts such as TiO_2 in order to convey electrons efficiently and boost the electron-hole separation, at the same time narrowing the band gap of the semiconductors [97–99]. The specific mechanism of GR doping has not been fully unveiled yet. It has been either ascribed to anionic substitution doping, where the lattice oxygen atoms of inorganic semiconductors are replaced by carbon (C), or to interstitial doping where C bears a positive charge. Thus, the oxidation state of carbon coming from GR varies from -4 to $+4$, as carbides with Ti–C bond (for the case of TiO_2 doping) or carbonates with C–O bond, respectively. While Ti–C bond was usually found in composites fabricated by flame pyrolysis and ion-assisted electron beam evaporation, C–O bond was frequently seen in those synthesized via sol-gel. The degree of C doping affects the band gap with a reduction ranging from 0.1 to 1.05 eV [98]. However, the dopant loading has a threshold depending on the fabrication method: a further increase results in the formation of a dopant segregated phase [100]. Along with the extension of light absorption to the visible range, it has been demonstrated that TiO_2 composited with GR has an electron-hole recombination rate slower than bare TiO_2 upon UV light excitation.

On the other hand, the chemical doping in GR and GR-inorganic semiconductor composites is a relevant approach to modulate the electronic properties of these materials. Chemically modified GR can be produced by the adsorption of gases, metals or organic molecules or through substitution doping, thus introducing heteroatoms such as nitrogen (N), boron (B) and sulphur (S), into the C lattice of GR. Specifically, the aim of performing non-metal doping

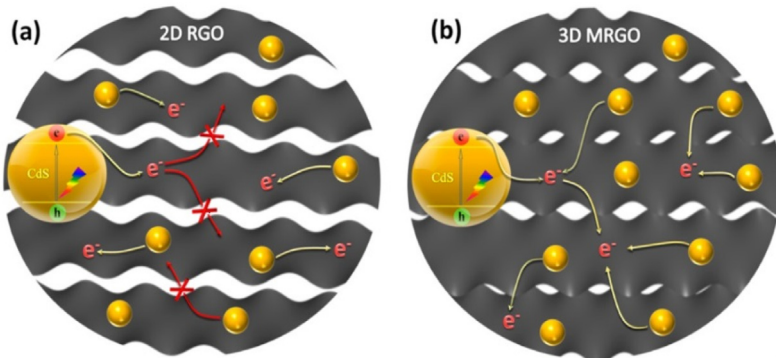


Fig. 4. Schematic illustrating the charge transfer mechanism at interfaces of 3D CdS-MRGO and 2D CdS-RGO. Reprinted with permission from Ref. [96]. Copyright 2015 American Chemical Society.

with N or B is to narrow the wide gap of GR-based semiconductors boosting their activity in the visible region. Electron withdrawing or electron donating functionalities GR can act as dopants by modifying the chemical structure of GR [52,89].

Substitutional N doping is the most common approach due to the comparable size of C and N. There are 3 common bonding configurations of N atoms within the C lattice, including graphitic N (quaternary), pyridinic N, and pyrrolic N [58]. N-dopant both affects the spin density and charge distribution of C atoms, also fostering GR electron density close to the Fermi level above Dirac point, eventually supporting the charge transfer in the course of photocatalytic reactions [101]. In addition, it was demonstrated that N-doping enhances the thermal stability of GR [102]. A recent case study reported by Xu et al. [63] involves N-doped GR-TiO₂ prepared by a hydrothermal method with different nitrogen sources including ammonia, hydrazine and urea. While N-doping of GR-TiO₂ by urea and ammonia brought to more than 70% pyrrolic N and 10% pyridinic N, on the other hand, using hydrazine as nitrogen source produced ca. 63% pyrrolic N and ca. 37% graphitic N. All of the N-doped composites, especially when hydrazine is used, displayed a better photocatalytic activity compared to GR-TiO₂ and TiO₂, with

an improvement of ca. 2 and 3 times, respectively. According to this result, Xu et al. [63] proposed that the graphitic N acts as an electron mediator for the photogenerated electrons, whereas the pyrrolic N serves as an active site for oxygen reduction to rapidly induce the subsequent interfacial catalytic conversion, as shown in Fig. 5. Liu et al. have also found that N-doped GR-TiO₂ has a good stability over time and it can be recycled and reused after several reactions without any loss of activity [56].

P-doped GR photocatalysts, produced by pyrolysis of phosphate modified alginate at 900 °C under inert atmosphere, was showed to have wider optical band gap and better photocatalytic performance on H₂ production from H₂O-CH₃OH solutions, compared to bare GR under UV irradiation [103]. This study shows how GR itself can be used as a photocatalyst for reductions without coupling with inorganic semiconductors.

In our opinion, nitrogen still remains the most utilized heteroatom non-metal dopant for GR and GR-inorganic composites. This owes to the thermal stability it imparts to composites alongside narrowing their band gap towards the visible light region. Various sources of nitrogen that have been used in the literature includes urea, hydrazine, ammonia, and ammonium nitrate.

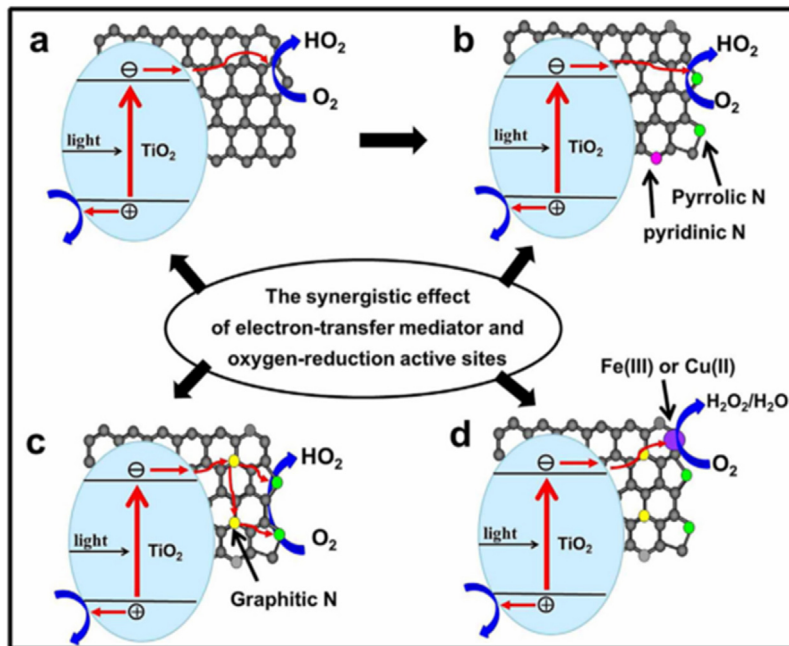


Fig. 5. Synergistic effect of GR-TiO₂ photocatalysts: (a) RGO/TiO₂; (b) N-RGO/TiO₂ (N sources: NH₃ or CO(NH₂)₂); (c) N-RGO/TiO₂ (N source: N₂H₄); and (d) Cu(II) or Fe(III)/N-RGO/TiO₂ (N Source: N₂H₄). Reprinted with permission from Ref. [63]. Copyright 2016 Elsevier.

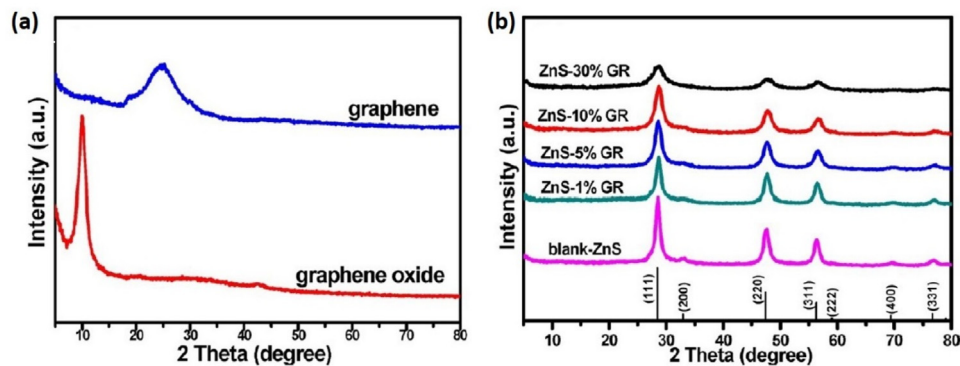


Fig. 6. XRD patterns of (a) GR and GO, (b) ZnS and ZnS-GR semiconductor photocatalyst with an increasing loading of GR. Reprinted with permission from Ref. [104]. Copyright 2012 American Chemical Society.

5. Characterization strategies

The features of composite photocatalysts containing GR are complex and a straightforward assessment is hard if not impossible. Since the physicochemical properties of semiconductors, including crystal phase, size, dimensionality, morphology, and exposed facets, play a role in both generation and transfer of charge carriers on the composite surface, eventually resulting in a better or worse interaction between semiconductor and GR. It is essential to deeply study the impact of the different catalyst properties on the photocatalytic activity.

XRD is firstly employed to analyze the crystallinity of the semiconductors. An estimation of the crystallite size can be done by using the main diffraction peaks according to the Debye-Scherrer formula [80]. The diffraction peaks of RGO, when prepared from graphite flakes by the Hummer's method, are three, located at 26.5°, 44.3°, and 54.5° corresponding to planes (002), (101), and (004),

respectively. The interplanar spacing can be calculated by using Bragg's equation from the observed position of the (002) peak. The interplanar distance in GO between consecutive C basal planes, ca. 9 Å, is attributed to the presence of hydroxyl, epoxy, and carboxyl groups bound to the GR sheets (Fig. 6) [104]. On the other hand, a positive shift of (002) peak in RGO, corresponding to a d-spacing of ca. 4 Å, indicates that the sp^2 carbon lattice within the GR network is significantly restored during the reduction process of GO, mainly due to the epoxides ring breakage [105]. However, in GR modified composites, GR, RGO and GO crystal peaks are often not detectable, since GR loading is usually far below the detection limit of XRD [78]. Moreover, Bhirud et al. [78] indicated that an increased amount of GR in the composite may restrict the degree of crystallization of the inorganic semiconductor ZnS, as illustrated in Fig. 6b. Thus, the presence of GR, even in trace amounts, needs to be confirmed via Raman spectroscopy and XPS rather than XRD.

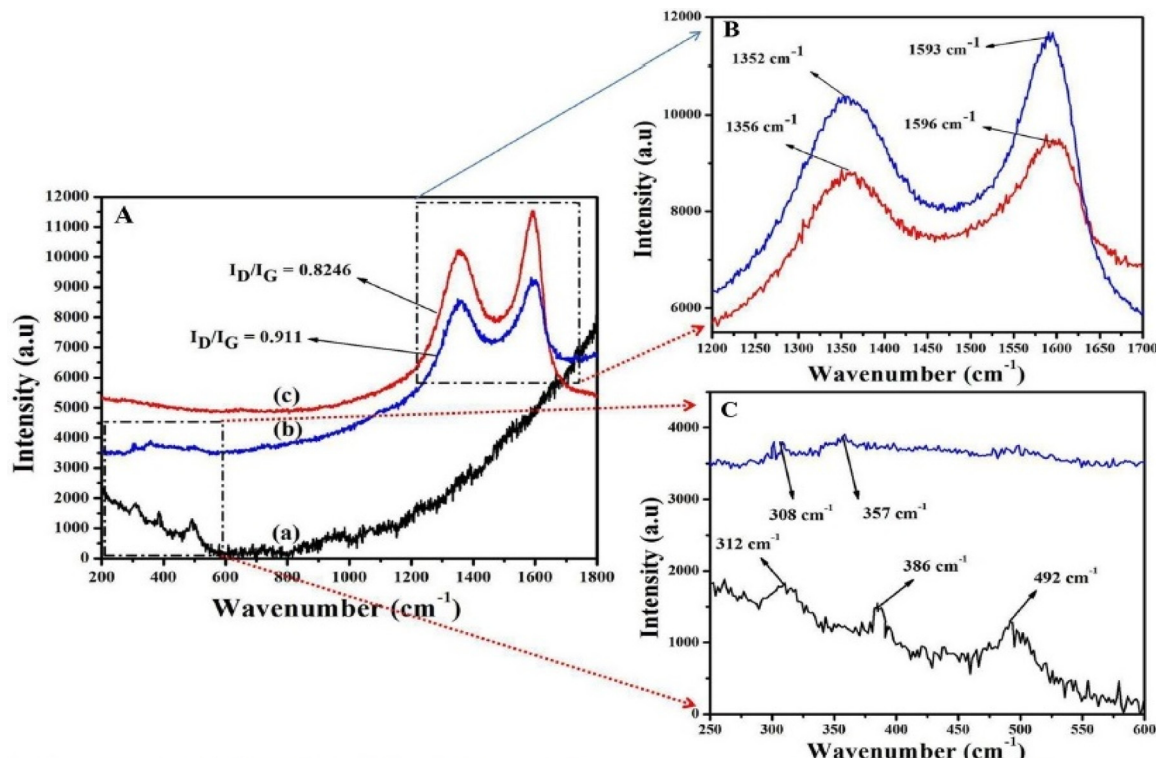


Fig. 7. Raman spectra of [A] (a) Gd(OH)₃ nanorod, (b) Gd(OH)₃ nanorod/RGO, (c) GO, [B] Raman shift of 'D' and 'G' band and [C] characteristics Raman peak of Gd(OH)₃ nanorods. Reprinted with permission from Ref. [81]. Copyright 2014 Elsevier.

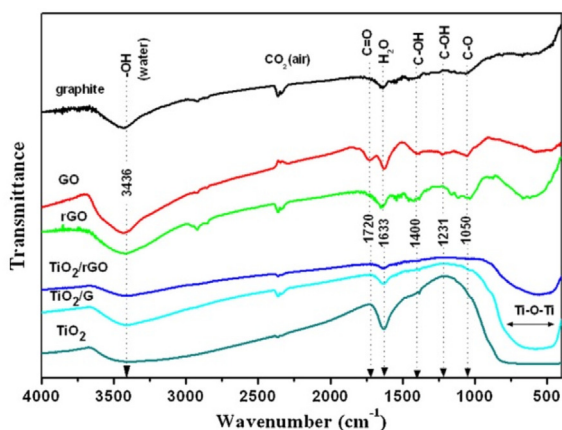


Fig. 8. FT-IR spectra of natural graphite, GO, RGO, TiO_2 , 1% GR- TiO_2 and 1% RGO- TiO_2 . Reprinted with permission from Ref. [83]. Copyright 2016 Elsevier.

Raman spectroscopy is a useful technique to evaluate the state of dispersion and the interaction of photocatalysts with GR as well as the disorder and defect structures of GR in the composites materials, reflected by shifts, width changes, and varying relative intensities of the peaks. When GO or RGO are used as precursors of GR in the fabrication of composite semiconductors, the Raman spectrum shows the two peaks located at around $1550\text{--}1600\text{ cm}^{-1}$ (G band) and $1300\text{--}1400\text{ cm}^{-1}$ (D), corresponding to the first order scattering of E_{2g} phonon of sp^2 bonded C hybridization and to the breathing mode of K-point phonons of A_{1g} symmetry in GR, respec-

tively [106]. The D/G peak intensities ratio indicates the defects level and disorder degree of sp^2 type C atoms in the GR structure. When analyzing the Raman spectra of a composite, such as Gd(OH)_3 nanorod/RGO, prepared starting from GO (getting reduced during the composite formation), the intensity ratio of D/G bands of the composite is greater than the same ratio in the absence of inorganic semiconductor. The last insight suggests that the interaction between the inorganic semiconductor and RGO sheets result in a shrinking of sp^2 domains upon reduction of GO to RGO (Fig. 7A) [81]. The G' band (also referred to as 2D band), located at around 2700 cm^{-1} , deriving from the second order of zone boundary phonons activated by a two-phonon (opposite momentum) assisted double resonance process, is used to assess the presence of a single or a few layers of GR in the composites. Thus, as the number of layers increases, the G' band peak can be slightly shifted and become broader with a shoulder towards lower wavenumbers. Moreover, upon incorporation of GR into the composites, the inorganic semiconductor Raman peaks may also shift due to the interaction of inorganic semiconductors with GR as illustrated in Fig. 7B and C. Haldorai et al. [77] indicated that D and G peak of RGO shift slightly to smaller wavenumbers in RGO/ TiO_2 composite compared to bare RGO.

The occurrence of different kinds of bonds in GO, RGO, and GR-modified composites can be investigated by Fourier transform infrared spectroscopy (FT-IR). The predominant characteristic bands of GO, at ca. $1720\text{--}1740\text{ cm}^{-1}$ and 1630 cm^{-1} , are assigned to $\text{C}=\text{O}$ (carbonyl) stretching mostly originating from the edge of GR surface, and $\text{C}=\text{C}$ stretching deriving from skeletal vibrations of non-oxidized sp^2 -hybridized C, respectively [83,106]. The other

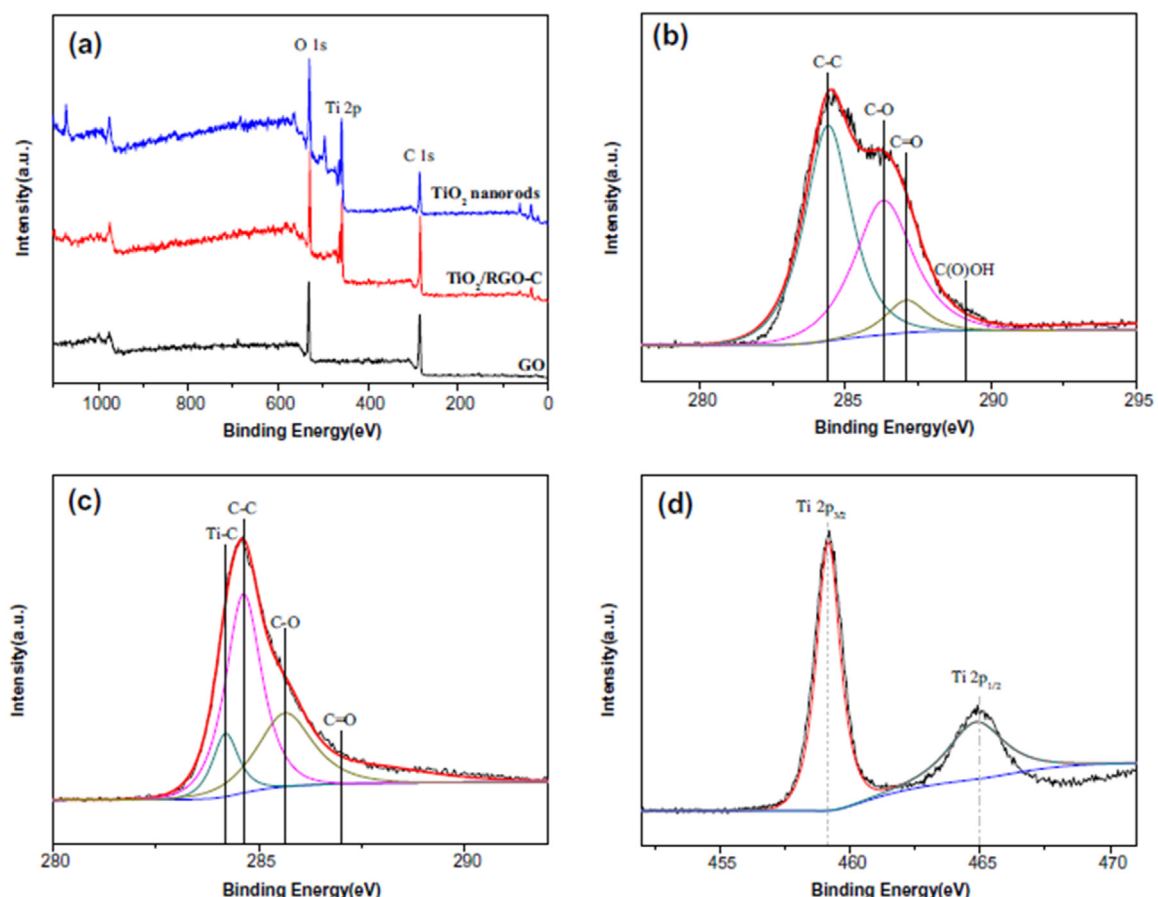


Fig. 9. X-ray photoelectron spectra of composite photocatalysts obtained with and without cetyltrimethyl ammonium bromide (-C) as a surfactant: (a) GO, TiO_2 nanorods and 0.6% TiO_2 /RGO-CTAB (C); (b) C 1s for GO; (c) C 1s for 0.6% TiO_2 /RGO-C; (d) Ti 2p for 0.6% TiO_2 /RGO-C. Reprinted with permission from Ref. [108]. Copyright 2015 Elsevier.

peaks of GO at ca. 3440 cm^{-1} , 1400 cm^{-1} , 1230 cm^{-1} and 1050 cm^{-1} are assigned to O—H (stretching), C—O (carboxyl), C—O (epoxy) and C—O (alkoxy) vibrations, respectively, as duly illustrated in Fig. 8. In the FT-IR spectra of RGO, the OH stretching peak at ca. 3440 cm^{-1} is significantly reduced in terms of full width at half maximum (FWHM) and intensity when compared to GO. The bands associated with oxygen stretching in RGO spectra are typically absent indicating a significant degree of hydroxyl and carbonyl groups removal after reduction of GO.

Coupling thermogravimetry (TGA) with FT-IR, and/or with a MS detector, enables determination of evolved gaseous products during thermal treatment of a photocatalyst. This method is useful in determining the optimal calcination temperature of GR-semiconductor composites to promote the crystallization of inorganic semiconductors, at the same time preventing the deterioration of the GR moiety in the composites. According to the TGA analysis reported on GO, there are two characteristic weight losses at 218 and 424°C corresponding to the thermal removal of oxygen containing species (mainly —OH) and degradation of hexagonal GR structure, respectively [71]. Overlapping of weight losses due to the inorganic semiconductor is possible and can be misleading, therefore, high precaution is needed in this analysis.

X-ray photoelectron spectroscopy (XPS) is employed to identify the composition and the surface electronic state of GR semiconductor photocatalysts upon the composite formation, in order to reveal the interaction of GR and catalysts, as shown in Fig. 9. The successful incorporation of GR into the catalyst can be investigated by checking the XPS spectrum of C 1s from GO, convoluted into 5 peaks, 284.5 , 285.4 , 286.5 , 287.6 , and 288.9 eV , which correspond to sp^2 bonded carbon (C—C), carbon atoms with sp^3 hybridization, epoxy/hydroxyl (C—O), carbonyls (C=O) or quinone groups, and carboxyl groups, respectively (see Fig. 9b) [107,108]. According to XPS, the percentage of GR in the composite photocatalyst and the doping at either substitution or interstitial regions can be inferred, keeping in mind that the sensitivity of this technique allows to analyze only the surface composition (down to depth of ca. 10 nm), hence a difference between bulk and surface composition can bring misleading results.

UV-vis diffuse reflectance spectra (UV-DRS) is used to determine the light absorption properties of both crystalline and amorphous materials in the 200 – 800 nm range as %R and as Kubelka-Munk (K-M) function. In films, the transmittance and reflectance allow to estimate the optical band gap through the Tauc equation, which links the ratio between the absorption and scattering coefficients and the photon energy for semiconductors with (in) direct band energy. The UV-vis spectra of GO show two absorption peaks, ca. 237 nm and ca. 307 nm , attributed to p-p* transition

of aromatic C=C bonds and n-p* transition of C=O bonds, respectively. On the other hand, RGO displays an absorption peak at ca. 270 nm , which results from the red-shift of the former peak of GO, whereas the latter peak of GO vanishes owing to the removal of oxygen containing functional groups [109]. Adamu et al. reported that the band gap was slightly narrowed to 0.21 and 0.26 eV when TiO_2 was doped with 0.25% GO and RGO, respectively [110]. UV-DRS also highlighted a red shift in the optical absorption and extended visible light absorption edge with the incorporation of GR into the composite.

The photoluminescence (PL) spectra are among the best techniques to assess the efficiency of electron migration, transfer, trapping, allowing to draw conclusions on the surface structure and excited states of a semiconductor, along with the recombination extent of electron-hole pairs. PL emission at wavelengths equal (band-to-band transition) or greater (transitions occurring in intra-band gap states and due to semiconductor defects acting as recombination centers) than the optical absorbance threshold of the semiconductor can be indeed ascribed to the recombination produced by electron-hole recombination. A lower PL emission, generally, indicates a lower recombination rate of electrons and holes under a given wavelength excitation, and a more efficient charge separation at the surface junctions. Assembling an inorganic semiconductor with GR leads to defects on the surface of the catalyst, acting as active sites where the photogenerated electrons are trapped and also as an interface between the two constituents of the composite, where electrons can be efficiently separated and conveyed far away from holes. As a result, the PL intensity is significantly lower in composite materials [111].

The morphology of GR-semiconductor photocatalytic surfaces are characterized by scanning electron microscopy (SEM) and transmission electron microscopy (TEM). The wrinkles of GR, the uniformity and the shape of the composite photocatalysts can be observed through SEM. A more detailed morphology characterization can be performed with TEM, allowing also to observe the lattice fringes and to deduce interplanar spacing (d) and Miller indices of the observed crystal planes. The crystallite sizes of inorganic semiconductor particles can be identified along with the corresponding crystal planes, as illustrated in Fig. 10*. The size of the agglomerates can also be identified easily, although few layers of GR are tougher to be observed due to the high electron transparency, resulting in a color quite close to the background one. Low applied voltages, along with the identification of GR wrinkles and edges of the composite, however, are helpful to perform a proper observation. Moreover, selected area electron diffraction (SAED) is a powerful means to obtain information on diffraction rings of GR, with its asymmetric six fold pattern with the corresponding Miller Bravais indices,

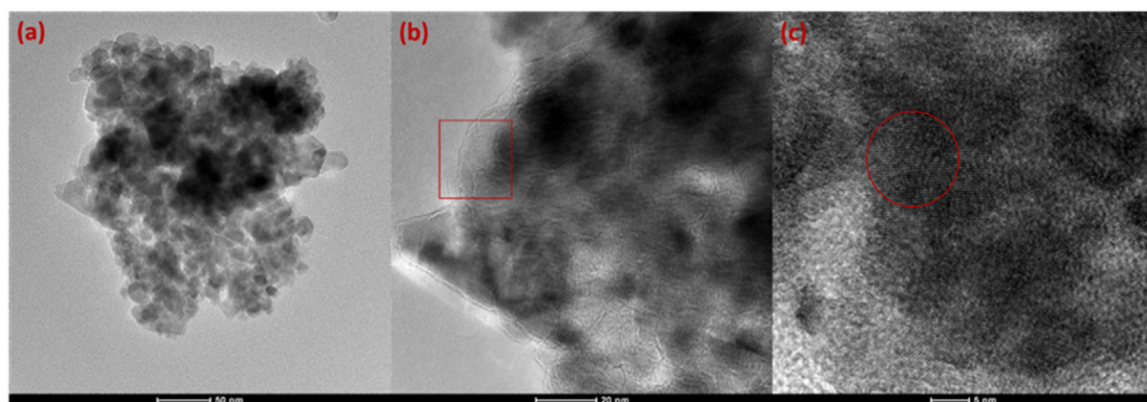


Fig. 10. TEM images of N-doped $\text{TiO}_2/1\%$ GR. GR in (b) is shown in the red rectangular; (c) shows crystal fringes of rutile (110) plane. This sample is made of N-doped brookite-rutile grown on graphene and it was recently developed in Khalifa University of Science and Technology, Masdar Institute, by some of the authors.

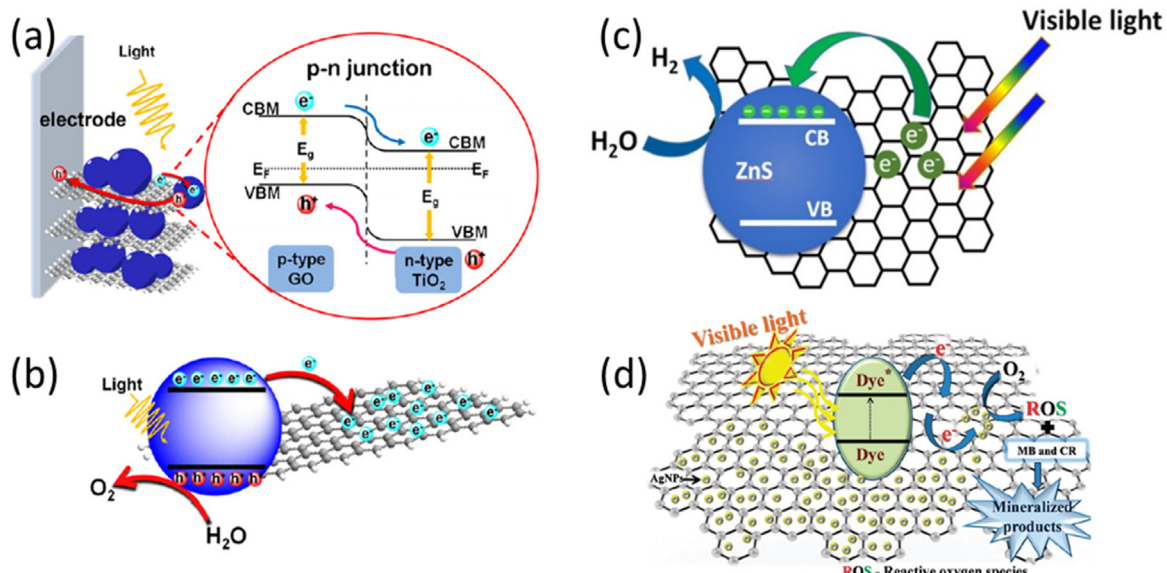


Fig. 11. Representation of possible electron transfer and scavenger mechanisms in different semiconductors: a) p-n heterojunction formed between GO and TiO₂, b) schematic of GO function in the electron separation and storage, c) photo-generated electron separation and transfer in the ZnS-GR composites under visible light irradiation, d) self-oxidation of dyes under visible light irradiation. Reprinted with permission from Ref. [61,115,116]. Copyright 2013 Elsevier, 2015 IOP Publishing and 2015 Royal Society of Chemistry.

enabling to safely differentiate between GR and the inorganic semiconductors [106].

Concerning the textural properties of the composite photocatalysts, the specific surface area, the total pore volume, and the pore size distribution need to be determined and correlated to the reactivity results. The specific surface area of GR semiconductor photocatalyst is usually calculated by the multi-point Brunauer-Emmett-Teller (BET) model and the correlation of isotherms and hysteresis loops to the pore-size distribution curves can be unveiled through Barrett-Joyner-Halenda (BJH) model. With combination of GR with inorganic semiconductors, higher specific surface areas and large pore volumes are expected, producing an enhanced photocatalytic performance due to a larger extent of adsorption and a more effective mobility of target molecules and products. Accordingly, Chun et al. have reported that the specific surface area and pore volume of GO-TiO₂, 68.5 m² g⁻¹ and 0.23 cm³ g⁻¹ higher than those of pure P25, 38.7 m² g⁻¹ and 0.14 cm³ g⁻¹, respectively. In addition, post treated GO-TiO₂ composite at 500 °C had higher surface areas and pore volumes, 113.8 m² g⁻¹ and 0.47 cm³ g⁻¹, respectively [79].

Electrochemical impedance spectroscopy (EIS) is employed to characterize the charge-carrier migration and electron-hole recombination behavior of the composites at semiconductor-electrolyte interface. The EIS spectra are represented as Nyquist plots consisting of semicircle and straight line. The diameter of semicircle represents the charge-transfer resistance (R_{ct}) and constant phase element (CPE) at the interfacial contact between composites and the electrolyte solution. The arc radius reflects recombination resistance and the semicircle at high frequency is a feature of the charge transfer process. On the other hand, the straight line in the Nyquist plot signifies the diffuse resistance of the electrolyte in the surface of the semiconductor. According to Chen et al. [112], the radius of semicircle decreased with RGO introduction in comparison to bare Bi₂S₃ photocatalyst, manifesting that the introduction of graphene reduced the charge transfer resistance on the surface, improved the transfer of the photogenerated charges and the separation of photogenerated electron-hole pairs at interfaces.

6. Cooperative mechanism at graphene-inorganic semiconductor interface

GR is a versatile component that can be functionalized in a range of different ways to tune its electronic properties [113]. It can be either p-type or n-type, upon chemical doping with electron withdrawing oxygen functionalities or electron-donating nitrogen functionalities, as illustrated in Fig. 11.

Chemically derived GO has a variable amount of oxygen in its structure owing to the difference in the preparation process. These functional groups, which can be located either on the basal plane or at the edges of GO, lead to the occurrence of sp² hybridization, conductive π states, and sp³ hybridized carbon atoms, derived from σ states. The tailoring of the amount of sp² and sp³ by chemical or thermal reduction allows for tuning of the optical band gap [48]. RGO, having aromatic sp² domains surrounded by sp³ domains, shows a p-type semiconductor activity [114]. Under UV radiation, these sp³ domains can be further reduced with the incorporation of metal oxides such as TiO₂, thus providing an efficient charge separation spot in the composite photocatalysts [53].

The interaction mechanisms among GR and inorganic semiconductors, resulting in suppressed recombination of photogenerated electrons and holes, extended excitation wavelength and increased surface-adsorption of reactants, are still not fully unveiled: several operational schemes have been proposed so far, as illustrated in Figs. 11 and 12 [61,115–117].

The function of GO in the electron transfer and scavenging mechanisms, taking place under UV and visible radiation, can be either electron donor or acceptor, depending on the energy levels of the inorganic semiconductors, and depending on oxidation/reduction potentials of the involved species. When GR is incorporated into a semiconductor in which the CB is more positive than the Fermi level of GR, the photo-generated electrons can be transferred from VB to either (i) GR by passing through CB or (ii) CB by passing through GR [118–120]. GR with π-conjugated 2D structure allows electrons to transfer as much as 1.5 × 10⁴ cm² V⁻¹ s⁻¹ to target pollutants. As a result, the photo-generated electron path-

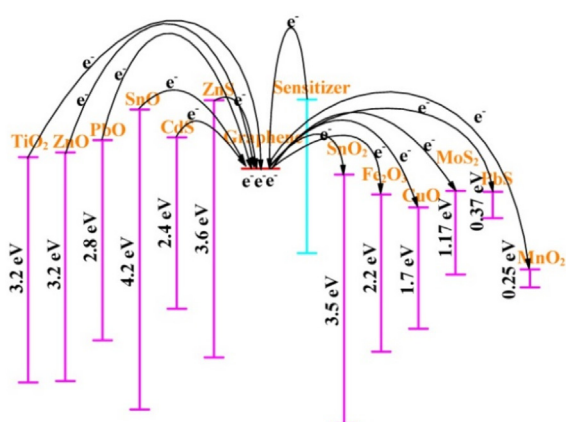


Fig. 12. Schematic representation of energy bands of GR and common semiconductors. Reprinted with permission from Ref. [117]. Copyright 2013 Elsevier.

way is prolonged, thus promoting the production of highly reactive radicals. Beside the transportation of photo-generated electrons, Wang et al. [121] proposed that a valence hole can move from VB to the phenol molecules on the RGO surface for immediate degradation. In some cases, the Fermi level of GR is more positive than the CB of photocatalyst, so electrons can be transferred from the semiconductor to GR only in the presence of sensitizers leading to an increased mean free path of electrons and consequently to a decrease in the recombination rate. Accordingly, the photocatalytic quantum efficiency of semiconductor/GR composites is enhanced as illustrated in Fig. 12 [117]. However, beside the photo-generated electron transfer from GR to inorganic semiconductors or vice versa, the photogenerated empty states (holes in semiconduc-

tor VB and in GR) can produce a direct oxidation of organic species if their energy is low enough.

Moreover, the precise band positions in semiconductors need to be carefully measured for the specific materials under study, since they can change significantly depending, for instance, on preparation methods and amorphous vs. crystalline contents; diverse reaction environments can also produce a diverse band bending resulting in different performance [122].

Another mechanism can be considered in the presence of dyes, which are able to absorb visible radiation themselves. According to Pastrana-Martinez et al., the photocatalytic activity of GR-modified composites with adsorbed dye is due to dye self-sensitized photocatalytic activation, which occurs under visible light irradiation leading to the direct self-degradation of colored pollutants [120,123]. The photo-excited electrons in the dye can be delocalized in the electronic diffuse states of RGO and/or of the CB of inorganic semiconductors, resulting in the degradation of the dye, going through a transient intermediates or stable by-products. However, this mechanism, which might partially explain the photocatalytic degradation of organic dyes under visible irradiation, cannot be applied to species not absorbing visible radiation, unless the visible absorbing complex is formed upon adsorption of the organic species on the composite catalyst.

It must also be underlined that the intrinsically heterogeneous GO electronic structure, containing many electronic states derived from different sp² and sp³ hybridized carbon atoms can boost the electron transfer from GO to TiO₂ under visible light irradiation. Visible light excited electrons in localized sp² states of GO with adequate energy can be delocalized in the CB of TiO₂ [123]. However, the self-sensitized photocatalytic activity can be dominant under visible light irradiation.

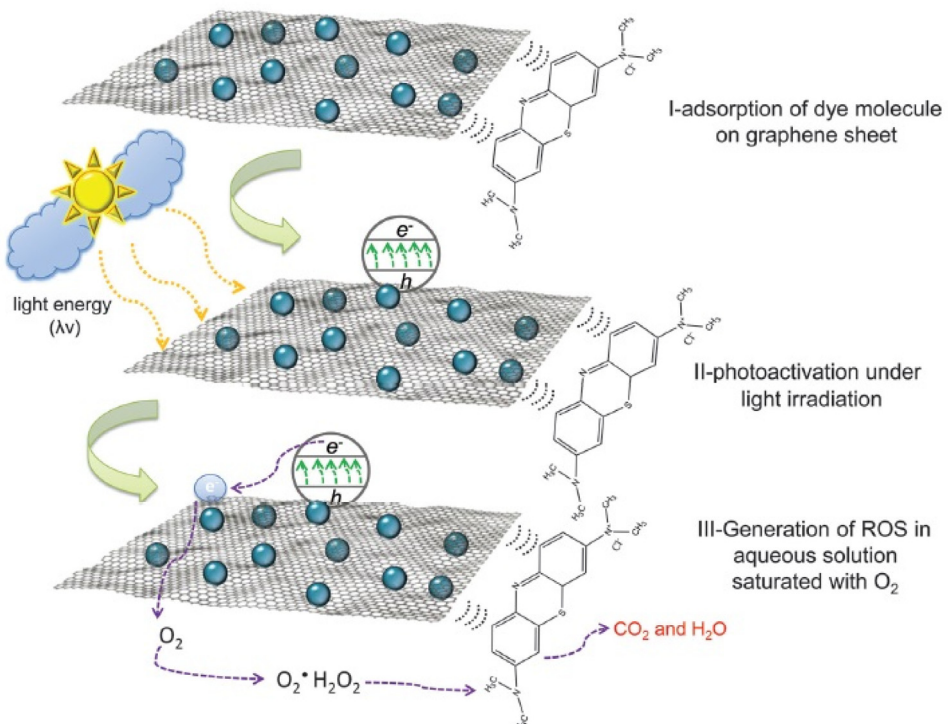


Fig. 13. Representation of the three step mechanism proposed for the degradation of organic dyes such as MB by GR-inorganic semiconductors. Reprinted with permission from Ref. [126]. Copyright 2015 Royal Society of Chemistry.

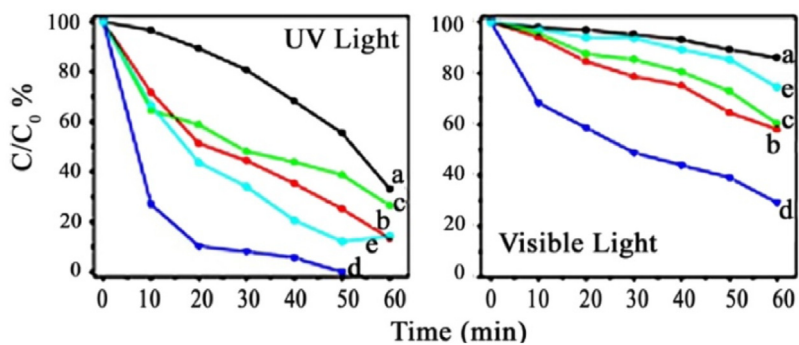


Fig. 14. Photodegradation of MB under UV light and visible light (a) TiO₂; (b) TiO₂/GR; (c) HRTiO₂; (d) HRTiO₂/GR and (e) P25. Reprinted with permission from Ref. [137]. Copyright 2016 Elsevier.

7. Applications

7.1. Pollutants degradation

With the increase in energy consumption and industrial water discharge, environmental pollutants such as organic dyes, hydrocarbons, heavy metals and metal oxides, have become a serious threat to the ecosystem. Many efforts have been directed towards the degradation of water and air pollutants through redox processes. In order to achieve a complete mineralization of organic pollutants into CO₂ and H₂O, the use of photocatalytic semiconductors represents one of the most sustainable techniques. Notably, semiconductors such as but not limited to TiO₂ have proved to be effective in the removal of mutagenic and carcinogenic species, including both organic and inorganic compounds [10,124]. However, their relatively low efficiency under solar radiation restricts their practical use. For this reason, the incorporation of GR into photocatalysts has been applied to synergistically enhance the degradation efficiency. The improvement in activity is correlated to the ability of GR to promote reactants adsorption, extend the absorption range of photocatalysts towards the visible region and suppress electron-hole recombination [125–128].

Schematically, the steps involved in photocatalytic activation of GR-inorganic semiconductors for the degradation of dyes can be summarized as follows: (1) adsorption of pollutant on the surface of GR through π–π stacking interactions, (2) photo-excitation of electron from VB to CB of the composite under UV or visible light and, lastly, (3) generation of reactive oxygen species obtained through the transfer of promoted electrons to O₂ molecules, through a pathway shown in Fig. 13 [126]. However, it should be emphasized that dyes and other species are also prone to absorb light themselves triggering the photocatalytic oxidation processes, especially after adsorption on a semiconductor through the formation of complexes. Accordingly, the excited electrons of dyes can be delocalized in the electronic diffuse states of RGO and/or be injected into the CB of inorganic semiconductors, finally activating a self-degradation process [120,129].

Due to the complexity of the reactions going on, which is often related to the reactivity of the complex formed upon adsorption of the dye, rather than to the intrinsic reactivity of the photocatalyst, it is hard to have a reliable quantitative assessment of comparable reaction rates for different catalysts [130]. However, synthetic dyes are relevant pollutants, since they find applications in a multitude of industries including textile, paper, plastic and rubber. Alarmingly, nearly 10% of them are released directly into the environment [131]. Such dyes, including MB, RhB and methylene orange, are some of the water pollutants, whose degradation is a major concern [132]. Also, some of these dyes are toxic and carcinogenic in

nature [133], thus adding to the harmful impact they have on the environment and living beings.

A recent case study reported by Chang et al. [65] involves RGO-TiO₂ hybrids prepared by a hydrothermal method at temperatures of 120, 150 and 180 °C. The catalyst prepared at a temperature of 180 °C showed an improved homogeneity when compared to those prepared at lower temperatures. A higher temperature fostered the homogeneity of the composite and PL emission because electron-hole recombination was significantly quenched, thus resulting in an efficient degradation of MB. After 10 min in dark, 50% MB was adsorbed on the surface of RGO-TiO₂, with an 8 fold improvement in performance when compared to pure TiO₂. The strong adsorption was generated by the non-covalent interaction driven by the π–π stacking between aromatic regions of MB and GR. After 3 h of exposure to natural solar light, MB was completely degraded. A limited electron-hole recombination and the extension of absorption range towards the visible were reported as the reasons for such performance. Upon exposure to a low (15 μW cm⁻²) and a high (120 μW cm⁻²) radiation intensity, an enhancement of the photocatalytic activity from 25.5% for low intensity to 98.8% for high intensity was reported.

The organic degradation can be carried out contemporaneously to metal cation reduction, as shown by Kumordzi et al. [16], who reported the photoreduction of Zn²⁺ using a hydrothermally synthesized TiO₂/GR 1% (w/w) in the presence of sunlight and H₂O₂. This photodegradation was carried out anaerobically by purging the reaction medium with nitrogen, thereby retaining the generated H₂ in its form without being converted into water. The incorporation of GR enhanced the reduction of Zn²⁺ to metal Zn, ca. 20% under solar light compared to pristine TiO₂, by narrowing the band gap of the semiconductor from 3.1 eV to 2.2 eV. The combination of metal oxide nanoparticles with GR derivatives leads to the narrowing of the metal oxide band gap by energetically favored hybridization of O 2p and C 2p atomic orbitals resulting in the formation of new valence bands [78,134–136]. The proposed mechanism of Zn²⁺ reduction by using TiO₂/GR nanocomposites can be divided into 3 steps: catalyst activation, oxidation of water and organic compounds present, and reduction of Zn²⁺.

The exposed facets of semiconductors can affect reactivity in a strong way: studies by Mukthar Ali et al. [137] on the effects of the {001} facet of GR-modified TiO₂ composite (HRTiO₂/GR) has been reported very recently. The composite, which was prepared by a photochemical reduction method, was applied on the photodegradation of 4-chlorophenol (4CP) and different dyes including MB, RhB and methyl orange (MO). Under visible light, the extent of adsorption and photodegradation of the dyes on prepared composites was found to follow the trend MB > RhB > MO > 4CP. Comparing the performance of HRTiO₂/GR composite with TiO₂/GR on the photodegradation of MB revealed a higher efficiency of the former

under both visible light and UV radiation (Fig. 14). This indicated that the exposure of {001} facet on TiO₂ in HRTiO₂/GR composite has a significant effect on the photocatalytic activity of the composite. In addition to the MB, the performance was also found to be better for RhB and MO degradation, whereas worse photodegradation of 4CP was observed when using the composite instead of commercial P25. Another important feature of HRTiO₂/GR composite is the selectivity towards the reduction of positive dyes (MB and RhB), a property attributed to the negative charges on GR. Higher selectivity in the photodegradation of the positive dyes is observed in the mixture of the positive and negative dyes.

Reactions similar to those described above can be carried out by using a configuration in which an ultra-thin anatase TiO₂ nanosheet is combined with GO by self-assembly [90]. The optimum GO content was found to be 5% (w/w) yielding a 91.2% degradation of MB as compared to 53.2% when pure TiO₂ was used under exposure to UV irradiation. The authors mentioned that one of the major reasons for this improvement was attributed to increased specific surface area resulting from interspace between the TiO₂ nanosheet and GO. Yang et al. [138] reported the preparation of a porous TiO₂/RGO composite via the permeation of TiO₂ into GO-PS microspheres followed by calcination. The prepared photocatalysts were applied to the degradation of MB under visible light in the presence of photoelectron scavengers. The TiO₂/RGO porous composite exhibited 6.5 improvement in efficiency for the degradation of MB under visible-light as compared to bare P25. In this photodegradation process, the major reactive species were holes (h⁺), O₂^{•-} and OH[•]. Owing to the high surface area and good permeability of the as-synthesized photocatalyst, the number of active sites increased and the light utilization was also enhanced thanks to the multi-scattering of incident photons. According to Xu et al. [54], the small size of TiO₂ spheres was the key for a good interaction with GO sheets, yielding an enhanced photocatalytic activity in the degradation of MO compared to that obtained with large TiO₂ spheres, thanks to the maximized interfacial contact area between TiO₂ and GO and increased specific light absorption provided by the former material. In two separate studies [139,140] the enhancement in the photoreduction of Cr (VI) to Cr (III) by incorporation of GR into TiO₂ was reported, as illustrated in Fig. 15. The optimum RGO content in the TiO₂ microsphere/RGO composite was also found to be 5% (w/w), similar to the conclusions given by Luan et al. [90]. The authors reported 98% reduction of Cr (VI) for the as-synthesized composite compared to 30% by P25 TiO₂ when exposed to visible light for 180 min. On the other hand, the photocatalytic activity of optimum 20% TiO₂/GR hydrogel was 98% for a UV light exposure time of 30 min. TiO₂/GR hydrogel has a large surface area with interconnected pores, which facilitate higher active sites for adsorption and crossed open channels for the diffusion of adsorbates, mostly in the forms of HCrO₄⁻ and CrO₄²⁻. It was also demonstrated that the oxygen functional groups of GR provide more active sites for adsorption, thereby fostering the uptake of Cr (VI), which can be quantitatively reduced to Cr (III). Accordingly, the results pointed to a strong enhancement upon tuning the morphology and size of TiO₂ and the distribution of TiO₂ nanoparticles on GR sheets.

Modification of GR-TiO₂ semiconductor using different doping agents has been investigated with the aim of extending its visible light absorption range, eventually narrowing the band gap. Liu et al. [56] reported the importance of GR moiety in N-doped TiO₂ nanowires supported on N-doped GR (with an optimum GR content of 7% (w/w)) fabricated by a facile hydrothermal method using urea as a nitrogen source at relatively low temperatures. The efficiency of the composite was compared to TiO₂ nanowires and N-doped TiO₂ nanowires by degrading MB and, under visible radiation, N-TiO₂ nanowire/N-GR showed a superior activity with an improvement of 8.6 and 5 fold, respectively. This suggests that excited electrons from N 2p impurity energy levels migrate to the CB of the com-

posite and, later on, they are transferred to GO sheets via Ti—O—C bonds. This is possible due to the favorable intra-band gap level of N 2p impurities in N-TiO₂, which is located above the VB maximum (corresponding to O 2p), as illustrated in Fig. 16. Meanwhile, the holes on the surface of N-doped GO migrate to the VB of TiO₂ thus separating the electron-hole pairs and inhibiting the recombination of charge carriers. As a result, the electrons gathered on the GR sheets leaving holes behind on TiO₂ surface. The electrons can be scavenged by O₂ thus generating reactive intermediates (i.e. superoxide radical anions, O₂^{•-}). The positive holes on TiO₂ VB react with H₂O molecules leading to the generation of many mobile free OH[•] radicals and hydrogen ions, which eventually oxidize MB as shown in Eqs. (3)–(7).



Wang et al. [141] studied the effect of RGO content and catalyst dose by preparing TiO₂-CdS/RGO nanocomposites via a solvothermal method, with RGO ranging from 3 to 10%, and performing the degradation of MB and RhB under visible light. The authors reported the optimum concentration of RGO in the composite to be 5%. When the sample with optimum RGO content was utilized for the photodegradation of MB and RhB, the degradation extent was 97.5% and 93.5%, respectively. The high activity was attributed to a promoted adsorption of pollutants and the suppressed recombination of photogenerated electrons and holes due to the presence of GR. Beyond the optimum concentration of RGO and catalyst weight, the photocatalytic efficiency was found to be reduced owing to the decreased active sites and to the decreased light transmittance. CdS served as a sensitizer, trapping photons from visible light and exciting electrons of CdS to the VB of TiO₂, whereas RGO acted as photo-excited electron mediator, which absorb photogenerated electrons and transported them to TiO₂, thereby minimizing the electron-hole pair recombination rate. This is due to its efficient charge carrier transfer as well as to its high adsorption capacity.

Apart from TiO₂, several other GR-based composite of inorganic semiconductors such as ZnO, CdO, MoS₂, Bi₂WO₆ have been used for oxidative degradation purposes. For instance, Ding et al. [142] found that among GO/MoS₂ hydrogel composites with loadings of MoS₂ ranging from 5% to 20%, the most efficient degradation of MB was attained with a GO/10% MoS₂ hydrogel. For an exposure time of 60 min under visible light, 99% degradation of the MB was achieved for the optimum GO content. Gan et al. [143] also used the hydrothermal method in the fabrication of WO₃/GO with different loadings of GO from 1% to 10%, where the WO₃/7% GO had the highest degradation efficiency under both visible light (400–700 nm) and combined UV-vis light spectra (below 700 nm). Qin et al. [144] reported that, though the band gap of ZnO microspheres did not remarkably change when coupled with RGO, the increase in absorption extent in UV and visible light regions obtained by increasing the RGO content was due to the enhanced surface electric charges on ZnO composited with RGO, also to a change in the mechanism of electron-hole pair formation, as illustrated in Fig. 17. ZnO microspheres-RGO composites, fabricated by a facile solution method improved photodegradation of MB, whereas the photogenerated holes and superoxide radical, O₂^{•-}, induced the generation of active species.

Kumar et al. [145] reported that hydrothermally fabricated CdO-RGO mineralized MB up to 80% under UV radiation. However, bare CdO was able to degrade only 65% in the same reaction time. Xu et al. [93] suggested an interesting photodegradation mechanism

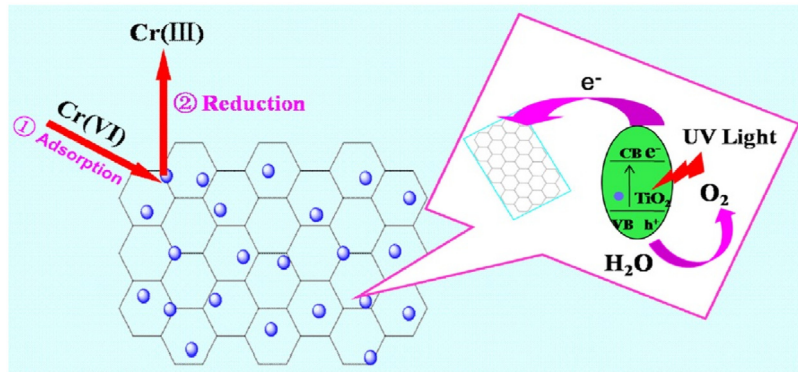


Fig. 15. Schematic diagram of TiO₂/GR hydrogel-mediated reduction of Cr (VI). Reprinted with permission from Ref. [140]. Copyright 2016 Elsevier.

of RhB by using a Bi₂WO₆/RGO aerogel: the electrons excited from the VB to the CB of Bi₂WO₆ under visible light leaving holes in VB, but recombination of the migrated electrons with holes was massive as the concentration of the promoted electrons increase. However, the interaction of GR and Bi₂WO₆ in the Bi₂WO₆/RGO aerogel demonstrates that separation of electrons and holes was highly facilitated.

A magnetically recoverable catalyst, i.e. Fe₃O₄/RGO, was used by Boruah et al. [146] in different pH media affecting the surface charge of the composite, and the adsorption of the degraded pollutants eventually altered their degradation efficiency. At the negative surface of Fe₃O₄/RGO, where pH was above 5.5, better

adsorption for cationic RhB and methyl green (MG) led to a better photocatalytic efficiency. Conversely, the positive surface adsorbs the anionic form of methyl blue (aniline blue) and Cr (VI) with a pH below 5.5. This study also showed that an increased loading of the catalyst up to 0.5 g L⁻¹ enhanced the efficiency of degradation of the dye due to the increase in available surface catalytic active sites thereby resulting in a better maximization of the available photons. However, a further increase leads to the loss of some activity owing to agglomeration, which minimizes the exposed catalytic sites and the chemical interaction between dye molecules and the nanoparticles. After 120 min of direct sunlight irradiation, the enhanced degradation of MG, MB and RhB on Fe₃O₄/RGO was 99.31, 98.97 and

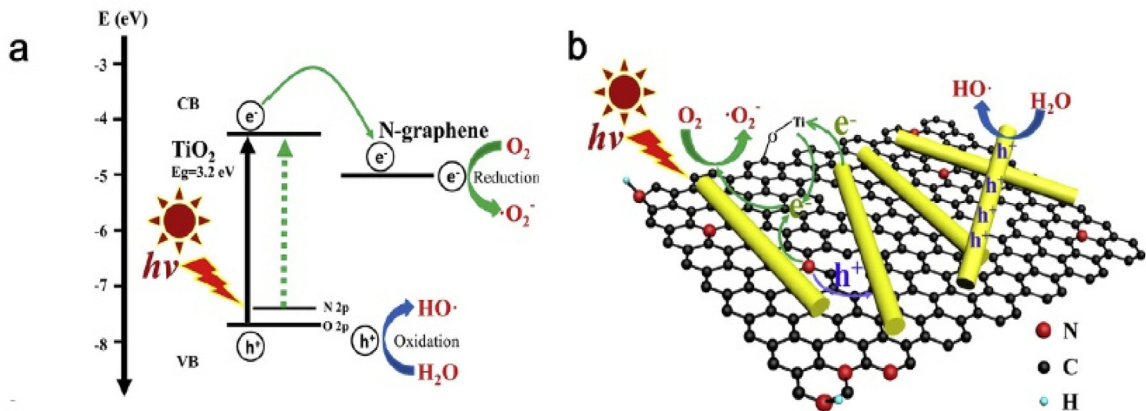


Fig. 16. Representation of (a) photogenerated electron transfer between N-TiO₂ nanowires and N-GR; (b) photo-generated electrons and holes exchanged between N-TiO₂ nanowires and N-GR nanosheets. Reprinted with permission from Ref. [56]. Copyright 2016 Elsevier.

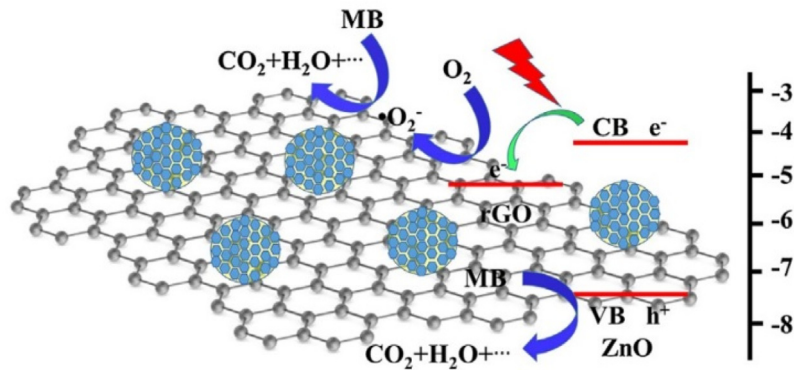


Fig. 17. Schematic diagram for the energy levels of ZnO microspheres-RGO composites and the proposed photocatalytic mechanism. Reprinted with permission from Ref. [144]. Copyright 2017 Elsevier.

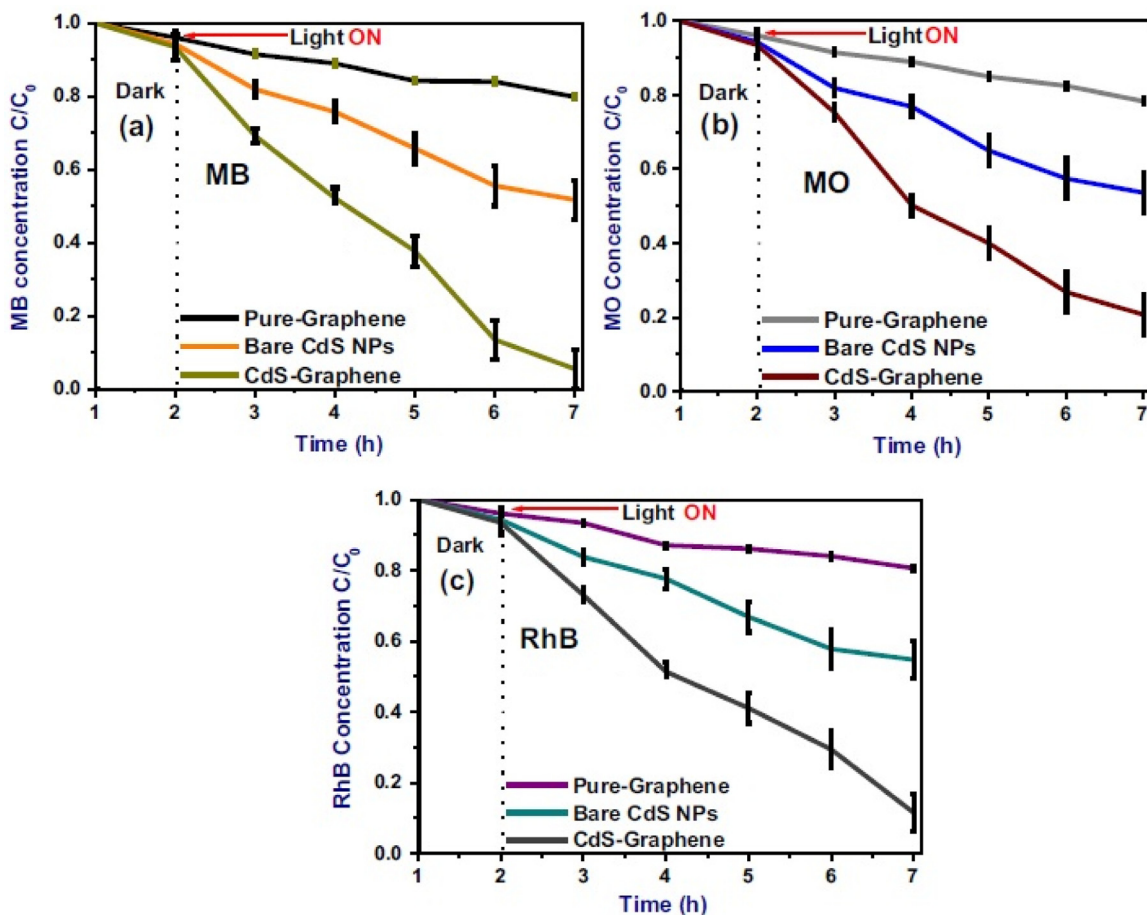


Fig. 18. The photodegradation/decolorization of (a) MB, (b) MO, and, (c) RhB using pure-GR, bare CdS NPs, and CdS-GR nanocomposite in the dark and under visible light irradiation. The kinetics of the reaction was plotted as the photodegradation constant of the model dye $\ln(C/C_0)$ vs. time (t). Adapted with permission from Ref. [132]. Copyright 2016 Elsevier.

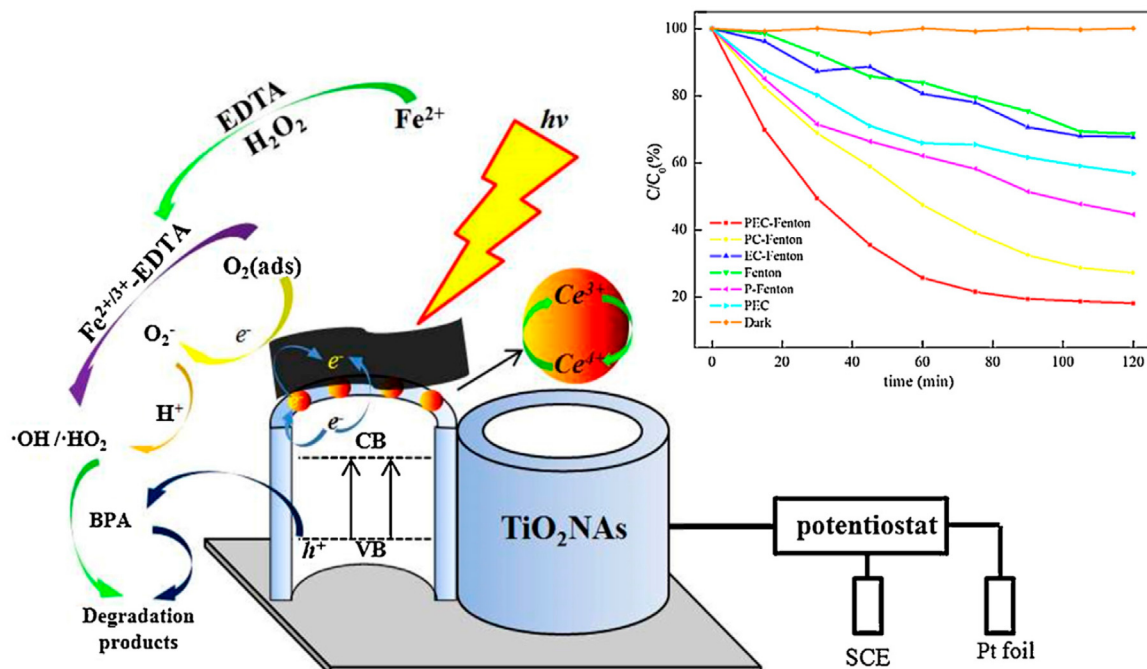
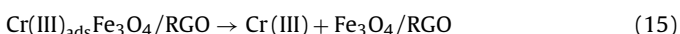
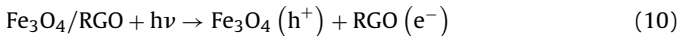


Fig. 19. Schematic for PEC degradation towards bisphenol A (BPA) using RGO-CeO₂-TNAs. Reprinted with permission from Ref. [153]. Copyright 2016 Elsevier.

87.13%, respectively. In the case of Cr (VI) reduction, the GR-based Fe_3O_4 also showed an improvement of 96% after an exposure time of 25 min, as compared to bare Fe_3O_4 , which only attained 66.17% reduction. The proposed mechanism for the degradation of dyes (Eqs. (8)–(13)) and the reduction of Cr (VI) (Eqs. (10), (14) and (15)) using $\text{Fe}_3\text{O}_4/\text{RGO}$ nanocomposites are as shown below.



In the field of oxidative degradation, photoelectrocatalysis has turned out to be a boon for its degradation ability to boost photocatalytic activity through the application of a bias. Numerous semiconductor photocatalysts such as TiO_2 , Cu_2O , CdS have been used in conjunction with GR or RGO as a route for the degradation of such dyes.

Different combinations of GR or RGO with metal oxides have been used for the degradation of synthetic dyes. Faraji et al. [133], for instance, have shown that the deposition of silver metal/ TiO_2 nanotubes/RGO coated Ti plate, exhibiting the best separation efficiency of photogenerated electron-hole pairs and the smallest charge transfer resistance, enhanced photoelectrocatalytic performance for the degradation of MB. They achieved excellent results, where more than 89% of MB was degraded within 2 h under UV light. These results were much better compared to the use of bare titanium electrodes [147]. Silver metal can enhance the binding of the metal oxide with GR, as has been shown earlier with carbon nanotubes [148]. Elsewhere, methylene orange was also effectively degraded when GR was combined with flocculent like TiO_2 : more than 75% of methylene orange was degraded within an hour [149]. The use of flocculent like TiO_2 along with GR increased the photocurrent density, ca. 10.31 mA cm^{-2} , at 0.6 V bias versus Ag/AgCl, as well as the available surface area for the reaction and consistency in the results was seen, even after 4 cycles.

Degradation of such dyes under visible light range does not only make the process technically simple but also economically desirable. Han et al. [150] demonstrated the degradation of MB under visible light by combining RGO with Cu_2O . They observed that, when the composite consisted of a mere 0.2% of RGO, good results were obtained compared to other combinations or even bare Cu_2O . Liu et al. [56] have shown that N-doping of the TiO_2/GR composite can enhance the efficiency of degradation of MB under visible light. They found that N-doping increased the reaction rate by more than 2.2 times. 87% degradation of MB was seen after 3 h of visible light irradiation where only 7% of GR was added. Under the influence of visible light and voltage in between -0.5 V and 0.7 V (versus the reference electrode), the excitation of electrons takes place to the CB of N-doped TiO_2 from the VB. These excited electrons can now be transferred to the CB of N-doped GR giving rise to holes in the VB, effectively separating the electron-hole pairs. This process therefore inhibits the recombination of charge carriers, efficiently enhancing the photocatalytic activity.

Recently, a CdS/GR nanocomposite was found to be effective in the degradation of multiple dyes including MB, MO and RhB. Close to 95% MB and 80% MO were found to be degraded in around 5 h as shown in Fig. 18 [132]. The time required for degradation

was relatively longer compared to other composites but with the advantage of utilizing visible light radiation.

Apart from synthetic dyes, various organic compounds such as quinoline and bisphenol A (BPA) have been degraded using photoelectrocatalysis [151,152]. Zhou et al. have shown that combining cerium (IV) oxide (CeO_2) with RGO and TiO_2 modified nanotube arrays gave excellent results for BPA degradation [153]. Using this composite in the optimized conditions allowed to achieve a degradation extent of more than 80% degradation of BPA in 2 h. Fig. 19 shows the used setup and the results obtained by combining photocatalysis, electrocatalysis and the photo-Fenton reaction. Zhang et al. [154] have shown successful reduction of bromate using fluorine co-doped TiO_2 and GO composites. Their process removed more than 90% of bromate in less than 15 min under UV radiation.

To sum up, GR improves the degradation of pollutants by fostering adsorption, by extending the catalyst absorbance towards visible region, by narrowing the band gap and reducing the electron-hole recombination rate. The discrepancies in the photocatalytic results obtained with different materials highlight the peculiarity of each of the discussed process and different effect of varying parameters, such as composite synthetic methods, RGO loading, pH, light intensity and initial concentration of pollutants.

The comprehensive role associated with GR derivatives in the photodegradation of pollutants appear very interesting and complex, and more efforts in these studies are expected along this direction. Briefly, the possible role of GR in the improvement of photocatalytic processes needs to be investigated in detail to optimize the implementation of GR in the photocatalytic oxidation of target pollutants.

7.2. H_2 production by H_2O and H_2S splitting

Hydrogen has long been identified as a sustainable and renewable source of clean energy due to its high energy density and environmental friendliness. As abundant as hydrogen is in nature it does not occur naturally on its own, but, it is found in various compounds, such as H_2O , H_2S , hydrocarbons, hydrides etc. The waste product from burning hydrogen is water, meaning that hydrogen, as a fuel, produces almost no pollutant when used as a source of energy [155–157]. One way to produce hydrogen is through heterogeneous photocatalysis which involves splitting of water, or even H_2S , through a process that can make use of solar energy as a source of photons. Bare inorganic semiconductors (such as TiO_2 , CdS , etc.) which are the most widespread inorganic photocatalyst have poor and limited performance for hydrogen production from splitting of water and H_2S ; thus, it is imperative to improve their photoactivity [156,158,159]. One of the approaches to improve performance of inorganic semiconductors is coupling with carbonaceous materials such as GR. Coupling of GR, for instance, with TiO_2 helps to increase the electron-hole pair recombination time thereby increasing hydrogen production thanks to the higher degree of mobile electrons available for reduction of hydrogen proton [126,156,160–165]. There exist extensive body of literature on coupling of GR sheets with semiconductor photocatalysts for enhanced photocatalytic activity in pollutant decomposition, water treatment and hydrogen production through splitting of water and hydrogen sulfide [126].

Recently, GO-CdS nanocomposite was synthesized to improve bare CdS photocatalytic activity for hydrogen production; the optimum photocatalyst was 5% GO in CdS with hydrogen production rate of $314 \mu\text{mol h}^{-1}$ under visible light irradiation [155]. Peng et al. [155] proposed a reaction mechanism for photocatalytic hydrogen production of their optimized GO/CdS nanocomposites, as shown in Fig. 20.

Li et al. [166] boosted hydrogen production rate to $1120 \mu\text{mol h}^{-1}$ under visible light irradiation using 1% GR-

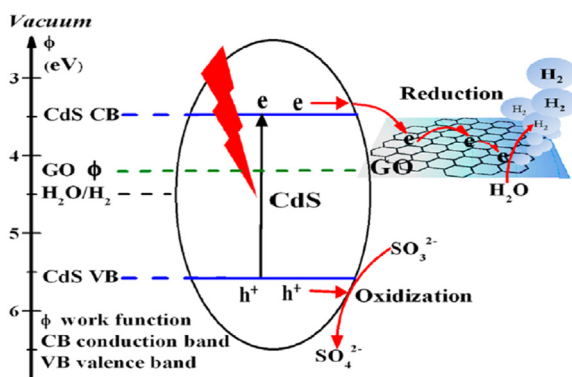


Fig. 20. Diagrammatic representation of proposed mechanism for photocatalytic hydrogen evolution of CdS/GO nanocomposites. Reprinted with permission from Ref. [155]. Copyright 2012 American Chemical Society.

CdS nanocomposites with 0.5% Pt as a cocatalyst which was ca. 5 times higher than what pure CdS nanoparticles produced. In the quest to finding suitable noble metal free composites, Lv et al. [167] prepared CdS-modified GR and TiO₂ (P25)-GR nanocomposites through an electrostatic assembly process for efficient photocatalytic hydrogen production, whose results are as shown in Fig. 21, and the results compared positively with respect to Pt-modified inorganic semiconductors under same operating conditions.

Chang et al. [163] synthesized CdS/MoS₂-GR nanocomposites for improved hydrogen production under visible light irradiation. This photocatalyst nanocomposites was tested and compared in lactic acid and Na₂S-Na₂SO₃ solutions, and the findings (as shown

in Fig. 22) highlighted that lactic acid could be a better sacrificial agent for MoS₂-based materials. CdS/MoS₂-GR nanocomposites produced 1800 μmol h⁻¹ of hydrogen in lactic acid solution and 1200 μmol h⁻¹ in Na₂S-Na₂SO₃ solution.

In order to improve charge transfer and binding energy of hydrogen on MoS₂/GR photocatalyst for enhanced hydrogen evolution reaction, Behranginia et al. [168] synthesized a 3D structured MoS₂ with Mo-edge atoms and a high degree of crystallinity on GR films. Analogously, Zheng et al. [169] prepared MoS₂/RGO using a solvent-evaporation-assisted intercalation different from the conventional pre-exfoliation method. This new method significantly improved the photoelectrocatalytic activity of MoS₂/RGO for hydrogen production, because of additional exposed active edge sites available for the catalytic reactions. On the whole, the major improvements could be credited to more active edge sites and increased electro-conductivity of the composite. Ng et al. [170] also prepared BiVO₄/RGO nanocomposites for improved photoelectrocatalytic hydrogen production from water under visible light irradiation. There was a 10-folds enhancement in photoelectrochemical water splitting compared to the pure BiVO₄. This improvement is credited to extended lifetime of excited BiVO₄ electrons and better interfacial contact between BiVO₄ particles and RGO sheets.

Jia et al. [171] reported the synthesis of a highly robust N-doped GR/CdS nanocomposite where N-doped GR served as a cocatalyst and protective layer to prevent CdS from photo-corrosion, and led to a higher hydrogen production from water under visible light irradiation, which yielded better result than pure CdS semiconductor. Zeng et al. [172] found that photocatalytic hydrogen production from water under visible light irradiation was improved when they used a one-pot solvothermal method to synthesize their RGO/CdS

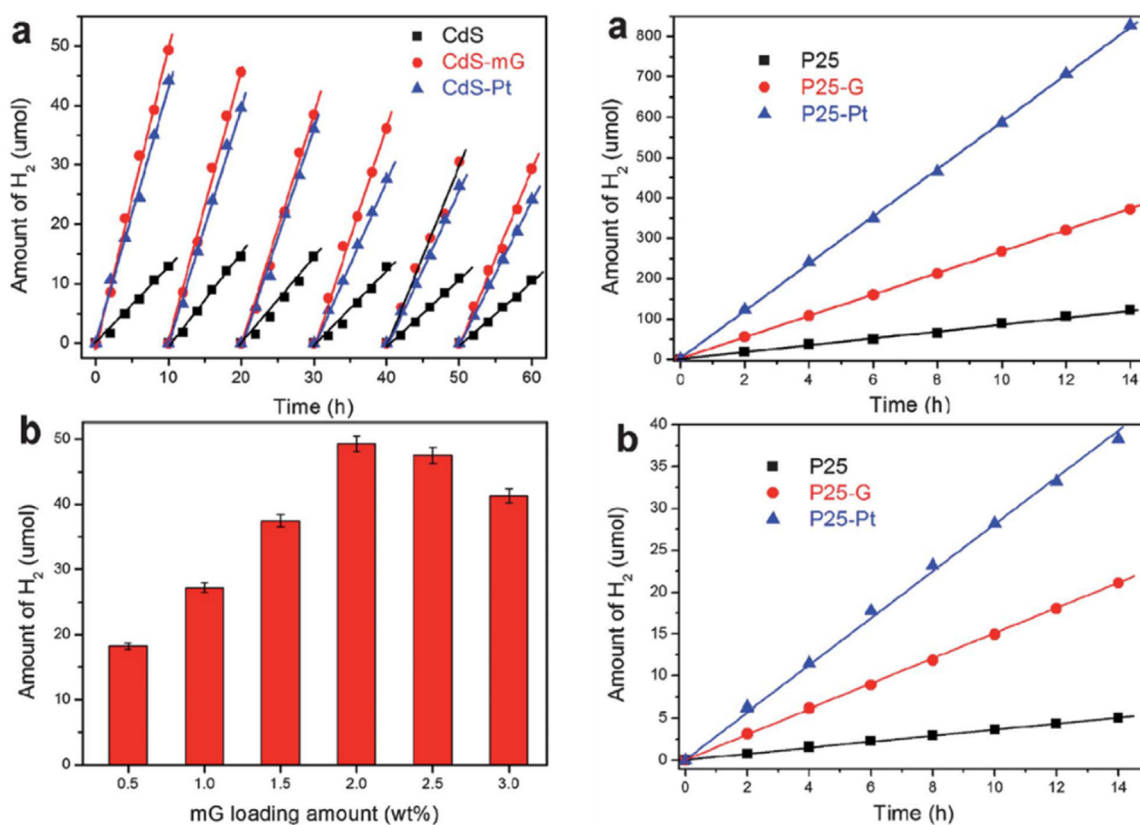


Fig. 21. Left: (a) Hydrogen production from CdS nanoparticles, CdS-modified GR (mG) and CdS-Pt composites in 20 mL Na₂S (0.05 M) and Na₂SO₃ (0.07 M) aqueous solution under visible light irradiation ($\lambda > 380$ nm); (b) effect of varying the weight% of mG in CdS-mG photocatalyst on hydrogen production after 10 h. Right: hydrogen production from P25 and its composite photocatalyst in 30 mL water and methanol (v/v 2:1) solution under (a) UV-vis and (b) visible light irradiation ($\lambda > 380$ nm). Reprinted with permission from Ref. [167]. Copyright 2012 Royal Society of Chemistry.

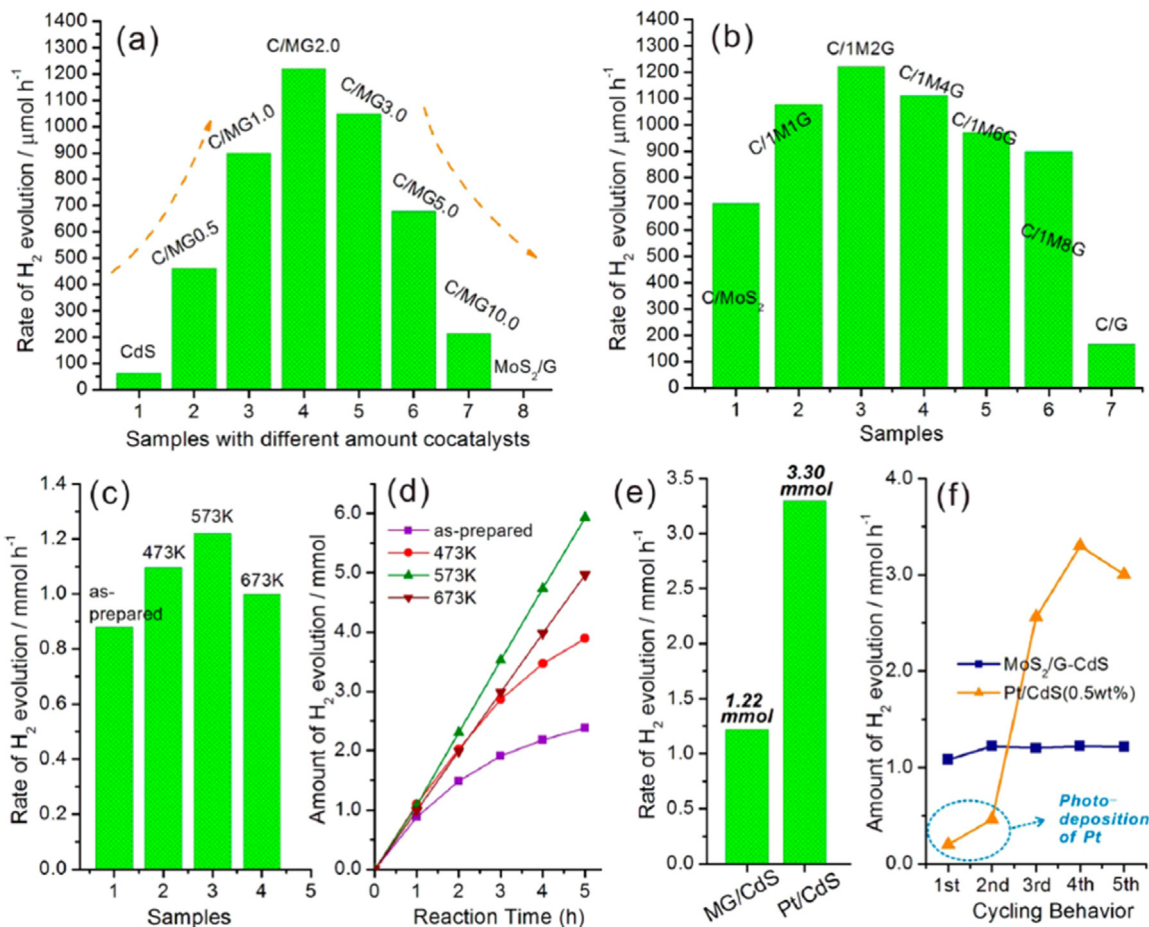


Fig. 22. Photocatalytic hydrogen evolution rate of MoS₂-Graphene (G)/CdS and Pt/CdS. (a) comparing hydrogen production of different samples with varying weight amount of cocatalyst (MoS₂-G) after 1 h. (b) hydrogen production from CdS for different molar concentration of cocatalyst. (c) Photocatalytic hydrogen production activities of MoS₂-G/CdS samples at different temperatures and (d) their cycling behavior for 5 h. (e) photocatalytic activities of MoS₂-G/CdS and Pt/CdS for hydrogen production for 1 h and (f) their cycling behavior after 5 h. Reprinted with permission from Ref. [163]. Copyright 2014 American Chemical Society.

nano-composites compared to the use of a precipitation method. The proposed mechanism is as shown in Fig. 23. The sacrificial agent used here is a Na₂S/Na₂SO₃ solution, which is replaced for every run due to drastic oxidation to SO₄²⁻ and S₂²⁻ by the hole in the VB of CdS.

Zhu et al. [173] prepared ZnS/GR/MoS₂ nanocomposites using a one-pot hydrothermal process to get an improved photocatalytic

hydrogen production from water splitting. Their major intention was to exploit the co-catalytic properties of GR and MoS₂. The result yielded hydrogen production rate of 2258 $\mu\text{mol h}^{-1} \text{ g}^{-1}$ under simulated solar irradiation, which was twice the one obtained from using pure ZnS. Yan et al. [174] synthesized and optimized Ni(OH)₂-CdS/RGO composites for hydrogen production from water under visible light irradiation. This new composite yielded an optimum hydrogen production rate of 4731 $\mu\text{mol h}^{-1} \text{ g}^{-1}$, which was ca. 10 times higher than the production rate from CdS/RGO composites. The result shows that there is strong synergy among all the constituents of the Ni(OH)₂-CdS/RGO nanocomposites. Tran et al. [175] reported the synthesis of Cu₂O/RGO composite capable of solving the photo-corrosion problem associated with using pure Cu₂O nanoparticles. An optimum Cu₂O/RGO composite with ca. 4% RGO showed a hydrogen production rate of 264.5 $\mu\text{mol h}^{-1} \text{ g}^{-1}$. Sulphonated GO was mixed with cerium-doped zinc(oxy)sulfide by Chang et al. [164] to produce [zinc (oxy) sulfide-sulphonated GR sheet] composite photocatalyst. This composite enhanced the photocatalytic hydrogen production both under UV and visible light irradiation with hydrogen production rate of 2100 $\mu\text{mol h}^{-1} \text{ g}^{-1}$ and 700 $\mu\text{mol h}^{-1} \text{ g}^{-1}$, respectively. The proposed reaction mechanism for photocatalytic hydrogen production is shown in Fig. 24. The improved photocatalytic activity was reported to be associated with presence of GR and cerium dopant which helped in narrowing zincoxysulfide band gap. Lately, sulphonated GR sheet (SG)-TiO₂ composite was synthesized using ultrasonic mixing of SG sheets

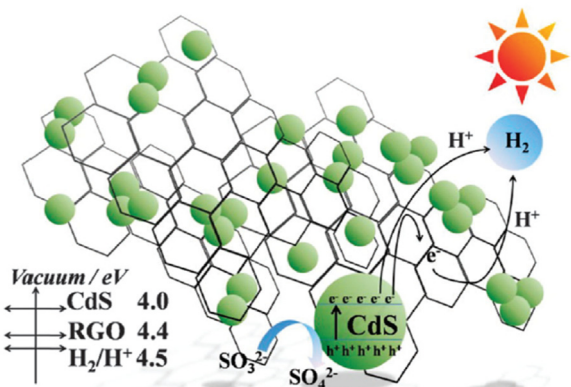


Fig. 23. Schematic illustration for mechanism of CdS/RGO composites for photocatalytic hydrogen production. Reprinted with permission from Ref. [172]. Copyright 2011 Royal Society of Chemistry.

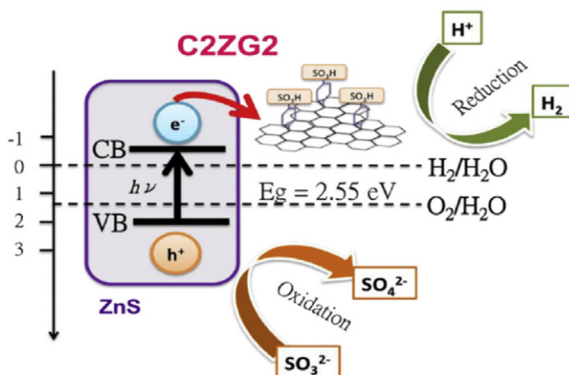


Fig. 24. The energy level diagram for Ce-doped zinc(oxy)sulfide/sulphonated GR nanocomposites photocatalyst related to redox potential of water splitting. Reprinted with permission from Ref. [164]. Copyright 2016 Elsevier.

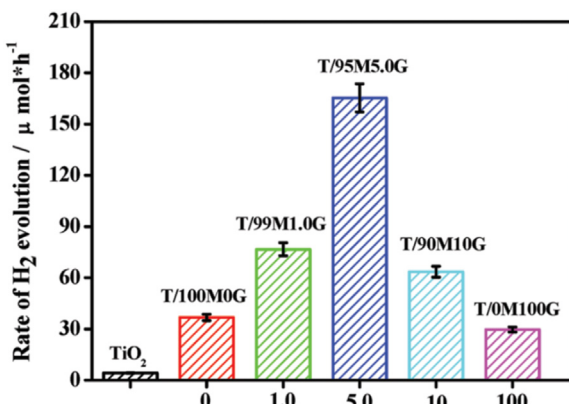


Fig. 25. Photocatalytic hydrogen production over TiO₂/MoS₂-GR composites with different weight ratio of MoS₂ and GR in the MoS₂-G cocatalyst, using 25 (v/v) % of ethanol-water solution under UV irradiation. Reprinted with permission from Ref. [156]. Copyright 2012 American Chemical Society.

and spheres of TiO₂. This composite showed excellent hydrogen production from water under visible light irradiation in a wide range of pH (from 3 to 11) where the optimum production rate of 260 μmol h⁻¹ was achieved at a pH of 7 with 2% SG sheet in composite [176].

Adsorption sites can be increased as shown by Xiang et al. [156], who succeeded in having more photoreaction centers and better interfacial charge transfer, at the same time decreasing the frequency of electron-hole pair recombination, by adding layered MoS₂/GR hybrid as co-catalyst to bare TiO₂ nanoparticles. A 0.5% MoS₂/GR hybrid in TiO₂/MoS₂ (95%)/GR (5%) nanocomposite produced an optimum hydrogen rate of 165 μmol h⁻¹, as evident in Fig. 25.

Pei et al. [177] showed that N-doped-TiO₂/GO nanocomposite succeeded in yielding a noble hydrogen production rate under both UV and visible light irradiation. This N-doped-TiO₂/GO nanocomposite produced 716 and 112 μmol h⁻¹ g⁻¹ using UV and visible light irradiation, respectively. These results are 9.2 and 13.6 times the value obtained for TiO₂ P25 photocatalyst under the same condition. Fig. 26 shows the proposed mechanism for hydrogen production from N-doped TiO₂/GO nanocomposites. It can be noticed that electrons in N-doped TiO₂ are excited from N 2p impurity energy level to the CB energy level under visible irradiation and electrons are excited from VB of TiO₂ under UV irradiation. The GR serves as the electron-transporting bridge and sink, which helps to increase the lifespan of the photogenerated electrons and to radically mitigate the recombination of electron-hole pairs; as

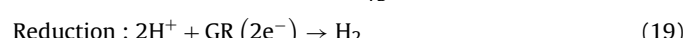
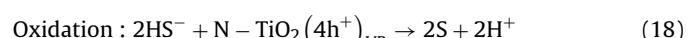
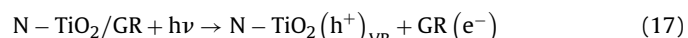
a result, an enhancement in the production of hydrogen in aqueous solutions in presence of sacrificial agent like methanol can be achieved efficiently. The hole in VB serves as an oxidizing agent which oxidizes methanol to produce CO₂ [156,162].

Fujishima and Honda with their pioneering work first demonstrated the photoelectrocatalytic production of hydrogen using TiO₂ electrode [178]. This photoelectrocatalytic process makes use of semiconductors, the practical use of which is limited by rapid recombination of electrons and holes. GR or RGO, thanks to their excellent electrical properties, can suppress electron-hole recombination and hasten charge transfer, demonstrating to be ideal components of photoelectrocatalyst composites. Kim et al. [179] used nano-sized GR/TiO₂ composites for hydrogen production. They found that nano-sized GR sheets were more efficient in production of hydrogen compared to larger GR sheets in combination with TiO₂ particles. They showed that, compared to TiO₂, the composite produced 5 times more hydrogen and impressively better results were obtained when platinum was included in the composite. The wide band gap of TiO₂ along with faster recombination rates of electron-hole carriers [56] has motivated researchers to look into other semiconductors for photoelectrocatalytic hydrogen production. Alternatively, CdS is being studied for such applications because of its appropriate band gap [180] and high adsorption ability [132]. Fig. 27 displays a schematic in which the production of hydrogen under visible light irradiation is shown, using a CdS/GR composite, in the presence of platinum. On the incidence of visible light, excitation of electrons from the VB to the CB of the CdS semiconductor takes place. The electron is then transferred to either platinum or to the GR sheet where it eventually reacts with adsorbed H⁺ to form H₂. GR here serves as an electron collector and transporter, efficiently separating the electron-hole pairs and increasing the life time of charge carriers [166].

Though photo-corrosion and faster recombination of electron hole pairs are some of the disadvantages of CdS, Han et al. [181] have proposed its combination with ZnO and GR. The high efficiency of this composite could be attributed to the presence of GR with photocurrent density as high as 16.7 mA cm⁻² being achieved. This photocurrent density was 3–4 times higher than CdS or ZnO. Again, a major advantage of this composite is its activity under visible light radiation.

Hydrogen can also be produced by photocatalytic splitting of H₂S, which is an abundant waste product from refineries and during sour gas sweetening processes. A study by Bhirud et al. [78] revealed that N-doped-TiO₂/GR nanocomposite can efficiently exploit the visible spectrum of solar radiation for an improved hydrogen production from H₂S. The optimized nanocomposite containing 2% GR showed the highest hydrogen production at ca. 5941 μmol h⁻¹. The improved result was associated with the narrowing of band gap due to nitrogen doping and excellent physical and chemical properties of GR. Authors reported that the more heterogeneous the nanocomposites the better the photocatalytic activity, since a heterogeneous structure helps to increase specific surface area, to increase the interfacial surfaces and provide additional reaction sites.

The proposed mechanism for H₂S splitting using N-TiO₂/GR nanocomposites is shown in Eqs. (16)–(19).



Among the few examples on H₂S splitting, it is worthy to report that Chaudhari et al. [12] synthesized a complex marigold flower like nanostructure of N-doped TiO₂ by applying a facile and template free solvothermal method. The hydrogen evolution rate was

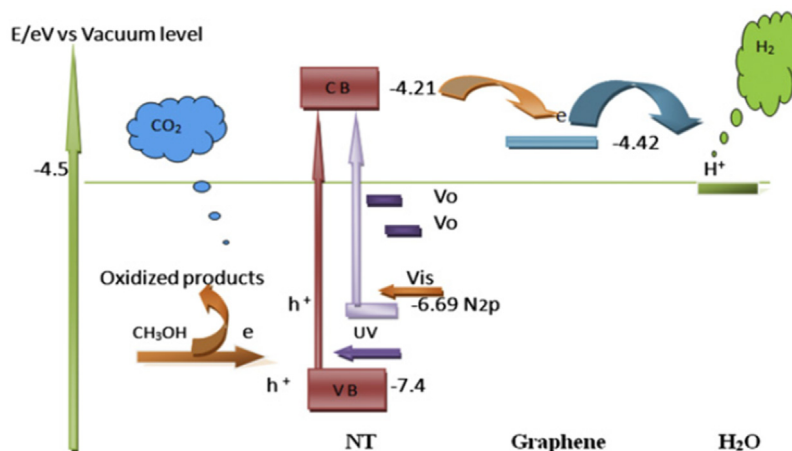


Fig. 26. Energy diagram of N-doped-TiO₂/GO for hydrogen evolution. Reprinted with permission from Ref. [177]. Copyright 2013 Elsevier.

about 8800 μmol h⁻¹ g⁻¹. This complex nanocomposite yielded result better than pure CdS and TiO₂ spheres under visible irradiation.

By looking at literature data as a whole, CdS and TiO₂ are the most sought inorganic semiconductors for hydrogen generation, and it is evident that GR and its derivatives enhance the photocatalytic properties of pure semiconductors. While in some studies they have been used as cocatalyst, in other ones they were applied as supporting matrix and means to improve conductivity of semiconductors. It is also evident that MoS₂ is a very popular cocatalyst because of the additional photoreaction sites it creates through its edge atoms sites. On one hand, H₂S splitting is not well explored compared to H₂O, but there is great need to synthesize and optimize nanocomposites effective for hydrogen production from both of these molecules, since the Clausius process currently employed to convert H₂S is producing water (instead of hydrogen) and elemental sulphur. It should also be finally underlined that the reaction mechanisms proposed in literature for hydrogen evolution on composite semiconductors appear to be in agreement [163,164,166,171,173,174,176,182,183].

7.3. Organic synthesis

Heterogeneous photocatalytic systems have garnered tremendous attention owing to their easy recycling and simple chemical work-up, which are essential qualities in order to ensure a green organic synthesis route to many industrially relevant chemicals. However, the use of semiconductor-based photocatalysis for selective organic synthesis remains modest if compared to other applications such as pollutants degradation [184–187]. One of the main issues resides in the lack of selectivity, especially in photocatalytic oxidations [188]. Two main types of organics syntheses over GR-based photocatalysts have been reported so far: selective oxidation of alcohols into corresponding aldehydes and selective reduction of nitro organics to corresponding amino organics.

The selective oxidation of alcohols into aldehydes is one of the most important synthesis for laboratory research and commercial production, since aldehydes are widely used in the food industries, beverages and drugs and as a precursor for many fine chemicals and intermediates [189–191]. In such chemical syntheses, water is considered the best solvent due to its environmental friendliness, safety and low cost. Nevertheless, the hydroxyl radicals generated in aqueous systems following UV-vis irradiation unavoidably attack the desired products, reducing the selectivity of the process [192]. Growing attention has been paid to exploring the potential of GR-based nanocomposites for these processes, carried out mainly in

aqueous systems, in the attempt to enhance the conversion and selectivity.

This last topic was addressed by Yuan et al. [193], who compared the photocatalytic performance of solvent exfoliated graphene-TiO₂ (SEG-TiO₂) and RGO-TiO₂ for the aerobic selective oxidation of benzylic alcohols to the corresponding aldehydes and acids in water under simulated solar light. Both photocatalysts, showed the best selectivity toward target products (>85%) when SEG or RGO amounted to 5% of the composite material. However, activity was greater for SEG-TiO₂, showing conversions in the range 46–57% against 30–37% in RGO-TiO₂. This was due to the much lower defects density, and better electron conductivity of SEG as compared to RGO. Further addition of SEG or RGO above 5% in the photocatalyst led to lower conversions and selectivities, with benzoic acid as the main byproduct. Alfè et al. [194] compared the reactivity of two kind of TiO₂/GR photocatalysts: water stable graphene-like (GL) layers were used in two different forms, that is in water suspensions (GLW) and shaped as flat platelets of assembled GL layers (GLP), to eventually fabricate composites with TiO₂ nanoparticles (TiO₂/GLW and TiO₂/GLP, respectively). The prepared photocatalysts were tested for the selective conversion of 3-pyridine methanol (3-PMA) to 3-pyridine carboxyaldehyde (3-PCA) and nicotinic acid (NA, vitamin B3), under simulated solar light and de-aerated conditions, in the presence of cupric ions as electron scavengers. The reaction mechanism involved the formation

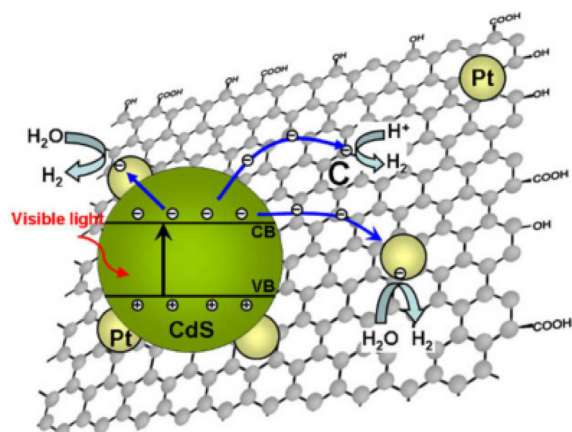


Fig. 27. Schematic showing the photoelectrocatalytic production of hydrogen under visible light. The charge transfer between the valence and conduction band is also seen. Reprinted with permission from Ref. [166]. Copyright 2011 American Chemical Society.

of 3-PCA as a primary intermediate following the reaction of holes with 3-PMA, then conversion of 3-PCA to NA and, finally, the photoreduction of cupric ions to zero-valent copper. TiO₂/GLP showed the best performance with a 3-PMA conversion of 63.3% and selectivities of 62.4% to 3-PCA and 34.6% to vitamin B3. The enhanced reactivity, in comparison with bare TiO₂, was both ascribed to a larger variety of stable free-radical species generated within the delocalized π -electron systems of the TiO₂/GLP and to a minor hydroxyl radicals formation. On the other hand, the well dispersed GL layers into TiO₂/GLW composites interfered with the TiO₂ crystallization process resulting in a lower NA conversion. Conversely, GLP offered a flat surface that was beneficial to the TiO₂ growing and crystallization.

Semiconductors different from TiO₂ were recently used to synthesize GR-based materials, where the alternative inorganic semiconductors were ZnS, In₂S₃, ZnO, Bi₂WO₆ [104,195–197]. The last one was considered a promising candidate for many photocatalytic reactions [195,196]. However, despite its good stability and recyclability, its performance is still modest, due to the low separation efficiency of electron-hole pairs and the low selectivity in synthetic reactions. To address this problem, Yang et al. [192,198] prepared Bi₂WO₆-RGO (BWO-RGO) nanocomposites via electrostatic self-assembly for the selective photocatalytic oxidation of alcohols in water. The valence and conduction edges of Bi₂WO₆ were finely tuned by the addition of RGO, causing an upward shift of the VB edge of Bi₂WO₆ (Fig. 28a), resulting in a minor generation of OH[•] and an enhanced selectivity. Despite this shift, which might have led to a decrease in oxidation capacity, BWO-RGO showed excellent photocatalytic activity, which also improved significantly with the increasing reduction degree of RGO owing to the low recombination phenomena in highly reduced RGO. Upon using the BWO-RGO 2% photocatalyst, the conversions of an extensive variety of alcohols and the selectivities towards the corresponding aldehydes were above 80 and 90% respectively. The proposed reaction mechanism (Fig. 28b) involves the trapping of the photogenerated electrons by O₂ to produce O₂^{•-}, which react with protons to form H₂O₂. Meanwhile, benzylic alcohol is oxidized through a two-step oxidation pathway, during which it reacts with a hole, giving rise to radicals that are further oxidized to produce the desired aldehydes by deprotonation. The reaction between O₂, O₂^{•-} or H₂O₂ and carbon radicals can take place simultaneously toward the selective conversions of alcohols on the BWO-RGO 2% photocatalyst.

Even when the band gap and the band edges of the photoactive material remain unchanged following the addition of GR, the latter might still lead to an increase of the visible light activity acting as a photosensitizer for wide-band gap materials. Accordingly, Zhang et al. [104] reported the assembly of nano-sized ZnS particles on GO (ZnS-GR) where GR acted as an organic dye-like photosensitizer for ZnS rather than an electronic reservoir, resulting in a visible-light photocatalyst for the selective aerobic oxidation of a wide range of alcohols and alkenes. After 10 h of irradiation, the selectivity to target products was in the range 88–98% over a ZnS-5% GR photocatalyst. As expected, the photocatalytic oxidation of the alkene –C=C– groups, was more challenging compared to the selective oxidation of –CH₂OH groups in alcohols, leading to conversions in the range 9–13% for alkenes against 33–51% for alcohols. The reaction mechanism envisaged the photoexcitation of GR from its ground state and the subsequent electron injection into the CB of ZnS. Electrons could then be trapped by molecular oxygen in the reaction system generating O₂^{•-} radicals. The alcohols or alkenes were finally converted to the corresponding aldehydes or epoxides over the ZnS-GR photocatalyst thanks to the activated oxygen.

Still on the theme of sulfides, Li et al. [199] fabricated hierarchical petal-like In₂S₃ structures grown on GR sheets with much larger surface area than the blank flowerlike In₂S₃, allowing for an

Table 1

Photocatalytic oxidation of several typical aromatic alcohols over the pure C₃N₃S₃ Polymer (CNS) and the RGO/C₃N₃S₃ Hybrid (0.3 RGO-CNS)^a. Reprinted with permission from Ref. [201]. Copyright 2014 American Chemical Society.

R groups	Photocatalysts	Conversion (%)	Selectivity (%) ^c	
H	CNS 0.3RGO-CNS	28.2	51.5	100 100
NO ₂ ^b	CNS 0.3RGO-CNS	22.3	34.1	100 100
F	CNS 0.3RGO-CNS	13.5	25.4	100 100
CH ₃	CNS 0.3RGO-CNS	34.7	54.4	100 100
H ^d	0.3RGO-CNS TiO ₂	45.9	24.3	100 92.7

^a Reaction conditions: aromatic alcohols (0.5 mmol), photocatalysts (0.03 g), solvent of benzotrifluoride (BTF) (2.5 mL) prior to being saturated with molecular oxygen, visible light irradiation ($\lambda > 420$ nm), irradiation time (8 h).

^b 4-nitrobenzyl alcohol (0.05 mmol), solvent of BTF (3.5 mL).

^c The selectivity is indicated to the corresponding aldehydes.

^d The photoreaction proceeds for 4 h with sunlight irradiation.

excellent interfacial contact between In₂S₃ and GR, which markedly boosted charge mobility and reduced electron-hole recombination. The proposed mechanism included the oxidation of the adsorbed alcohol by the photogenerated holes to form alcohol radical cation, thus reacting with O₂ or O₂^{•-} to give rise to the target aldehyde. When the GR loading was 1%, the conversion of benzyl alcohol was about 55% with high selectivity (ca. 99%) toward benzaldehyde after visible light irradiation for 2 h. Xu et al. [200] reported hierarchical nanoarchitectures of photoactive metal organic frameworks (MOFs) of UiO-66-NH₂ combined with GR, and they applied them in the oxidation of 4-nitrobenzyl alcohol, 4-methylbenzyl alcohol and 4-fluorobenzyl alcohol to the corresponding aldehydes. After visible light irradiation for 8 h, the conversions for the different benzylic alcohols were in the range 18.6–43.1% in presence of 1% RGO (1.0 RGO/UiO-66-NH₂). The addition of pyrene⁺, acting as a linker for RGOs and MOFs, was crucial for the self-assembly of the photocatalyst to form a layered sandwich-like heterostructure, in which electrons could be transferred effectively. The improved utilization of the photocarriers, as well as the more effective activation of surface-adsorbed oxygen, was corroborated by electron spin resonance (ESR) spectroscopy which showed enhanced oxygen activation to O₂^{•-} in the 1.0 RGO/UiO-66-NH₂ photocatalyst as compared with the bare UiO-66-NH₂. Such radicals, which were generated in large quantities following the quick transfer of electrons on the GR layer, caused the oxidation of the positive carbonium ions of aromatic alcohols to form the corresponding aldehydes.

The same group also attempted to use GR as a framework and support for metal-free photocatalysts intended for alcohols oxidation. They synthesized layered sandwich RGO/C₃N₃S₃ hybrids, by applying an *in situ* two-step polymerization, proving visible-light activity for selective photocatalytic oxidation of benzylic alcohols to aldehydes [201]. 4-Nitrobenzyl alcohol, 4-methylbenzyl alcohol, and 4-fluorobenzyl alcohol were oxidized and, as shown in Table 1, 100% selectivity was achieved in all cases, conversions being strongly dependent on the electron donor property of the –R group, which decreased in the following order: –CH₃ (54.4%) > –H (51.5%) > –NO₂ (34.1%) > –F (25.4%). In comparison to the reactivity of the pure C₃N₃S₃ polymer, the conversions over the RGO/C₃N₃S₃ photocatalysts with 0.3% of RGO (0.3 RGO-CNS) were almost double.

The photocatalytic selective reduction of nitro to amino group in organic molecules is widespread, since amino organics serve as raw materials for many chemical reactions [202–204]. Growing endeavors have been devoted to using GR-based materials for such selective reductions [202,205,206]. Xu et al. [202] prepared

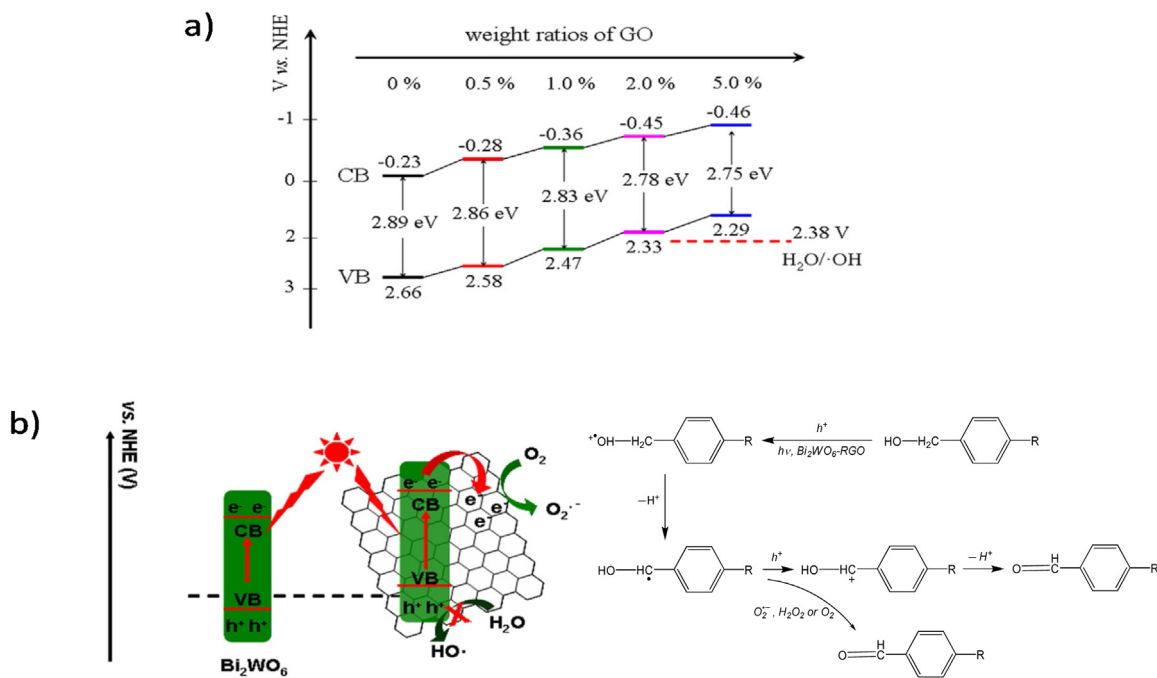


Fig. 28. (a) Estimated band structures of bare Bi_2WO_6 and various Bi_2WO_6 -RGO samples. (b) Tentative mechanism of the selective oxidation of benzylic alcohols over Bi_2WO_6 -RGO under light irradiation. Adapted with permission from Ref. [192]. Copyright 2016 Wiley VCH.

TiO_2 -GR hybrids by electrostatic assembly, where the incorporation of GR sheets minimized the recombination phenomena and encouraged the separated electrons to take part more effectively in nitro-aromatics reduction, using oxalic acid as a hole scavenger. As shown in Fig. 29a, after 1 h UV irradiation, 4-nitrophenol was almost completely converted to 4-aminophenol over the photocatalyst with 1% GO, with a 95% yield, which outperformed, by far, the yield obtained over pure TiO_2 (14%). Upon the photocarrier generation under UV irradiation, the excited-state electrons could be transferred from the TiO_2 to the GR sheets, shuttled freely along the network of the latter, and thus moved to the surface, finally reacting with nitro-aromatics to form the corresponding amino-aromatics, as schematically depicted in Fig. 29b.

The use of hybrid nanocomposites containing CdS has proved effective to carry out such organic synthesis for a number of reasons. CdS has been extensively investigated owing to its suitable band gap (2.4 eV), well matching the spectrum of sunlight [207]. Liu et al. [187] prepared CdS nanowires-RGO nanocomposites

(CdS NWs-RGO NCs) via electrostatic self-assembly. These photocatalysts exhibited superior photocatalytic performance for the selective oxidation of nitro organics in water under visible-light owing to the greater lifetime and transfer of the charge carriers in conjunction with enhanced adsorption capacity of CdS NWs-RGO NCs towards aromatic nitro organics. For similar purposes, the same group reported the synthesis of CdS nanospheres/GR (CdS NSPs/GR) hybrid nanocomposites via an electrostatic self-assembly combined with hydrothermal process [206]. In such photocatalysts, the intimate interfacial contact between CdS NSPs and the GR sheets benefited the electron conductivity and mobility of GR, as well as inhibited the photo-corrosion of CdS NSPs, along with the ammonium nitrate, which quenched the holes during the photocatalytic reaction.

Synthesis of organic compounds in photocatalysis is still in its early stage of development with application limited to selective oxidation of alcohol to aldehydes, and reduction of nitro organic compound to amino organics. Even these available routes for

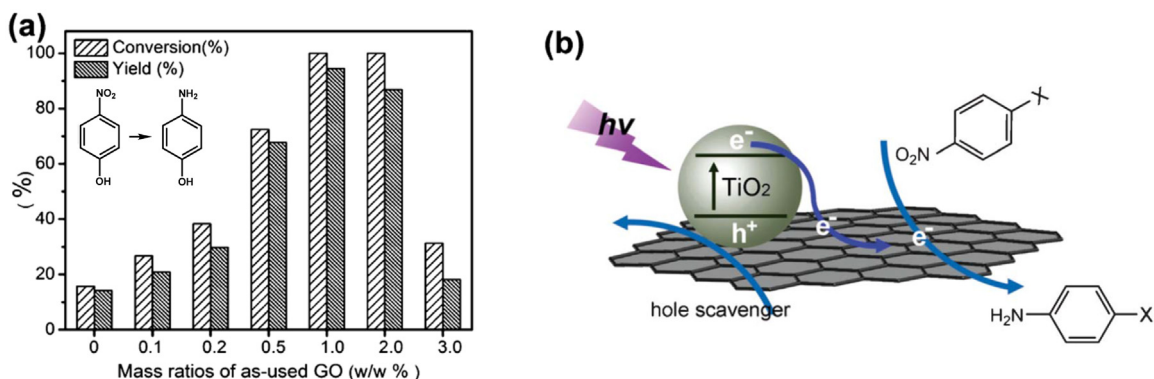


Fig. 29. Comparison of photocatalytic performances of different TiO_2 -GR hybrids for the 4-nitrophenol reduction to 4-aminophenol under irradiation for 1 h. (b) Schematic illustration of the charge separation and transfer in TiO_2 -GR system and photoreduction of nitro-organics into amino-organics under UV light irradiation in the presence of hole scavengers. (The adsorption of products and by-products are not listed in this illustration). Reprinted with permission from Ref. [202]. Copyright 2013 Royal Society of Chemistry.

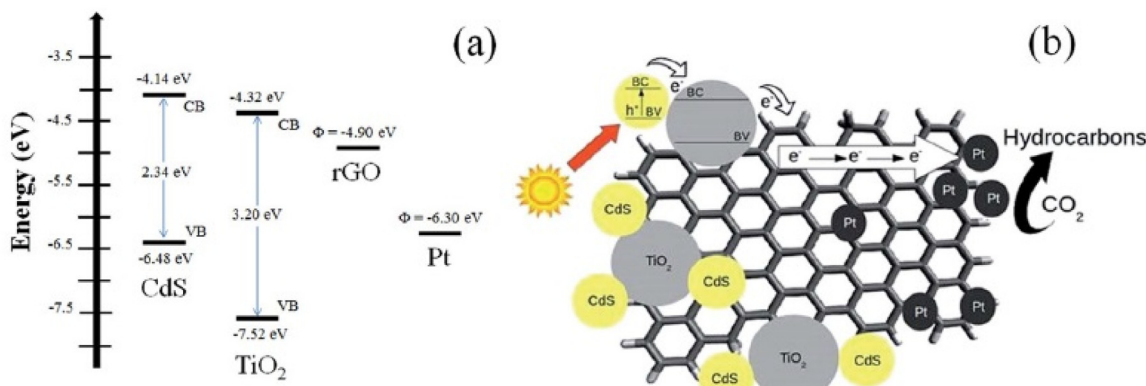


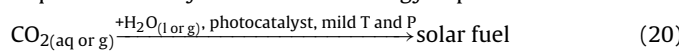
Fig. 30. (a) Energy level diagram for the CB and VB for CdS and TiO₂ together with work function of GR and platinum (b) Schematic representation of the migration of electron from CdS to TiO₂ through GR. Reprinted with permission from Ref. [214]. Copyright 2015 Royal Society of Chemistry.

production of aldehydes and amino compound are not yet fully understood. Highly oxidant hydroxyl radicals and other oxygen-bearing radicals remain the significant barrier to achieving high selectivity in aldehyde production from the selective alcohol oxidation. We believe a lot of research is still required to better optimize the available technologies in this area of application.

7.4. CO₂ reduction

Being one of the major greenhouse gases, various approaches have been employed for the reduction of the level of CO₂ in the atmosphere, which is considered one of the challenges to be urgently addressed in today's society [208]. The present focus in the scientific world is the valorization of CO₂ to produce useful chemicals rather than its traditional capture without any specific use after. Since CO₂ is thermodynamically stable [209], most of these valorization techniques require the use of catalyst and a high temperature and pressure in order to achieve the set objective [210].

Due to the depletion of fossil fuel, the conversion of CO₂ into solar fuel is being given great consideration. By so doing, the CO₂ level in the atmosphere will be maintained constant because the CO₂ formed after the combustion of such solar fuel will be recycled back into fuel. Solar conversion also has an edge over the traditional catalytic synthesis of fuel from CO₂ in that the later requires high temperature (which involves the burning of fuel) while the former requires the freely available solar energy to proceed:



Photocatalytic reduction of CO₂ into solar fuel (Eq. (20)) remains the most sustainable, eco-friendly and environmentally benign

technique of capturing CO₂ and addressing the world energy demand [211]. A peculiar challenge to the CO₂ reduction is the appropriateness of the CB level of the photo-excited semiconductor, where electrons are available to trigger reductions after their promotion from the VB. Most semiconductors perform well in the photoreduction of water due to the positive reduction potential of water (E^o = +0.82 V) [212]. This is not the case when one needs to perform the reduction of CO₂ (with E^o between -0.61 and -0.24 V) [212]. Looking into these challenges holistically, various techniques have been utilized to overcome them. The incorporation of GR into the chemical structure of photocatalysts is one efficient way of boosting the reduction ability of photocatalysts, thanks to its special features including high mobility of electrons, large surface area and remarkable chemical stability.

Some of the solar fuels derivable from the photocatalytic valorization are methane [213–215], methanol [216–218], ethane [219], carbon monoxide [220,221]. Other reported products are formic acid [222] and formaldehyde [223]. It should be noted that the peculiar photocatalytic reduction product is influenced by many factors, such as the presence of GR in the composite, the physical state of CO₂ and the reductant used, among others.

The proposed mechanism for CO₂ photoreduction into the various organic species has been reported by a number of authors such as Inoue et al. [224].

According to the mechanism, the reduction of CO₂ into the various hydrocarbons requires significant electrons, with methane formation, for instance, needing eight electrons. Thus, long living electrons are essential to favor such reductions and electron-hole recombination needs to be suppressed to the extent possible. Consider a typical photocatalytic mechanism as illustrated in Fig. 30:

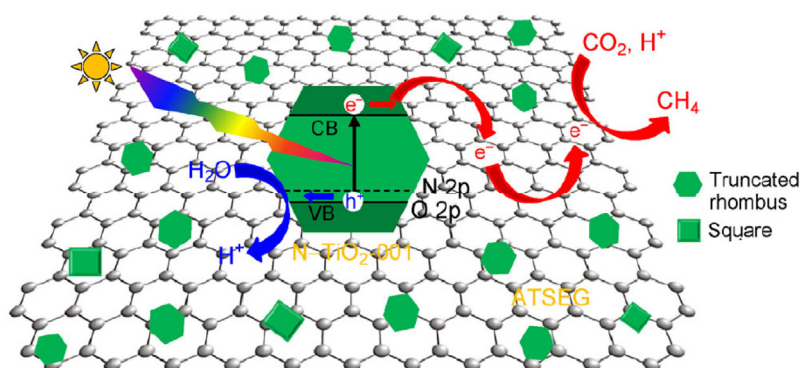


Fig. 31. Schematic representation of the reaction mechanism and the electron-hole pair separation quality of GR. Reprinted with permission from Ref. [213]. Copyright 2014 Springer.

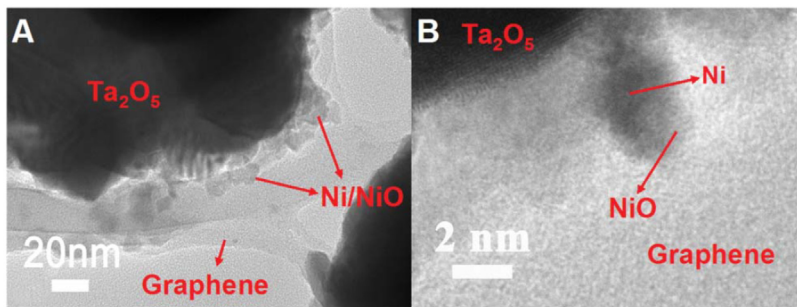
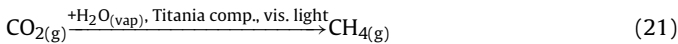


Fig. 32. Transmission Electron Micrograph of GR-based $\text{NiO}_x\text{-Ta}_2\text{O}_5$ composite for methanol synthesis. Reprinted with permission from Ref. [216]. Copyright 2013 Royal Society of Chemistry.

the facilitation of electron flow within the composite (Fig. 30b) is attained with the aid of GR 2D layers with their high electrical conductivity. The energy levels of the CB for both CdS and TiO_2 , on one hand, and the work function for GR and platinum on the other hand (Fig. 30a) suggest the direction of the photogenerated electron flow. Since the energy level of the CB of CdS (-4.14 V) is more positive than that of TiO_2 (-4.32 V), photogenerated electrons from CdS migrate to the CB of TiO_2 as illustrated in Fig. 30b. Furthermore, these electrons, in their new location, migrate quickly through GR, thereby effectively separating the charge carriers. The migration of the holes is however in the opposite direction (from lower to higher energy level) with the holes left behind in the TiO_2 migrating to VB of CdS. In the following, the description of the design of photocatalysts, using GR, for the reduction of CO_2 into specific value added product, is made.

The reduction of CO_2 into methane is the most reported photocatalytic conversion of CO_2 owing to the small reduction potential ($E^\circ = -0.24\text{ eV}$). Recently, Ong et al. [213] described the first examples of the application of GR based N-doped TiO_2 on CO_2 photoreduction, prepared by a solvothermal treatment of acid treated SEG (ATSEG) and TBOT in NH_4F , 2-propanol and diethylenetriamine (DETA) solution upon treatment at $190\text{ }^\circ\text{C}$ for 10 h. The used TiO_2 had predominant exposed $\{001\}$ facet with a high surface energy, 0.9 J m^{-2} as compared to the most stable $\{101\}$ facet with a surface energy of 0.44 J m^{-2} . The as-synthesized photocatalysts were then applied on the photoreduction of CO_2 (Eq. (21)) using a gas flow reactor and the reaction temperature and pressure were kept at ambient condition. Visible radiation, with wavelengths ranging between 400 and 625 nm was provided to the reaction system to obtain the following conversion:



The promoted electrons injected into the CB of TiO_2 are then conveyed through GR and, aiding charge transfer, eventually promoting the conversion of CO_2 into CH_4 .

Six different kinds of photocatalysts were employed on the photocatalytic reduction, namely (1) N- $\text{TiO}_2(001)$ -GR, (2) $\text{TiO}_2(001)$ -GR, (3) N- $\text{TiO}_2(101)$ -GR, (4) $\text{TiO}_2(101)$ -GR, (5) N- $\text{TiO}_2(001)$ and (6) $\text{TiO}_2(001)$. The GC analysis of the products indicated that in all the studied cases, only methane is formed and its yield reduces from $3.7\text{ }\mu\text{mol g}^{-1}$ for catalyst (1) through $0.34\text{ }\mu\text{mol g}^{-1}$ for catalyst (6). This is owing to the enhancement of the visible light absorbance (catalyst absorbance is in the following order: (1)>(2)>(3)>(4)>(5)>(6)) and the lower charge recombination rate (recombination rate is in the following order: (6)>(5)>(4)>(3)>(2)>(1)).

Accordingly, the authors proposed that the nitrogen doping and the sensitization effect of GR enhanced the absorbance of the photocatalysts in the visible region while low recombination rate was attributed to the high mobility of electron on GR as depicted in

Fig. 31. From this figure, it is also clear that GR provides a high surface area for the reduction to take place. The presence of GR has been found to increase the surface area of the composite by a factor of ca. 1.8.

More recently, Benedetti et al. [214] reported an enhanced photocatalytic activity of GR-based titania composites in the photoreduction of CO_2 into methane. The four kinds of catalytic systems used for the photoreduction were TiO_2 , TiO_2/CdS , $\text{TiO}_2/\text{CdS/Pt}$ and $\text{TiO}_2/\text{CdS/RGO/Pt}$. There was a 3-fold improvement in the yield of methane for the case of $\text{TiO}_2/\text{CdS/RGO/Pt}$ as compared to the TiO_2 . Again, the authors attributed the catalytic enhancement to a higher charge mobility coupled with the high surface area offered by GR for the homogeneous deposition of the Pt nanoparticles. The GR high surface area also made it possible for the TiO_2 and CdS nanoparticles to have a better interface contact.

Although GR composition enhances the activity of a semiconductor when compared to the bare semiconductor, the efficiency is further improved in the visible light region when single-walled CNT are incorporated into semiconductors due to their more strongly sensitizing effect. However, the GR composite performs better in the UV region than does the CNT semiconductor composite [225].

Lv et al. [216] described the photocatalytic reduction of CO_2 into methanol using GR modified $\text{NiO}_x\text{-Ta}_2\text{O}_5$ composite with water as the reductant. The TEM micrographs of the as-synthesized catalyst indicated the attachment of NiO_x to Ta_2O_5 and to the GR surface, as shown in Fig. 32, with GR offering a high surface area for the attachment, thereby giving an indication that the activated electron from the semi-conductor migrates either directly to the NiO_x or through the GR.

The photoactivity was found to improve by increasing in the quantity of the GR and the optimum weight percent of GR in the composite was found to be 1%, above which a continuous worsening of the performance was reported (Fig. 33), attributed by the authors to the screening effect of excessive carbon moiety on the light absorption ability of the composite catalyst. The yield improved by 3.4 folds when the optimum GR composition was used as compared to the bare catalyst.

Wang et al. [217] observed a similar result with 1.53 fold enhancement in the catalytic activity when GR was incorporated into Cu_2O photocatalyst utilized for a similar reaction. The authors similarly attributed the enhancement to increased catalytic sites and high electron mobility of GR. In order to study the effect of basic solvent on the photoreduction, Lv et al. [216] dissolved CO_2 in an aqueous solution of sodium hydroxide, observing a 3-fold increase in methanol yield. This was attributed to the higher solubility of CO_2 in basic rather than neutral H_2O , due to the acidic character of the former one. Not only did the NaOH increased the methanol yield, but it also increased the methanol selectivity by reducing the concentration of H^+ in the reaction medium. The reason for this behavior can be found in the competing photoreduction of H_2O to

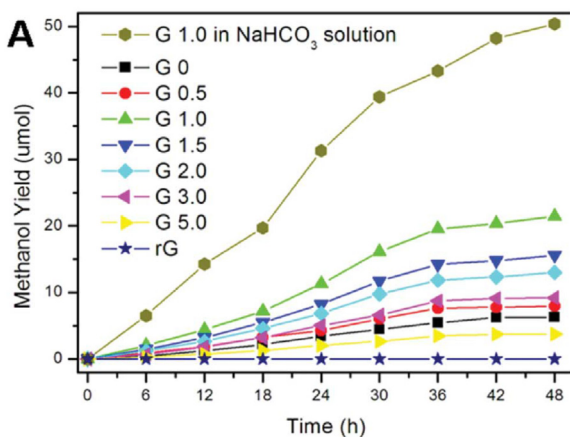


Fig. 33. Yield of methanol in the photoreduction of CO_2 dissolved in water and in NaOH using GR based $\text{NiO}_x\text{-Ta}_2\text{O}_5$ composite. Reprinted with permission from Ref. [216]. Copyright 2013 Royal Society of Chemistry.

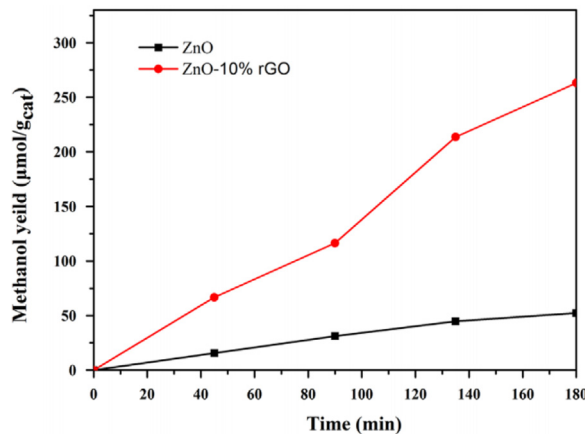


Fig. 34. Methanol yield based on ZnO and graphene based ZnO photocatalyst for the CO_2 photoreduction. Reprinted with permission from Ref. [228]. Copyright 2015 Elsevier.

H_2 , which is inhibited when the concentration of H^+ in solution is lower. A similar conclusion is drawn by Tseng et al. [218], but in that case the higher yield was mainly attributed to the scavenging of the holes by the OH^- , thereby further reducing the recombination rate of electrons and holes.

Methanol production was also enhanced by the doping of GR-based titania with tourmaline and making NaHCO_3 react upon irradiation with photons in the visible region ($\lambda > 400 \text{ nm}$) [226]. The yield of methanol (expressed in $\mu\text{mol h}^{-1} \text{g}^{-1}$) increased from 0.03 for TiO_2 , to 0.12 for 1% GR- TiO_2 , to 0.24 for 1% Tourmaline- TiO_2 , reaching the final value of 0.39 for 1% GR-1% Tourmaline- TiO_2 . The excellent performance was attributed to (i) high electron mobility on GR and electron acceptance by tourmaline, thereby reducing recombination, and to (ii) higher surface area thereby increasing the active sites.

The effect of GR composition in ZnO/RGO composite on the reduction of CO_2 to methanol, in two different studies, by Li et al. [227] and Zhang et al. [228] revealed a similar result. As expected, the yield of methanol was enhanced by the presence of RGO, which aided the transfer of electrons from the ZnO surface in order to reduce the recombination rate of the electrons and holes. Zhang et al. [228] made an advancement on the application of the as-prepared photocatalyst by obtaining the optimum GO composition of the composite to be 10% with a 5-fold improvement in the yield of methanol as compared to the case when RGO was absent (Fig. 34).

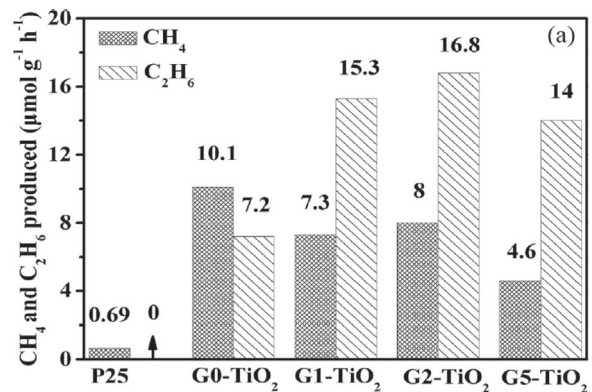


Fig. 35. Methane and ethane yield based on commercial P25 TiO_2 and series of GR based titania. Reprinted with permission from Ref. [219]. Copyright 2013 Wiley VCH.

Despite the ease of conversion of ethane into liquid fuel and into ethylene, which makes it more attractive than methane, very little work has been done on the reduction of CO_2 into ethane and only one, to the best of our knowledge, employed a GR-modified TiO_2 for this purpose. The GO was synthesized using modified Hummer's method, while hydrothermal conversion was used for the synthesis of the composite using the simultaneous reduction-hydrolysis technique as reported by Tu et al. [219]. A mixture of methane and ethane is formed as the reaction product, with an enhancement of selectivity to ethane achieved by an increase in GO loading. Although the optimum GR weight percent was found to be 2% to obtain the best yield, the selectivity for ethane was not very high (67.8%). However, for a composite with 5% GR, the ethane selectivity was found to increase up to 75% (but with a lower yield) as compared to 41% selectivity when no GR was used (Fig. 35). The modification of the catalyst for a simultaneous high selectivity and yield of ethane could be an interesting development to further studies.

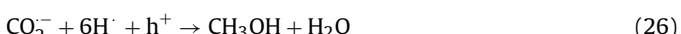
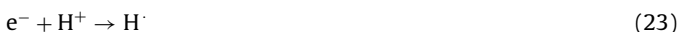
Tu et al. [220] produced a mixture of carbon monoxide (through a two-electron transfer process) and methane (involving a much more complex eight-electron transfer process) from hollow-sphere titania ($\text{Ti}_{0.91}\text{O}_2$)/GR composites (catalyst A) synthesized using the layer-by-layer method, comparing the performance with bare titania ($\text{Ti}_{0.91}\text{O}_2$) (catalyst B) and lastly with the benchmark Evonik P25 (TiO_2) (catalyst C). The efficiency and selectivity towards carbon monoxide were assessed by applying the three catalysts on the photoreduction reaction. While catalyst B led to a 100% selectivity towards methane, catalyst A was able to produce a quantifiable amount of carbon monoxide with a selectivity of 83% as compared to CO selectivity of 17% obtainable from the P25. The total yield was also found to increase by using the hollow-sphere titania/GR composite with $6 \mu\text{mol g}^{-1}$ in the case of catalyst C, $10 \mu\text{mol g}^{-1}$ for catalyst B and, finally, $45 \mu\text{mol g}^{-1}$ for catalyst A.

In some of the reported studies [62,118] the results were validated by using ^{13}C in the starting CO_2 , to rule out the possibility that the photodecomposition of graphene moieties or organic contaminants that could be adsorbed on the photocatalyst surface were the source of carbon in the reduced species. However, in other cases runs by using inert gases (Ar, N_2) instead of CO_2 were performed as blank experiments [218].

Owing to the special qualities of GR (high surface area, high mobility of electron), the comparison of the use of both Cu_2O and GR/ Cu_2O composite for the reduction of CO_2 into CO under visible light revealed that the latter is more efficient (by 10-fold). It was recently reported by An et al. [118] that the optimum GR content that produced the best catalytic activity is 0.5%.

The conversion of CO_2 into useful products is also performed by photoelectrocatalysis. For example, CO_2 has been shown to be

reduced into formic acid, formaldehyde, methanol and methane in the presence of various semiconductor powders by Inoue et al. [224]. Copper electrodes have shown to perform better in the synthesis of hydrocarbons including methane [229]. Li et al. [230] succeeded in synthesizing ethylene from an electrode made of copper nanoparticles on pyridinic-N rich GR in potassium bicarbonate electrolyte. Although they witnessed the synthesis of other products including methane, ethane and formate, a very high selectivity of 79% at -0.9 V (vs reversible hydrogen electrode) was seen for ethylene; 13-C tests were performed to confirm that the bicarbonate was the actual source of carbon in the reduced products. Hasan et al. [229] showed that, when a TiO_2/RGO composite was doped with copper and used in a photoelectrocatalytic setup, CO_2 was reduced to formic acid and methanol. Interestingly, longer reaction times resulted in increased methanol production, which was produced significantly at $189.06\text{ }\mu\text{mol h}^{-1}$. The reaction steps for the production of formic acid and methanol from CO_2 are shown below:



Under the influence of visible light and at an applied voltage of -0.61 V , the photo-oxidation of Cu/RGO/TiO_2 composite takes place releasing electrons and producing reactive holes. The initial oxidation reaction given by Eq. (22) is characterized by the reaction of these holes with water to form oxygen. Eqs. (23)–(24) show the initial reduction reaction where CO_2 and hydrogen radicals are generated which in subsequent reactions give rise to formic acid and methanol. It was recently shown that doping an RGO/TiO_2 composite with Ga leads to an increase in surface area for CO_2 absorption, thereby boosting the CO_2 conversion yield [76]. The main products of this photoreduction under visible light were methanol and formic acid.

It is quite noteworthy that pH has an effect on the product formed by photoreduction of CO_2 , as was demonstrated by Hasan et al. [231]. They observed that at a higher pH, a higher photocurrent response is seen. As a reason for this, they proposed that the recombination of electrons and holes might be mitigated, thereby increasing the global efficiency of the photoelectrocatalytic process.

On the basis of the literature results, GR has been demonstrated to improve the photoreduction of CO_2 by increasing the rate of the reaction [214,216,228] and the yield into specific products [219], even producing a reduced species that would have been otherwise absent [220]. All these improvements are mainly attributed to the ability of GR to convey multiple electrons to be used for the reduction of CO_2 . However, there is a trade-off among these improvements and the light absorption features of the composite when the GR content reaches a particular percentage, which varies from one composite to the other.

8. Conclusions and future outlook

The evolution of GR-inorganic semiconductor photocatalyst has been reviewed with emphasis on recent advancements in synthetic processes and photo(electro)catalytic applications, taking into account the continuously increasing understanding of the interaction mechanisms among the constituents of the composites. GR has remarkable properties, which significantly enhance

the photocatalytic activity of GR-based composites. However, high electron mobility and charge transfer of GR are greatly susceptible to changes in a GR-based composite photocatalyst affecting the behavior of GR at the interface with inorganic semiconductors. Therefore, other factors which include crystal phases, exposed crystal facets, particle size, dimensionality and morphology are also very important, as they all determine the photocatalytic performance of GR modified photocatalysts.

The current state of knowledge on interaction mechanisms at the GR-semiconductor interfaces emerging from this account highlights how electron-hole recombination rate is mitigated because of the long electron transport path and reduction of generated holes by available electron donor in the composites.

Synthetic methods are vital to foster the performance of GR-inorganic semiconductors. GR based composites are usually made either by growing nanoparticles of inorganic semiconductors on GO or RGO surfaces or, alternatively, by anchoring them on the oxygen sites through covalent and noncovalent interactions. The oxygen sites on GR precursors are essential: they act as nucleation points where size, morphology and degree of crystallinity of the composites can be tuned including strong interfacial contact. The dimensionality of the composites is also important to their performance: the higher the dimensionality of the semiconductor the higher the interfacial contact area and the better the electron charge transfer, resulting in an enhanced photocatalytic activity. 3D structures can also help to increase specific surface area, thus improving the photocatalytic performance by generating multidimensional electron transfer pathways and elongation of lifespan of electron-hole pair.

All the above mentioned properties make GR/RGO [232,233] an ideal candidate in photoelectrocatalyst composites. Creating a composite of GR and photocatalysts can give rise to groundbreaking applications such as degradation of harmful pollutants, hydrogen production and conversion of CO_2 . The applications stated are but a few among many others.

Detailed knowledge from characterization techniques reveal important features like pore size, crystal phases and facets, morphology, degree of crystallinity and eventually interaction mechanisms, is critical to optimizing the material properties in view of GR-semiconductor composites commercialization.

Concerning applications to water remediation, various parameters such as synthetic techniques, RGO loading, pH, and even light have substantial effect on the efficiency of the GR-semiconductor photocatalysts. Also, in hydrogen production through GR-modified composites based on TiO_2 and CdS as semiconductors of choice, the performance is greatly affected by the synthetic method, the nature of GR precursor, and the dimensionality of the resulting nanocomposites. The use of GR-semiconductor composites in organic synthesis is in its nascent stage. The major challenge faced in this area of application is lack of selectivity towards desired products due to the production of oxidizing radicals. Photoreduction of CO_2 is instead highly boosted by the high electron density in the GR moiety. In photoelectrocatalytic applications, it is advisable to leverage the electrical properties and large surface area of GR moieties.

To wrap up, all reviewed works showed the great potential of GR in GR-semiconductor composites to be used in photo(electro)catalytic applications. More work to unveil the full potential of GR-based composites should concentrate not only on leveraging the GR properties but rather focus on studying and optimizing the GR interface with semiconductors and their electronic compatibility, with the final aim to tune and boost the performance of resulting composite materials.

Acknowledgements

Abu Dhabi Education Council is gratefully acknowledged for 2015 Award for Research Excellence (EX2016-000005).

References

- [1] F. Meneguzzo, R. Ciriminna, L. Albanese, M. Pagliaro, The energy-population conundrum and its possible solution, *ArXiv. org* (2016) <http://arxiv.org/abs/1610.07298>.
- [2] Y.-H.P. Zhang, Next generation biorefineries will solve the food, biofuels, and environmental trilemma in the energy-food-water nexus, *Energy Sci. Eng.* 1 (2013) 27–41, <http://dx.doi.org/10.1002/ese3.2>.
- [3] M.B. Hocking, *Handbook of Chemical Technology and Pollution Control*, 3rd ed., Academic Press Inc., USA, 2005.
- [4] F. Parrino, G. Camera-Roda, V. Loddo, G. Palmisano, V. Augugliaro, Combination of ozonation and photocatalysis for purification of aqueous effluents containing formic acid as probe pollutant and bromide ion, *Water Res.* 50 (2014) 189–199, <http://dx.doi.org/10.1016/j.watres.2013.12.001>.
- [5] R. Molinari, M. Borgese, E. Drioli, L. Palmisano, M. Schiavello, Hybrid processes coupling photocatalysis and membranes for degradation of organic pollutants in water, *Catal. Today* 75 (2002) 77–85, [http://dx.doi.org/10.1016/S0920-5861\(02\)00047-0](http://dx.doi.org/10.1016/S0920-5861(02)00047-0).
- [6] C.H. Ao, S.C. Lee, Indoor air purification by photocatalyst TiO₂ immobilized on an activated carbon filter installed in an air cleaner, *Chem. Eng. Sci.* 60 (2005) 103–109, <http://dx.doi.org/10.1016/j.ces.2004.01.073>.
- [7] J. Zhao, X. Yang, Photocatalytic oxidation for indoor air purification: a literature review, *Build. Environ.* 38 (2003) 645–654, [http://dx.doi.org/10.1016/S0360-1323\(02\)00212-3](http://dx.doi.org/10.1016/S0360-1323(02)00212-3).
- [8] Y. Yamazaki, H. Takeda, O. Ishitani, Photocatalytic reduction of CO₂ using metal complexes, *J. Photochem. Photobiol. C Photochem. Rev.* 25 (2015) 106–137, <http://dx.doi.org/10.1016/j.jphotochemrev.2015.09.001>.
- [9] K. Li, X. An, K.H. Park, M. Khrasheh, J. Tang, A critical review of CO₂ photoconversion: catalysts and reactors, *Catal. Today* 224 (2014) 3–12, <http://dx.doi.org/10.1016/j.cattod.2013.12.006>.
- [10] M. Pelaez, N.T. Nolan, S.C. Pillai, M.K. Seery, P. Falaras, A.G. Kontos, P.S.M. Dunlop, J.W.J. Hamilton, J.A. Byrne, K. O'Shea, M.H. Entezari, D.D. Dionysiou, A review on the visible light active titanium dioxide photocatalysts for environmental applications, *Appl. Catal. B* 125 (2012) 331–349, <http://dx.doi.org/10.1016/j.apcatb.2012.05.036>.
- [11] Y. Ma, X. Wang, Y. Jia, X. Chen, H. Han, C. Li, Titanium dioxide-based nanomaterials for photocatalytic fuel generations, *Chem. Rev.* 114 (2014) 9987–10043, <http://dx.doi.org/10.1021/cr50008u>.
- [12] N.S. Chaudhari, S.S. Warule, S.A. Dhanmane, M.V. Kulkarni, M. Valant, B.B. Kale, Nanostructured N-doped TiO₂ marigold flowers for an efficient solar hydrogen production from H₂S, *Nanoscale* 5 (2013) 9383–9390, <http://dx.doi.org/10.1039/c3nr02975a>.
- [13] S.M. El-Sheikh, T.M. Khedr, A. Hakki, A.A. Ismail, W.A. Badawy, D.W. Bahnemann, Visible light activated carbon and nitrogen co-doped mesoporous TiO₂ as efficient photocatalyst for degradation of ibuprofen, *Sep. Purif. Technol.* 173 (2017) 258–268, <http://dx.doi.org/10.1016/j.seppur.2016.09.034>.
- [14] X.H. Lin, Y. Wu, J. Xiang, D. He, S.F.Y. Li, Elucidation of mesopore-organic molecules interactions in mesoporous TiO₂ photocatalysts to improve photocatalytic activity, *Appl. Catal. B* 199 (2016) 64–74, <http://dx.doi.org/10.1016/j.apcatb.2016.06.023>.
- [15] S. Yang, L. Gao, Photocatalytic activity of nitrogen doped rutile TiO₂ nanoparticles under visible light irradiation, *Mater. Res. Bull.* 43 (2008) 1872–1876, <http://dx.doi.org/10.1016/j.materresbull.2007.06.058>.
- [16] G. Kumordzi, G. Malekshoar, E.K. Yanful, A.K. Ray, Solar photocatalytic degradation of Zn²⁺ using graphene based TiO₂, *Sep. Purif. Technol.* 168 (2016) 294–301, <http://dx.doi.org/10.1016/j.seppur.2016.05.040>.
- [17] V. Augugliaro, M. Bellardita, V. Loddo, G. Palmisano, L. Palmisano, S. Yurdakal, Overview on oxidation mechanisms of organic compounds by TiO₂ in heterogeneous photocatalysis, *J. Photochem. Photobiol. C Photochem. Rev.* 13 (2012) 224–245, <http://dx.doi.org/10.1016/j.jphotochemrev.2012.04.003>.
- [18] Q. Zhang, K. Zhang, D. Xu, G. Yang, H. Huang, F. Nie, C. Liu, S. Yang, CuO nanostructures: synthesis, characterization, growth mechanisms, fundamental properties, and applications, *Prog. Mater. Sci.* 60 (2014) 208–337, <http://dx.doi.org/10.1016/j.pmatsci.2013.09.003>.
- [19] X. Liu, J. Chen, P. Liu, H. Zhang, G. Li, T. An, H. Zhao, Controlled growth of CuO/Cu₂O hollow microsphere composites as efficient visible-light-active photocatalysts, *Appl. Catal. A* 521 (2016) 34–41, <http://dx.doi.org/10.1016/j.apcata.2015.10.005>.
- [20] D. Sudha, P. Sivakumar, Review on the photocatalytic activity of various composite catalysts, *Chem. Eng. Process. Process Intensif.* 97 (2015) 112–133, <http://dx.doi.org/10.1016/j.cep.2015.08.006>.
- [21] M. Shekofteh-Gohari, A. Habibi-Yangjeh, Fabrication of novel magnetically separable visible-light-driven photocatalysts through photosensitization of Fe₃O₄/ZnO with CuWO₄, *J. Ind. Eng. Chem.* 44 (2016) 174–184, <http://dx.doi.org/10.1016/j.jiec.2016.08.028>.
- [22] W.-J. Liu, F.-X. Zeng, H. Jiang, X.-S. Zhang, W.-W. Li, Composite Fe₂O₃ and ZrO₂/Al₂O₃ photocatalyst: preparation, characterization, and studies on the photocatalytic activity and chemical stability, *Chem. Eng. J.* 180 (2012) 9–18, <http://dx.doi.org/10.1016/j.cej.2011.10.085>.
- [23] O. Mehrraj, B.M. Pirzada, N.A. Mir, M.Z. Khan, S. Sabir, A highly efficient visible-light-driven novel p-n junction Fe₂O₃/BiOI photocatalyst: surface decoration of BiOI nanosheets with Fe₂O₃ nanoparticles, *Appl. Surf. Sci.* 387 (2016) 642–651, <http://dx.doi.org/10.1016/j.apsusc.2016.06.166>.
- [24] Z. Wei, X. Wei, S. Wang, D. He, Preparation and visible-light photocatalytic activity of α -Fe₂O₃/ γ -Fe₂O₃ magnetic heterophase photocatalyst, *Mater. Lett.* 118 (2014) 107–110, <http://dx.doi.org/10.1016/j.matlet.2013.12.051>.
- [25] M. Pagliaro, R. Ciriminna, G. Palmisano, Silica-based hybrid coatings, *J. Mater. Chem.* 19 (2009) 3116–3126, <http://dx.doi.org/10.1039/b819615j>.
- [26] X. Pan, M.-Q. Yang, Z.-R. Tang, Y.-J. Xu, Noncovalently functionalized graphene-directed synthesis of ultralarge graphene-based TiO₂ nanosheet composites: tunable morphology and photocatalytic applications, *J. Phys. Chem. C* 118 (2014) 27325–27335, <http://dx.doi.org/10.1021/jp507173a>.
- [27] H.-H. Chun, J.Y. Lee, J.-H. Lee, W.-K. Jo, Enhanced photocatalysis of graphene and TiO₂ dual-coupled carbon nanofibers post-treated at various temperatures, *Ind. Eng. Chem. Res.* 55 (2016) 45–53, <http://dx.doi.org/10.1021/acs.iecr.5b02751>.
- [28] N. Liu, L. Fu, B. Dai, K. Yan, X. Liu, R. Zhao, Y. Zhang, Z. Liu, Universal segregation growth approach to wafer-size graphene from non-noble metals, *Nano Lett.* 11 (2011) 297–303, <http://dx.doi.org/10.1021/nl103962a>.
- [29] C. Garlisi, G. Scandura, J. Szlachetko, S. Ahmadi, J. Sa, G. Palmisano, E-beam evaporated TiO₂ and Cu-TiO₂ on glass: performance in the discoloration of methylene blue and 2-propanol oxidation, *Appl. Catal. A* 526 (2016) 191–199, <http://dx.doi.org/10.1016/j.apcata.2016.08.022>.
- [30] B.S. Tek, S. Yurdakal, L. Özcan, V. Augugliaro, V. Loddo, G. Palmisano, N-doped anatase/rutile photocatalysts for the synthesis of aromatic aldehydes under ultraviolet and solar Irradiation, *Sci. Adv. Mater.* 7 (2015) 2306–2319, <http://dx.doi.org/10.1166/sam.2015.2280>.
- [31] C. Guarisco, G. Palmisano, G. Calogero, R. Ciriminna, G. Di Marco, V. Loddo, M. Pagliaro, F. Parrino, Visible-light driven oxidation of gaseous aliphatic alcohols to the corresponding carbonyls via TiO₂ sensitized by a perylene derivative, *Environ. Sci. Pollut. Res.* 21 (2014) 11135–11141, <http://dx.doi.org/10.1007/s11356-014-2546-z>.
- [32] K.S. Novoselov, A.K. Geim, S.V. Morozov, D. Jiang, Y. Zhang, S.V. Dubonos, I.V. Grigorieva, A.A. Firsov, Electric field effect in atomically thin carbon films, *Science* 306 (2004) 666–669, <http://dx.doi.org/10.1126/science.1102896>.
- [33] (a) M.D. Stoller, S. Park, Y. Zhu, J. An, R.S. Ruoff, Graphene-based ultracapacitors, *Nano Lett.* 8 (2008) 3498–3502, <http://dx.doi.org/10.1021/nl802558y>; (b) M.J. Allen, V.C. Tung, R.B. Kaner, Honeycomb carbon: A review of graphene, *Chem. Rev.* 110 (2010) 132–145, <http://dx.doi.org/10.1021/cr900070d>.
- [34] C. Lee, X. Wei, J.W. Kysar, J. Hone, Measurement of the elastic properties and intrinsic strength of monolayer graphene, *Science* 321 (2008) 385–388, <http://dx.doi.org/10.1126/science.1157996>.
- [35] A.A. Balandin, S. Ghosh, W. Bao, I. Calizo, D. Teweldebrhan, F. Miao, C.N. Lau, Superior thermal conductivity of single-layer graphene, *Nano Lett.* 8 (2008) 902–907, <http://dx.doi.org/10.1021/nl0731872>.
- [36] L. Liu, M. Qing, Y. Wang, S. Chen, Defects in Graphene: generation, healing, and their effects on the properties of graphene: A Review, *J. Mater. Sci. Technol.* 31 (2015) 599–606, <http://dx.doi.org/10.1016/j.jjmst.2014.11.019>.
- [37] (a) M.-Q. Yang, N. Zhang, M. Pagliaro, Y.-J. Xu, Artificial photosynthesis over graphene-semiconductor composites. Are we getting better? *Chem. Soc. Rev.* 43 (2014) 8240–8254, <http://dx.doi.org/10.1039/c4cs00213j>; (b) K. Kakaei, One-pot electrochemical synthesis of graphene by the exfoliation of graphite powder in sodium dodecyl sulfate and its decoration with platinum nanoparticles for methanol oxidation, *Carbon* 51 (2013) 195–201.
- [38] R. Ciriminna, N. Zhang, M.-Q. Yang, F. Meneguzzo, Y.-J. Xu, M. Pagliaro, Commercialization of graphene-based technologies: a critical insight, *Chem. Commun.* 51 (2015) 7090–7095, <http://dx.doi.org/10.1039/C5CC01411E>.
- [39] A. Ambrosi, C.K. Chua, A. Bonanni, M. Pumera, Electrochemistry of graphene and related materials, *Chem. Rev.* 114 (2014) 7150–7188, <http://dx.doi.org/10.1021/cr500023c>.
- [40] K. Ullah, A. Ullah, A. Aldalbahi, J. Chung, W.-C. Oh, Enhanced visible light photocatalytic activity and hydrogen evolution through novel heterostructure AgI–TiO₂ nanocomposites, *J. Mol. Catal. A Chem.* 410 (2015) 242–252, <http://dx.doi.org/10.1016/j.molcata.2015.09.024>.
- [41] R. Muñoz, C. Gómez-Aleixandre, Review of CVD synthesis of graphene, *Chem. Vap. Depos.* 19 (2013) 297–322, <http://dx.doi.org/10.1002/cvde.201300051>.
- [42] W.S. Hummers, R.E. Offeman, Preparation of graphitic oxide, *J. Am. Chem. Soc.* 80 (1958) 1339, <http://dx.doi.org/10.1021/ja01539a017>.
- [43] D.C. Marcano, D.V. Kosynkin, J.M. Berlin, A. Sinitskii, Z. Sun, A. Slesarev, L.B. Alemany, W. Lu, J.M. Tour, Improved synthesis of graphene oxide, *ACS Nano* 4 (2010) 4806–4814, <http://dx.doi.org/10.1021/nn1006368>.
- [44] M.J. McAllister, J.-L. Li, D.H. Adamson, H.C. Schniepp, A.A. Abdala, J. Liu, M. Herrera-Alonso, D.L. Milius, R. Car, R.K. Prud'homme, I.A. Aksay, Single sheet functionalized graphene by oxidation and thermal expansion of graphite, *Chem. Mater.* 19 (2007) 4396–4404, <http://dx.doi.org/10.1021/cm0630800>.
- [45] M. Acik, Y.J. Chabal, A review on thermal exfoliation of graphene oxide, *J. Mater. Sci. Res.* 2 (2013) 101–112, <http://dx.doi.org/10.5539/jmsr.v2n1p101>.

- [46] V.C. Tung, M.J. Allen, Y. Yang, R.B. Kaner, High-throughput solution processing of large-scale graphene, *Nat. Nanotechnol.* 4 (2009) 25–29, <http://dx.doi.org/10.1038/nano.2008.329>.
- [47] (a) C. Hu, T. Lu, F. Chen, R. Zhang, A brief review of graphene–metal oxide composites synthesis and applications in photocatalysis, *J. Chin. Adv. Mater. Soc.* 1 (2013) 21–39, <http://dx.doi.org/10.1080/22243682.2013.771917>; (b) X. Men, H. Chen, K. Chang, X. Fang, C. Wu, W. Qin, S. Yin, Three-dimensional free-standing ZnO/graphene composite foam for photocurrent generation and photocatalytic activity, *Appl. Catal. B* 187 (2016) 367–374, <http://dx.doi.org/10.1016/j.apcatb.2016.01.052>.
- [48] K.P. Loh, Q. Bao, G. Eda, M. Chhowalla, Graphene oxide as a chemically tunable platform for optical applications, *Nat. Chem.* 2 (2010) 1015–1024, <http://dx.doi.org/10.1038/nchem.907>.
- [49] Y. Qiu, F. Guo, R. Hurt, I. Külaots, Explosive thermal reduction of graphene oxide-based materials: mechanism and safety implications, *Carbon* 72 (2014) 215–223, <http://dx.doi.org/10.1016/j.carbon.2014.02.005>.
- [50] J. Song, X. Wang, C.-T. Chang, Preparation and characterization of graphene oxide, *J. Nanomater.* 2014 (2014) 1–6, <http://dx.doi.org/10.1155/2014/276143>.
- [51] X. An, J.C. Yu, Graphene-based photocatalytic composites, *RSC Adv.* 1 (2011) 1426–1434, <http://dx.doi.org/10.1039/c1ra00382h>.
- [52] N. Zhang, Y. Zhang, Y.-J. Xu, Recent progress on graphene-based photocatalysts: current status and future perspectives, *Nanoscale* 4 (2012) 5792–5813, <http://dx.doi.org/10.1039/c2nr31480k>.
- [53] G. Williams, B. Seger, P.V. Kamat, TiO₂-graphene nanocomposites. UV-assisted photocatalytic reduction of graphene oxide, *ACS Nano.* 2 (2008) 1487–1491, <http://dx.doi.org/10.1021/nn800251f>.
- [54] C. Xu, J. Zhu, R. Yuan, X. Fu, More effective use of graphene in photocatalysis by conformal attachment of small sheets to TiO₂ spheres, *Carbon* 96 (2016) 394–402, <http://dx.doi.org/10.1016/j.carbon.2015.09.088>.
- [55] A.N. Fouda, E.S.M. Durai, Self-assembled graphene oxide on a photo-catalytic active transparent conducting oxide, *Mater. Des.* 90 (2016) 284–290, <http://dx.doi.org/10.1016/j.matdes.2015.10.139>.
- [56] C. Liu, L. Zhang, R. Liu, Z. Gao, X. Yang, Z. Tu, F. Yang, Z. Ye, L. Cui, C. Xu, Y. Li, Hydrothermal synthesis of N-doped TiO₂ nanowires and N-doped graphene heterostructures with enhanced photocatalytic properties, *J. Alloys Compd.* 656 (2016) 24–32, <http://dx.doi.org/10.1016/j.jallcom.2015.09.211>.
- [57] M. Faraji, N. Mohaghegh, Ag/TiO₂-nanotube plates coated with reduced graphene oxide as photocatalysts, *Surf. Coat. Technol.* 288 (2016) 144–150, <http://dx.doi.org/10.1016/j.surfcoat.2016.01.022>.
- [58] N. Zhang, Y.-J. Xu, The endeavour to advance graphene–semiconductor composite-based photocatalysis, *CrystEngComm* 18 (2016) 24–37, <http://dx.doi.org/10.1039/c5ce01712b>.
- [59] S. Cao, T. Liu, Y. Tsang, C. Chen, Role of hydroxylation modification on the structure and property of reduced graphene oxide/TiO₂ hybrids, *Appl. Surf. Sci.* 382 (2016) 225–238, <http://dx.doi.org/10.1016/j.apsusc.2016.04.138>.
- [60] N.M. Julkapli, S. Bagheri, Graphene supported heterogeneous catalysts: an overview, *Int. J. Hydrogen Energy* 40 (2015) 948–979, <http://dx.doi.org/10.1016/j.ijhydene.2014.10.129>.
- [61] T.-F. Yeh, J. Cihlář, C.-Y. Chang, C. Cheng, H. Teng, Roles of graphene oxide in photocatalytic water splitting, *Mater. Today* 16 (2013) 78–84, <http://dx.doi.org/10.1016/j.mattod.2013.03.006>.
- [62] J. Low, J. Yu, W. Ho, Graphene-based photocatalysts for CO₂ reduction to solar fuel, *J. Phys. Chem. Lett.* 6 (2015) 4244–4251, <http://dx.doi.org/10.1012/acs.jpcllett.5b01610>.
- [63] Y. Xu, Y. Mo, J. Tian, P. Wang, H. Yu, J. Yu, The synergistic effect of graphitic N and pyrrolic N for the enhanced photocatalytic performance of nitrogen-doped graphene/TiO₂ nanocomposites, *Appl. Catal. B* 181 (2016) 810–817, <http://dx.doi.org/10.1016/j.apcatb.2015.08.049>.
- [64] J.T.-W. Wang, J.M. Ball, E.M. Barea, A. Abate, J.A. Alexander-Webber, J. Huang, M. Saliba, I. Mora-Sero, J. Bisquert, H.J. Snaith, R.J. Nicholas, Low-temperature processed electron collection layers of graphene/TiO₂ nanocomposites in thin film perovskite solar cells, *Nano Lett.* 14 (2014) 724–730, <http://dx.doi.org/10.1021/nl403997a>.
- [65] B.Y.S. Chang, M.S. Mahmood, A. Pandikumar, N.M. Huang, H.N. Lim, A.R. Marlinda, N. Yusoff, W.S. Chiu, Hydrothermally prepared graphene-titania nanocomposite for the solar photocatalytic degradation of methylene blue, *Desalin. Water Treat.* 57 (2015) 238–245, <http://dx.doi.org/10.1080/19443994.2015.1006816>.
- [66] N. Armaroli, V. Balzani, Solar electricity and solar fuels: status and perspectives in the context of the energy transition, *Chem. Eur. J.* 22 (2016) 32–57, <http://dx.doi.org/10.1002/chem.201503580>.
- [67] C.S.K. Lin, R. Luque, C. Webb, *Building a Biobased Economy a Global Perspective*, Taylor & Francis, Florida, 2014.
- [68] (a) W. Tu, Y. Zhou, Z. Zou, Versatile graphene-promoting photocatalytic performance of semiconductors: basic principles, synthesis, solar energy conversion, and environmental applications, *Adv. Funct. Mater.* 23 (2013) 4996–5008, <http://dx.doi.org/10.1002/adfm.201203547>; (b) Z. Jin, Q. Zhang, S. Yuan, T. Ohno, Synthesis high specific surface area nanotube g-C₃N₄ with two-step condensation treatment of melamine to enhance photocatalysis properties, *RSC Adv.* 5 (2015) 4026–4029, <http://dx.doi.org/10.1039/c4ra13355b>.
- [69] R. Long, N.J. English, O.V. Prezhdo, Photo-induced charge separation across the graphene–TiO₂ interface is faster than energy losses: a time-domain ab initio analysis, *J. Am. Chem. Soc.* 134 (2012) 14238–14248, <http://dx.doi.org/10.1021/ja3063953>.
- [70] S. Chowdhury, R. Balasubramanian, Graphene/semiconductor nanocomposites (GSNs) for heterogeneous photocatalytic decolorization of wastewaters contaminated with synthetic dyes: a review, *Appl. Catal. B* 160 (2014) 307–324, <http://dx.doi.org/10.1016/j.apcatb.2014.05.035>.
- [71] A.M. Jastrzebska, J. Karcz, R. Letmanowski, D. Zabost, E. Ciecielska, M. Siekierski, A. Olszyna, Synthesis of RGO/TiO₂ nanocomposite flakes and characterization of their unique electrostatic properties using zeta potential measurements, *J. Alloys Compd.* 679 (2016) 470–484, <http://dx.doi.org/10.1016/j.jallcom.2016.04.043>.
- [72] S. Liu, H. Sun, S. Liu, S. Wang, Graphene facilitated visible light photodegradation of methylene blue over titanium dioxide photocatalysts, *Chem. Eng. J.* 214 (2013) 298–303, <http://dx.doi.org/10.1016/j.cej.2012.10.058>.
- [73] A. Sharma, B.-K. Lee, Rapid photo-degradation of 2-chlorophenol under visible light irradiation using cobalt oxide-loaded TiO₂/reduced graphene oxide nanocomposite from aqueous media, *J. Environ. Manage.* 165 (2016) 1–10, <http://dx.doi.org/10.1016/j.jenvman.2015.09.013>.
- [74] J. Li, Q. Zhang, L. Zeng, D. He, Synthesis, characterization and photocatalytic study of graphene oxide and cerium co-doped in TiO₂, *Appl. Phys. A* 122 (2016) 51, <http://dx.doi.org/10.1007/s00339-015-9580-7>.
- [75] G. Dai, X. Wang, S. Liu, Y. Liang, K. Liu, Template-free fabrication of hierarchical macro-/mesoporous N-doped TiO₂/graphene oxide composites with enhanced visible-light photocatalytic activity, *J. Chin. Chem. Soc.* 62 (2015) 170–176, <http://dx.doi.org/10.1002/jccs.201400247>.
- [76] M.R. Hasan, S.B. Abd Hamid, W.J. Basirun, Z.Z. Chowdhury, A.E. Kandjani, S.K. Bhargava, Ga doped RGO–TiO₂ composite on an ITO surface electrode for investigation of photoelectrocatalytic activity under visible light irradiation, *New J. Chem.* 39 (2015) 369–376, <http://dx.doi.org/10.1039/c4nj01048e>.
- [77] Y. Haldorai, A. Rengaraj, C.H. Kwak, Y.S. Huh, Y.-K. Han, Fabrication of nano TiO₂/graphene composite: reusable photocatalyst for hydrogen production, degradation of organic and inorganic pollutants, *Synth. Met.* 198 (2014) 10–18, <http://dx.doi.org/10.1016/j.synthmet.2014.09.034>.
- [78] A.P. Bhirud, S.D. Sathaye, R.P. Waichal, J.D. Ambekar, C.-J. Park, B.B. Kale, In-situ preparation of N-TiO₂/graphene nanocomposite and its enhanced photocatalytic hydrogen production by H₂S splitting under solar light, *Nanoscale* 7 (2015) 5023–5034, <http://dx.doi.org/10.1039/c4nr06435f>.
- [79] H.-H. Chun, W.-K. Jo, Adsorption and photocatalysis of 2-ethyl-1-hexanol over graphene oxide–TiO₂ hybrids post-treated under various thermal conditions, *Appl. Catal. B* 180 (2016) 740–750, <http://dx.doi.org/10.1016/j.apcatb.2015.07.021>.
- [80] J. Wei, S. Xue, P. Xie, R. Zou, Synthesis and photocatalytic properties of different SnO₂ microspheres on graphene oxide sheets, *Appl. Surf. Sci.* 376 (2016) 172–179, <http://dx.doi.org/10.1016/j.apsusc.2016.03.058>.
- [81] D.K. Padhi, G.K. Pradhan, K.M. Parida, S.K. Singh, Facile fabrication of Gd(OH)₃ nanorod/RGO composite: synthesis, characterisation and photocatalytic reduction of Cr(VI), *Chem. Eng. J.* 255 (2014) 78–88, <http://dx.doi.org/10.1016/j.cej.2014.06.039>.
- [82] Y. Wang, Z. Mo, P. Zhang, C. Zhang, L. Han, R. Guo, H. Gou, X. Wei, R. Hu, Synthesis of flower-like TiO₂ microsphere/graphene composite for removal of organic dye from water, *Mater. Des.* 99 (2016) 378–388, <http://dx.doi.org/10.1016/j.matdes.2016.03.066>.
- [83] A. Trapalis, N. Todorova, T. Giannakopoulou, N. Boukos, T. Speliotis, D. Dimotikali, J. Yu, TiO₂/graphene composite photocatalysts for NOx removal: a comparison of surfactant-stabilized graphene and reduced graphene oxide, *Appl. Catal. B* 180 (2016) 637–647, <http://dx.doi.org/10.1016/j.apcatb.2015.07.009>.
- [84] M.S. Sher Shah, K. Zhang, A.R. Park, K.S. Kim, N.-G. Park, J.H. Park, P.J. Yoo, Single-step solvothermal synthesis of mesoporous Ag–TiO₂–reduced graphene oxide ternary composites with enhanced photocatalytic activity, *Nanoscale* 5 (2013) 5093–5101, <http://dx.doi.org/10.1039/c3nr0057h>.
- [85] L. Liu, Z. Liu, A. Liu, X. Gu, C. Ge, F. Gao, L. Dong, Engineering the TiO₂–graphene interface to enhance photocatalytic H₂ production, *ChemSusChem* 7 (2014) 618–626, <http://dx.doi.org/10.1002/cssc.201300941>.
- [86] S. Thangavel, K. Krishnamoorthy, S.-J. Kim, G. Venugopal, Designing ZnS decorated reduced graphene-oxide nanohybrid via microwave route and their application in photocatalysis, *J. Alloys Compd.* 683 (2016) 456–462, <http://dx.doi.org/10.1016/j.jallcom.2016.05.089>.
- [87] W. Xiao, Y. Zhang, L. Tian, H. Liu, B. Liu, Y. Pu, Facile synthesis of reduced graphene oxide/titania composite hollow microspheres based on sonication-assisted interfacial self-assembly of tiny graphene oxide sheets and the photocatalytic property, *J. Alloys Compd.* 665 (2016) 21–30, <http://dx.doi.org/10.1016/j.jallcom.2016.01.047>.
- [88] W.-N. Wang, Y. Jiang, J.D. Fortner, P. Biswas, Nanostructured graphene–titanium dioxide composites synthesized by a single-step aerosol process for photoreduction of carbon dioxide, *Environ. Eng. Sci.* 31 (2014) 428–434, <http://dx.doi.org/10.1089/ees.2013.0473>.
- [89] B. Luo, G. Liu, L. Wang, Recent advances in 2D materials for photocatalysis, *Nanoscale* 8 (2016) 6904–6920, <http://dx.doi.org/10.1039/c6nr00546b>.
- [90] X. Luan, M.T. Gutierrez Wing, Y. Wang, Enhanced photocatalytic activity of graphene oxide/titania nanosheets composites for methylene blue degradation, *Mater. Sci. Semicond. Process.* 30 (2015) 592–598, <http://dx.doi.org/10.1016/j.mssp.2014.10.032>.
- [91] R. Bera, S. Kundu, A. Patra, 2D hybrid nanostructure of reduced graphene oxide–CdS nanosheet for enhanced photocatalysis, *ACS Appl. Mater.*

- Interfaces 7 (2015) 13251–13259, <http://dx.doi.org/10.1021/acsmi.5b03800>.
- [92] M. Zeng, W.-L. Wang, X.-D. Bai, Preparing three-dimensional graphene architectures: review of recent developments, *Chin. Phys. B* 22 (98105) (2013), <http://dx.doi.org/10.1088/1674-1056/22/9/098105>.
- [93] X. Xu, F. Ming, J. Hong, Y. Xie, Z. Wang, Three-dimensional porous aerogel constructed by Bi_2WO_6 nanosheets and graphene with excellent visible-light photocatalytic performance, *Mater. Lett.* 179 (2016) 52–56, <http://dx.doi.org/10.1016/j.matlet.2016.05.031>.
- [94] R. Fang, Y. Liang, X. Ge, M. Du, S. Li, T. Li, Z. Li, Preparation and photocatalytic degradation activity of TiO_2/rGO /polymer composites, *Colloid. Polym. Sci.* 293 (2015) 1151–1157, <http://dx.doi.org/10.1007/s00396-015-3507-x>.
- [95] R. Fang, X. Ge, M. Du, Z. Li, C. Yang, B. Fang, Y. Liang, Preparation of silver/graphene/polymer hybrid microspheres and the study of photocatalytic degradation, *Colloid. Polym. Sci.* 292 (2014) 985–990, <http://dx.doi.org/10.1007/s00396-013-3148-x>.
- [96] B. Weng, Y.-J. Xu, What if the electrical conductivity of graphene is significantly deteriorated for the graphene–semiconductor composite-based photocatalysis? *ACS Appl. Mater. Interfaces* 7 (2015) 27948–27958, <http://dx.doi.org/10.1021/acsmi.5b10298>.
- [97] P. Magalhães, J. Ângelo, V.M. Sousa, O.C. Nunes, L. Andrade, A. Mendes, Synthesis and assessment of a graphene-based composite photocatalyst, *Biochem. Eng. J.* 104 (2015) 20–26, <http://dx.doi.org/10.1016/j.bej.2015.05.016>.
- [98] R. Leary, A. Westwood, Carbonaceous nanomaterials for the enhancement of TiO_2 photocatalysis, *Carbon* 49 (2011) 741–772, <http://dx.doi.org/10.1016/j.carbon.2010.10.010>.
- [99] H. Zhang, X. Lv, Y. Li, Y. Wang, J. Li, P25-graphene composite as a high performance photocatalyst, *ACS Nano* 4 (2010) 380–386, <http://dx.doi.org/10.1021/nm901221k>.
- [100] R. Krol, Photoelectrochemical hydrogen production, in: R. Krol, M. Gratzel (Eds.), *Princ. Photoelectrochem. Cells*, Springer, US, 2012, pp. 13–67, http://dx.doi.org/10.1007/978-1-4614-1380-6_2.
- [101] H. Wang, T. Maiyalagan, X. Wang, Review on recent progress in nitrogen-doped graphene: synthesis, characterization, and its potential applications, *ACS Catal.* 2 (2012) 781–794, <http://dx.doi.org/10.1021/cs200652y>.
- [102] S. Sandoval, N. Kumar, A. Sundaresan, C.N.R. Rao, A. Fuertes, G. Tobias, Enhanced thermal oxidation stability of reduced graphene oxide by nitrogen doping, *Chem. Eur. J.* 20 (2014) 11999–12003, <http://dx.doi.org/10.1002/chem.201403833>.
- [103] M. Latorre-Sánchez, A. Primo, H. García, P-doped graphene obtained by pyrolysis of modified alginate as a photocatalyst for hydrogen generation from water-methanol mixtures, *Angew. Chem. Int. Ed.* 52 (2013) 11813–11816, <http://dx.doi.org/10.1002/anie.201304505>.
- [104] Y. Zhang, N. Zhang, Z.-R. Tang, Y.-J. Xu, Graphene transforms wide band gap ZnS to a visible light photocatalyst. The new role of graphene as a macromolecular photosensitizer, *ACS Nano* 6 (2012) 9777–9789, <http://dx.doi.org/10.1021/nn304154s>.
- [105] A.M. Abdelkader, C. Vallés, A.J. Cooper, I.A. Kinloch, R.A.W. Dryfe, Alkali reduction of graphene oxide in molten halide salts: production of corrugated graphene derivatives for high-performance supercapacitors, *ACS Nano* 8 (2014) 11225–11233, <http://dx.doi.org/10.1021/nn505700x>.
- [106] S. Abdolhosseinzadeh, H. Asgharzadeh, H. Seop Kim, Fast and fully-scalable synthesis of reduced graphene oxide, *Sci. Rep.* 5 (10160) (2015), <http://dx.doi.org/10.1038/srep10160>.
- [107] S. Drewniak, R. Muzyka, A. Stolarczyk, T. Pustelnik, M. Kotyczka-Morańska, M. Setkiewicz, Studies of reduced graphene oxide and graphite oxide in the aspect of their possible application in gas sensors, *Sensors* 16 (2016), <http://dx.doi.org/10.3390/s16010103>.
- [108] J. Hu, H. Li, Q. Wu, Y. Zhao, Q. Jiao, Synthesis of TiO_2 nanowire/reduced graphene oxide nanocomposites and their photocatalytic performances, *Chem. Eng. J.* 263 (2015) 144–150, <http://dx.doi.org/10.1016/j.cej.2014.11.007>.
- [109] I. Roy, G. Sarkar, S. Mondal, D. Rana, A. Bhattacharyya, N.R. Saha, A. Adhikari, D. Khastgir, S. Chattopadhyay, D. Chattopadhyay, Synthesis and characterization of graphene from waste dry cell battery for electronic applications, *RSC Adv.* 6 (2016) 10557–10564, <http://dx.doi.org/10.1039/c5ra21112c>.
- [110] H. Adamu, P. Dubey, J.A. Anderson, Probing the role of thermally reduced graphene oxide in enhancing performance of TiO_2 in photocatalytic phenol removal from aqueous environments, *Chem. Eng. J.* 284 (2016) 380–388, <http://dx.doi.org/10.1016/j.cej.2015.08.147>.
- [111] N.R. Khalid, E. Ahmed, Z. Hong, Y. Zhang, M. Ahmad, Nitrogen doped TiO_2 nanoparticles decorated on graphene sheets for photocatalysis applications, *Curr. Appl. Phys.* 12 (2012) 1485–1492, <http://dx.doi.org/10.1016/j.cap.2012.04.019>.
- [112] Y. Chen, G. Tian, G. Mao, R. Li, Y. Xiao, T. Han, Facile synthesis of well-dispersed Bi_2S_3 nanoparticles on reduced graphene oxide and enhanced photocatalytic activity, *Appl. Surf. Sci.* 378 (2016) 231–238, <http://dx.doi.org/10.1016/j.apsusc.2016.03.194>.
- [113] (a) K. Kondo, N. Murakami, C. Ye, T. Tsubota, T. Ohno, Development of highly efficient sulfur-doped TiO_2 photocatalysts hybridized with graphitic carbon nitride, *Appl. Catal. B* 142 (2013) 362–367, <http://dx.doi.org/10.1016/j.apcatb.2013.05.042>; (b) Z. Jin, N. Murakami, T. Tsubota, T. Ohno, Complete oxidation of acetraldehyde over composite photocatalyst of graphitic carbon nitride and tungsten (VI) oxide under visible-light irradiation, *Appl. Catal. B* 150–151 (2014) 479–485, <http://dx.doi.org/10.1016/j.apcatb.2013.05.042>; (c) N. Sagara, S. Kamimura, T. Tsubota, T. Ohno, Photoelectrochemical CO_2 reduction by a p-type boron-doped $\text{g-C}_3\text{N}_4$ electrode under visible light, *Appl. Catal. B* 192 (2016) 193–198, <http://dx.doi.org/10.1016/j.apcatb.2016.03.055>.
- [114] H. Gao, W. Chen, J. Yuan, Z. Jiang, G. Hu, W. Shangguan, Y. Sun, J. Su, Controllable $\text{O}_2\text{-}$ oxidation graphene in TiO_2 /graphene composite and its effect on photocatalytic hydrogen evolution, *Int. J. Hydrogen Energy* 38 (2013) 13110–13116, <http://dx.doi.org/10.1016/j.ijhydene.2013.01.155>.
- [115] F. Wang, M. Zheng, C. Zhu, B. Zhang, W. Chen, L. Ma, W. Shen, Visible light photocatalytic H_2 -production activity of wide band gap ZnS nanoparticles based on the photosensitization of graphene, *Nanotechnology* 26 (2015) 345–402, <http://dx.doi.org/10.1088/0957-4484/26/34/345402>.
- [116] M.E. Khan, M.M. Khan, M.H. Cho, Biogenic synthesis of a Ag -graphene nanocomposite with efficient photocatalytic degradation, electrical conductivity and photoelectrochemical performance, *New J. Chem.* 39 (2015) 8121–8129, <http://dx.doi.org/10.1039/c5nj01320h>.
- [117] J. Chen, J. Shi, X. Wang, H. Cui, M. Fu, Recent progress in the preparation and application of semiconductor/graphene composite photocatalysts, *Chin. J. Catal.* 34 (2013) 621–640, [http://dx.doi.org/10.1016/S1872-2067\(12\)60530-0](http://dx.doi.org/10.1016/S1872-2067(12)60530-0).
- [118] X. An, K. Li, J. Tang, Cu_2O /reduced graphene oxide composites for the photocatalytic conversion of CO_2 , *ChemSusChem* 7 (2014) 1086–1093, <http://dx.doi.org/10.1002/cssc.201301194>.
- [119] Z. Ren, E. Kim, S.W. Pattinson, K.S. Subrahmanyam, C.N.R. Rao, A.K. Cheetham, D. Eder, Hybridizing photoactive zeolites with graphene: a powerful strategy towards superior photocatalytic properties, *Chem. Sci.* 3 (2012) 209–216, <http://dx.doi.org/10.1039/c1sc00511a>.
- [120] M. Minella, F. Sordello, C. Minero, Photocatalytic process in TiO_2 /graphene hybrid materials. Evidence of charge separation by electron transfer from reduced graphene oxide to TiO_2 , *Catal. Today* 281 (2017) 29–37, <http://dx.doi.org/10.1016/j.cattod.2016.03.040>.
- [121] P. Wang, J. Wang, X. Wang, H. Yu, J. Yu, M. Lei, Y. Wang, One-step synthesis of easy-recycling TiO_2 -rGO nanocomposite photocatalysts with enhanced photocatalytic activity, *Appl. Catal. B* 132 (2013) 452–459, <http://dx.doi.org/10.1016/j.apcatb.2012.12.009>.
- [122] (a) B. Ohtani, Revisiting the fundamental physical chemistry in heterogeneous photocatalysis: its thermodynamics and kinetics, *Phys. Chem. Chem. Phys.* 16 (2014) 1788–1797, <http://dx.doi.org/10.1039/C3CP53653j>; (b) B. Ohtani, Revisiting the original works related to titania photocatalysis: a review of papers in the early stage of photocatalysis studies, *Electrochemistry* 82 (2014) 414–425, <http://dx.doi.org/10.5796/electrochemistry.82.414>.
- [123] L.M. Pastrana-Martínez, S. Morales-Torres, V. Likodimos, J.L. Figueiredo, J.L. Faria, P. Falaras, A.M.T. Silva, Advanced nanostructured photocatalysts based on reduced graphene oxide– TiO_2 composites for degradation of diphenylhydramine pharmaceutical and methyl orange dye, *Appl. Catal. B* 123–124 (2012) 241–256, <http://dx.doi.org/10.1016/j.apcatb.2012.04.045>.
- [124] D.S. Bhatkhande, V.G. Pangarkar, A.A.C.M. Beenackers, Photocatalytic degradation for environmental applications – a review, *J. Chem. Technol. Biotechnol.* 77 (2002) 102–116, <http://dx.doi.org/10.1002/jctb.532>.
- [125] L. Wang, M. Wen, W. Wang, N. Momuiniun, Z. Wang, S. Li, Photocatalytic degradation of organic pollutants using rGO supported TiO_2 – CdS composite under visible light irradiation, *J. Alloys Compd.* 683 (2016) 318–328, <http://dx.doi.org/10.1016/j.jallcom.2016.05.111>.
- [126] F. Perreault, A. Fonseca de Faria, M. Elimelech, Environmental applications of graphene-based nanomaterials, *Chem. Soc. Rev.* 44 (2015) 5861–5896, <http://dx.doi.org/10.1039/c5cc00021a>.
- [127] C.-C. Wang, X.-D. Du, J. Li, X.-X. Guo, P. Wang, J. Zhang, Photocatalytic $\text{Cr}(\text{VI})$ reduction in metal–organic frameworks: a mini-review, *Appl. Catal. B* 193 (2016) 198–216, <http://dx.doi.org/10.1016/j.apcatb.2016.04.030>.
- [128] Q. Xiang, J. Yu, M. Jaroniec, Graphene-based semiconductor photocatalysts, *Chem. Soc. Rev.* 41 (2012) 782–796, <http://dx.doi.org/10.1039/c1cs15172j>.
- [129] L.M. Pastrana-Martínez, S. Morales-Torres, V. Likodimos, P. Falaras, J.L. Figueiredo, J.L. Faria, A.M.T. Silva, Role of oxygen functionalities on the synthesis of photocatalytically active graphene– TiO_2 composites, *Appl. Catal. B* 158–159 (2014) 329–340, <http://dx.doi.org/10.1016/j.apcatb.2014.04.024>.
- [130] (a) X. Yan, T. Ohno, K. Nishijima, R. Abe, B. Ohtani, Is methylene blue an appropriate substrate for a photocatalytic activity test? A study with visible-light responsive titania, *Chem. Phys. Lett.* 429 (2006) 606–610, <http://dx.doi.org/10.1016/j.cplett.2006.08.081>; (b) B. Ohtani, Photocatalysis A to Z—What we know and what we do not know in a scientific sense, *J. Photochem. Photobiol. C Photochem. Rev.* 11 (2010) 157–178.
- [131] A. Ahmad, S.H. Mohd-Setapar, C.S. Chuong, A. Khatoon, W.A. Wani, R. Kumar, M. Rafatullah, Recent advances in new generation dye removal technologies: novel search for approaches to reprocess wastewater, *RSC Adv.* 5 (2015) 30801–30818, <http://dx.doi.org/10.1039/C4RA16959j>.
- [132] M.E. Khan, M.M. Khan, M.H. Cho, CdS -graphene nanocomposite for efficient visible-light-driven photocatalytic and photoelectrochemical applications, *J. Colloid Interface Sci.* 482 (2016) 221–232, <http://dx.doi.org/10.1016/j.jcis.2016.07.070>.

- [133] M. Faraji, N. Mohaghegh, Ag/TiO₂-nanotube plates coated with reduced graphene oxide as photocatalysts, *Surf. Coat. Technol.* 288 (2016) 144–150, <http://dx.doi.org/10.1016/j.surfcoat.2016.01.022>.
- [134] K. Li, T. Chen, L. Yan, Y. Dai, Z. Huang, J. Xiong, D. Song, Y. Lv, Z. Zeng, Design of graphene and silica co-doped titania composites with ordered mesostructure and their simulated sunlight photocatalytic performance towards atrazine degradation, *Colloids Surf. A Physicochem. Eng. Asp.* 422 (2013) 90–99, <http://dx.doi.org/10.1016/j.colsurfa.2013.01.039>.
- [135] N. Prabhakarao, M.R. Chandra, T.S. Rao, Synthesis of Zr doped TiO₂/reduced Graphene Oxide (rGO) nanocomposite material for efficient photocatalytic degradation of Eosin Blue dye under visible light irradiation, *J. Alloys Compd.* 694 (2017) 596–606, <http://dx.doi.org/10.1016/j.jallcom.2016.09.329>.
- [136] R.K. Upadhyay, N. Soin, S.S. Roy, Role of graphene/metal oxide composites as photocatalysts, adsorbents and disinfectants in water treatment: a review, *RSC Adv.* 4 (2014) 3823–3851, <http://dx.doi.org/10.1039/c3ra45013a>.
- [137] M. Mukhtar Ali, K.Y. Sandhya, Selective photodegradation and enhanced photo electrochemical properties of titanium dioxide-graphene composite with exposed {001} facets made by photochemical method, *Sol. Energy Mater. Sol. Cells* 144 (2016) 748–757, <http://dx.doi.org/10.1016/j.solmat.2015.10.025>.
- [138] Y. Yang, L. Xu, H. Wang, W. Wang, L. Zhang, TiO₂/graphene porous composite and its photocatalytic degradation of methylene blue, *Mater. Des.* 108 (2016) 632–639, <http://dx.doi.org/10.1016/j.matdes.2016.06.104>.
- [139] L. Liu, C. Luo, J. Xiong, Z. Yang, Y. Zhang, Y. Cai, H. Gu, Reduced graphene oxide (rGO) decorated TiO₂ microspheres for visible-light photocatalytic reduction of Cr(VI), *J. Alloys Compd.* 690 (2017) 771–776, <http://dx.doi.org/10.1016/j.jallcom.2016.08.197>.
- [140] Y. Li, W. Cui, L. Liu, R. Zong, W. Yao, Y. Liang, Y. Zhu, Removal of Cr(VI) by 3D TiO₂-graphene hydrogel via adsorption enriched with photocatalytic reduction, *Appl. Catal. B* 199 (2016) 412–423, <http://dx.doi.org/10.1016/j.apcatb.2016.06.053>.
- [141] L. Wang, M. Wen, W. Wang, N. Momuinou, Z. Wang, S. Li, Photocatalytic degradation of organic pollutants using rGO supported TiO₂-CdS composite under visible light irradiation, *J. Alloys Compd.* 683 (2016) 318–328, <http://dx.doi.org/10.1016/j.jallcom.2016.05.111>.
- [142] Y. Ding, Y. Zhou, W. Nie, P. Chen, MoS₂–GO nanocomposites synthesized via a hydrothermal hydrogel method for solar light photocatalytic degradation of methylene blue, *Appl. Surf. Sci.* 357 (2015) 1606–1612, <http://dx.doi.org/10.1016/j.apsusc.2015.10.030>.
- [143] L. Gan, L. Xu, S. Shang, X. Zhou, L. Meng, Visible light induced methylene blue dye degradation photo-catalyzed by WO₃/graphene nanocomposites and the mechanism, *Ceram. Int.* 42 (2016) 15235–15241, <http://dx.doi.org/10.1016/j.ceramint.2016.06.160>.
- [144] J. Qin, X. Zhang, C. Yang, M. Cao, M. Ma, R. Liu, ZnO microspheres-reduced graphene oxide nanocomposite for photocatalytic degradation of methylene blue dye, *Appl. Surf. Sci.* 392 (2017) 196–203, <http://dx.doi.org/10.1016/j.apsusc.2016.09.043>.
- [145] S. Kumar, A.K. Ojha, B. Walkenfort, Cadmium oxide nanoparticles grown in situ on reduced graphene oxide for enhanced photocatalytic degradation of methylene blue dye under ultraviolet irradiation, *J. Photochem. Photobiol. B* 159 (2016) 111–119, <http://dx.doi.org/10.1016/j.jphotobiol.2016.03.025>.
- [146] P.K. Boruah, P. Borthakur, G. Darabdhara, C.K. Kamaja, I. Karbhal, M.V. Shelke, P. Phukan, D. Saikia, M.R. Das, Sunlight assisted degradation of dye molecules and reduction of toxic Cr(VI) in aqueous medium using magnetically recoverable Fe₃O₄/reduced graphene oxide nanocomposite, *RSC Adv.* 6 (2016) 11049–11063, <http://dx.doi.org/10.1039/c5ra25035h>.
- [147] J. Li, L. Zheng, L. Li, Y. Xian, L. Jin, Fabrication of TiO₂/Ti electrode by laser-assisted anodic oxidation and its application on photoelectrocatalytic degradation of methylene blue, *J. Hazard. Mater.* 139 (2007) 72–78, <http://dx.doi.org/10.1016/j.jhazmat.2006.06.003>.
- [148] F. Zhang, M. Chen, W. Oh, Photoelectrocatalytic properties of Ag-CNT/TiO₂ composite electrodes for methylene blue degradation, *New Carbon Mater.* 25 (2010) 348–356, [http://dx.doi.org/10.1016/S1872-5805\(09\)60038-X](http://dx.doi.org/10.1016/S1872-5805(09)60038-X).
- [149] W. Han, L. Ren, Z. Zhang, X. Qi, Y. Liu, Z. Huang, J. Zhong, Graphene-supported flocculent-like TiO₂ nanostructures for enhanced photoelectrochemical activity and photodegradation performance, *Ceram. Int.* 41 (2015) 7471–7477, <http://dx.doi.org/10.1016/j.ceramint.2015.02.068>.
- [150] F. Han, H. Li, J. Yang, X. Cai, L. Fu, One-pot synthesis of cuprous oxide-reduced graphene oxide nanocomposite with enhanced photocatalytic and electrocatalytic performance, *Phys. E* 77 (2016) 122–126, <http://dx.doi.org/10.1016/j.physE.2015.11.020>.
- [151] T. An, W. Zhang, X. Xiao, G. Sheng, J. Fu, X. Zhu, Photoelectrocatalytic degradation of quinoline with a novel three-dimensional electrode-packed bed photocatalytic reactor, *J. Photochem. Photobiol. A* 161 (2004) 233–242, <http://dx.doi.org/10.1016/j.jphoto.2003.08.004>.
- [152] X.Z. Li, C. He, N. Graham, Y. Xiong, Photoelectrocatalytic degradation of bisphenol A in aqueous solution using a Au-TiO₂/ITO film, *J. Appl. Electrochem.* 35 (2005) 741–750, <http://dx.doi.org/10.1007/s10800-005-1385-5>.
- [153] Q. Zhou, A. Xing, J. Li, D. Zhao, K. Zhao, M. Lei, Synergistic enhancement in photoelectrocatalytic degradation of bisphenol A by CeO₂ and reduced graphene oxide co-modified TiO₂ nanotube arrays in combination with Fenton oxidation, *Electrochim. Acta* 209 (2016) 379–388, <http://dx.doi.org/10.1016/j.electacta.2016.05.094>.
- [154] Y. Zhang, L. Li, H. Liu, T. Lu, Graphene oxide and F co-doped TiO₂ with {001} facets for the photocatalytic reduction of bromate: synthesis, characterization and reactivity, *Chem. Eng. J.* 307 (2017) 860–867, <http://dx.doi.org/10.1016/j.cej.2016.08.139>.
- [155] T. Peng, K. Li, P. Zeng, Q. Zhang, X. Zhang, Enhanced photocatalytic hydrogen production over graphene oxide–cadmium sulfide nanocomposite under visible light irradiation, *J. Phys. Chem. C* 116 (2012) 22720–22726.
- [156] Q. Xiang, J. Yu, M. Jaroniec, Synergetic effect of MoS₂ and graphene as cocatalysts for enhanced photocatalytic H₂ production activity of TiO₂ nanoparticles, *J. Am. Chem. Soc.* 134 (2012) 6575–6578.
- [157] A. Kudo, Y. Miseki, Heterogeneous photocatalyst materials for water splitting, *Chem. Soc. Rev.* 38 (2009) 253–278.
- [158] O. Carp, C.L. Huisman, A. Reller, Photoinduced reactivity of titanium dioxide, *Prog. Solid State Chem.* 32 (2004) 33–177.
- [159] S. Liu, J. Yu, M. Jaroniec, Anatase TiO₂ with dominant high-energy {001} facets: synthesis, properties, and applications, *Chem. Mater.* 23 (2011) 4085–4093.
- [160] I.V. Lightcap, T.H. Kosel, P.V. Kamat, Anchoring semiconductor and metal nanoparticles on a two-dimensional catalyst mat: Storing and shuttling electrons with reduced graphene oxide, *Nano Lett.* 10 (2010) 577–583.
- [161] Y. Liang, Y. Li, H. Wang, J. Zhou, J. Wang, T. Regier, H. Dai, Co₃O₄ nanocrystals on graphene as a synergistic catalyst for oxygen reduction reaction, *Nat. Mater.* 10 (2011) 780–786.
- [162] N. Gao, X. Fang, Synthesis and development of graphene–inorganic semiconductor nanocomposites, *Chem. Rev.* 115 (2015) 8294–8343.
- [163] K. Chang, Z. Mei, T. Wang, Q. Kang, S. Ouyang, J. Ye, MoS₂/graphene cocatalyst for efficient photocatalytic H₂ evolution under visible light irradiation, *ACS Nano* 8 (2014) 7078–7087.
- [164] C.-J. Chang, K.-L. Huang, K.-W. Chu, Y.-H. Wei, I.-H. Tseng, Sulfonated graphene oxide-doped zincoxysulfide composites with enhanced photocatalytic hydrogen production performance, *Int. J. Hydrogen Energy* 41 (2016) 21755–21763.
- [165] L.-C. Chen, T.-F. Yeh, Y.-L. Lee, H. Teng, Incorporating nitrogen-doped graphene oxide dots with graphene oxide sheets for stable and effective hydrogen production through photocatalytic water decomposition, *Appl. Catal. A* 521 (2016) 118–124.
- [166] Q. Li, B. Guo, J. Yu, J. Ran, B. Zhang, H. Yan, J.R. Gong, Highly efficient visible-light-driven photocatalytic hydrogen production of CdS-cluster-decorated graphene nanosheets, *J. Am. Chem. Soc.* 133 (2011) 10878–10884, <http://dx.doi.org/10.1021/ja2025454>.
- [167] X.-J. Lv, W.-F. Fu, H.-X. Chang, H. Zhang, J.-S. Cheng, G.-J. Zhang, Y. Song, C.-Y. Hu, J.-H. Li, Hydrogen evolution from water using semiconductor nanoparticle/graphene composite photocatalysts without noble metals, *J. Mater. Chem. B* 22 (2012) 1539–1546.
- [168] A. Behranginia, M. Asadi, C. Liu, P. Yasaei, B. Kumar, P. Phillips, T. Foroozan, J.C. Waranius, K. Kim, J. Abiade, R.F. Klie, L.A. Curtiss, A. Salehi-Khojin, Highly efficient hydrogen evolution reaction using crystalline layered three-dimensional molybdenum disulfides grown on graphene film, *Chem. Mater.* 28 (2016) 549–555, <http://dx.doi.org/10.1021/acs.chemmater.5b03997>.
- [169] X. Zheng, J. Xu, K. Yan, H. Wang, Z. Wang, S. Yang, Space-confined growth of MoS₂ nanosheets within graphite: the layered hybrid of MoS₂ and graphene as an active catalyst for hydrogen evolution reaction, *Chem. Mater.* 26 (2014) 2344–2353.
- [170] Y.H. Ng, A. Iwase, A. Kudo, R. Amal, Reducing graphene oxide on a visible-light BiVO₄ photocatalyst for an enhanced photoelectrochemical water splitting, *J. Phys. Chem. Lett.* 1 (2010) 2607–2612.
- [171] L. Jia, D.-H. Wang, Y.-X. Huang, A.-W. Xu, H.-Q. Yu, Highly durable N-doped graphene/CdS nanocomposites with enhanced photocatalytic hydrogen evolution from water under visible light irradiation, *J. Phys. Chem. C* 115 (2011) 11466–11473.
- [172] P. Zeng, Q. Zhang, T. Peng, X. Zhang, One-pot synthesis of reduced graphene oxide–cadmium sulfide nanocomposite and its photocatalytic hydrogen production, *Phys. Chem. Chem. Phys.* 13 (2011) 21496–21502.
- [173] B. Zhu, B. Lin, Y. Zhou, P. Sun, Q. Yao, Y. Chen, B. Gao, Enhanced photocatalytic H₂ evolution on ZnS loaded with graphene and MoS₂ nanosheets as cocatalysts, *J. Mater. Chem. A* 2 (2014) 3819–3827, <http://dx.doi.org/10.1039/C3TA14819J>.
- [174] Z. Yan, X. Yu, A. Han, P. Xu, P. Du, Noble-metal-free Ni(OH)₂-modified CdS/reduced graphene oxide nanocomposite with enhanced photocatalytic activity for hydrogen production under visible light irradiation, *J. Phys. Chem. C* 118 (2014) 22896–22903, <http://dx.doi.org/10.1021/jp5065402>.
- [175] P.D. Tran, S.K. Batabyal, S.S. Pramanika, J. Barber, L.H. Wong, S.C.J. Loo, A cuprous oxide-reduced graphene oxide (Cu₂O-rGO) composite photocatalyst for hydrogen generation: employing rGO as an electron acceptor to enhance the photocatalytic activity and stability of Cu₂O, *Nanoscale* 4 (2012) 3875–3878, <http://dx.doi.org/10.1039/C2nr30881a>.
- [176] P. Gao, D.D. Sun, Hierarchical sulfonated graphene oxide–TiO₂ composites for highly efficient hydrogen production with a wide pH range, *Appl. Catal. B* 147 (2014) 888–896, <http://dx.doi.org/10.1016/j.apcatb.2013.10.025>.
- [177] F. Pei, Y. Liu, S. Xu, J. Lü, C. Wang, S. Cao, Nanocomposite of graphene oxide with nitrogen-doped TiO₂ exhibiting enhanced photocatalytic efficiency for hydrogen evolution, *Int. J. Hydrogen Energy* 38 (2013) 2670–2677.
- [178] A. Fujishima, K. Honda, Electrochemical photolysis of water at a semiconductor electrode, *Nature* 238 (1972) 37–38, <http://dx.doi.org/10.1038/238037a0>.
- [179] H. Kim, G. Moon, D. Monllor-Satoca, Y. Park, W. Choi, Solar photoconversion using Graphene/TiO₂ composites: nanographene shell on TiO₂ core versus

- TiO₂ nanoparticles on graphene sheet, *J. Phys. Chem. C* 116 (2012) 1535–1543, <http://dx.doi.org/10.1021/jp209035e>.
- [180] R. Banerjee, R. Jayakrishnan, R. Banerjee, P. Ayyub, Effect of the size-induced structural transformation on the band gap in CdS nanoparticles, *J. Phys. Condens. Matter.* 12 (2000) 10647–10654, <http://dx.doi.org/10.1088/0953-8984/12/50/325>.
- [181] W. Han, L. Ren, X. Qi, Y. Liu, X. Wei, Z. Huang, J. Zhong, Synthesis of CdS/ZnO/graphene composite with high-efficiency photoelectrochemical activities under solar radiation, *Appl. Surf. Sci.* 299 (2014) 12–18, <http://dx.doi.org/10.1016/j.apsusc.2014.01.170>.
- [182] X. Lv, G. Zhang, W. Fu, Highly efficient hydrogen evolution using TiO₂/graphene composite photocatalysts, *Procedia Eng.* 27 (2012) 570–576.
- [183] Q. Xiang, J. Yu, M. Jaroniec, Preparation and enhanced visible-light photocatalytic H₂-production activity of graphene/C₃N₄ composites, *J. Phys. Chem. C* 115 (2011) 7355–7363.
- [184] G. Palmisano, V. Augugliaro, M. Pagliaro, L. Palmisano, Photocatalysis: a promising route for 21st century organic chemistry, *Chem. Commun.* 95 (2007) 3425–3437, <http://dx.doi.org/10.1039/b700395c>.
- [185] G. Palmisano, E. García-López, G. Marcí, V. Loddo, S. Yurdakal, V. Augugliaro, L. Palmisano, Advances in selective conversions by heterogeneous photocatalysis, *Chem. Commun.* 46 (2010) 7074–7089, <http://dx.doi.org/10.1039/c0cc02087g>.
- [186] M.A. Fox, Organic heterogeneous photocatalysis: chemical conversions sensitized by irradiated semiconductors, *Acc. Chem. Res.* 16 (1983) 314–321, <http://dx.doi.org/10.1021/ar00093a001>.
- [187] S. Liu, Z. Chen, N. Zhang, Z.-R. Tang, Y.-J. Xu, An efficient self-assembly of CdS nanowires-reduced graphene oxide nanocomposites for selective reduction of nitro organics under visible light irradiation, *J. Phys. Chem. C* 117 (2013) 8251–8261.
- [188] D. Friedmann, A. Hakki, H. Kim, W. Choi, D. Bahnenmann, Heterogeneous photocatalytic organic synthesis: state-of-the-art and future perspectives, *Green Chem.* 18 (2016) 5391–5411, <http://dx.doi.org/10.1039/C6GC01582D>.
- [189] G.-J. ten Brink, I.W.C.E. Arends, R.A. Sheldon, Green, Catalytic oxidation of alcohols in water, *Science* 287 (2000) 1636–1639.
- [190] M. Qamar, M.O. Waheed, A.-M. Azad, M.I. Ahmed, A. Khan, T.A. Saleh, Selective photocatalytic oxidation of aromatic alcohols into aldehydes by tungsten blue oxide (TBO) anchored with Pt nanoparticles, *RSC Adv.* 6 (2016) 71108–71116.
- [191] D. Ravelli, D. Dondi, M. Fagnoni, A. Albini, Photocatalysis. A multi-faceted concept for green chemistry, *Chem. Soc. Rev.* 38 (2009) 1999–2011.
- [192] J. Yang, X. Shen, Y. Li, L. Bian, J. Dai, D. Yuan, Bismuth tungstate-reduced graphene oxide self-assembled nanocomposites for the selective photocatalytic oxidation of alcohols in water, *ChemCatChem* 8 (2016) 1399–1409, <http://dx.doi.org/10.1002/cctc.201501370>.
- [193] L. Yuan, Q. Yu, Y. Zhang, Y.-J. Xu, Graphene-TiO₂ nanocomposite photocatalysts for selective organic synthesis in water under simulated solar light irradiation, *RSC Adv.* 4 (2014) 15264–15270.
- [194] M. Alfè, D. Spasiano, V. Gargiulo, G. Vitiello, R. Di Capua, R. Marotta, TiO₂/graphene-like photocatalysts for selective oxidation of 3-pyridine-methanol to vitamin B3 under UV/solar simulated radiation in aqueous solution at room conditions: the effect of morphology on catalyst performances, *Appl. Catal. A* 487 (2014) 91–99, <http://dx.doi.org/10.1016/j.apcata.2014.09.002>.
- [195] C. Zhang, Y. Zhu, Synthesis of square Bi₂WO₆ nanoplates as high-activity visible-light-driven photocatalysts, *Chem. Mater.* 17 (2005) 3537–3545.
- [196] C. Wang, H. Zhang, F. Li, L. Zhu, Degradation and mineralization of bisphenol A by mesoporous Bi₂WO₆ under simulated solar light irradiation, *Environ. Sci. Technol.* 44 (2010) 6843–6848.
- [197] Y. Wang, X. Zhang, L. Wang, Y. Chen, Photocatalytic oxidation of benzyl alcohols by three-dimensional reduced graphene oxide/nano zinc oxide catalyst under visible light, *J. Chem. Res.* 39 (2015) 727–730.
- [198] J. Yang, X. Wang, X. Zhao, J. Dai, S. Mo, Synthesis of uniform Bi₂WO₆-reduced graphene oxide nanocomposites with significantly enhanced photocatalytic reduction activity, *J. Phys. Chem. C* 119 (2015) 3068–3078.
- [199] X. Li, B. Weng, N. Zhang, Y.-J. Xu, In situ synthesis of hierarchical In₂S₃–graphene nanocomposite photocatalyst for selective oxidation, *RSC Adv.* 4 (2014) 64484–64493.
- [200] J. Xu, S. He, H. Zhang, J. Huang, H. Lin, X. Wang, J. Long, Layered metal-organic framework/graphene nanoarchitectures for organic photosynthesis under visible light, *J. Mater. Chem. A* 3 (2015) 24261–24271, <http://dx.doi.org/10.1039/C5TA06838J>.
- [201] J. Xu, L. Luo, G. Xiao, Z. Zhang, H. Lin, X. Wang, J. Long, Layered C₃N₃S₃ polymer/graphene hybrids as metal-free catalysts for selective photocatalytic oxidation of benzylic alcohols under visible light, *ACS Catal.* 4 (2014) 3302–3306.
- [202] C. Xu, Y. Yuan, R. Yuan, X. Fu, Enhanced photocatalytic performances of TiO₂-graphene hybrids on nitro-aromatics reduction to amino-aromatics, *RSC Adv.* 3 (2013) 18002–18008.
- [203] S. Füldner, P. Pohla, H. Bartling, S. Dankesreiter, R. Stadler, M. Gruber, A. Pfitzner, B. König, Selective photocatalytic reductions of nitrobenzene derivatives using PbBiO₂X and blue light, *Green Chem.* 13 (2011) 640–643.
- [204] A. Maldotti, L. Andreotti, A. Molinari, S. Tollari, A. Penoni, S. Cenini, Photochemical and photocatalytic reduction of nitrobenzene in the presence of cyclohexene, *J. Photochem. Photobiol. A* 133 (2000) 129–133.
- [205] B. Weng, S. Liu, N. Zhang, Z.-R. Tang, Y.-J. Xu, A simple yet efficient visible-light-driven CdS nanowires-carbon nanotube 1D-1D nanocomposite photocatalyst, *J. Catal.* 309 (2014) 146–155.
- [206] Z. Chen, S. Liu, M.-Q. Yang, Y.-J. Xu, Synthesis of uniform CdS nanospheres/graphene hybrid nanocomposites and their application as visible light photocatalyst for selective reduction of nitro organics in water, *ACS Appl. Mater. Interfaces* 5 (2013) 4309–4319.
- [207] D. Jing, L. Guo, A novel method for the preparation of a highly stable and active CdS photocatalyst with a special surface nanostructure, *J. Phys. Chem. B* 110 (2006) 11139–11145.
- [208] A. ElMekawy, H.M. Hegab, G. Mohanakrishna, A.F. Elbaz, M. Bulut, D. Pant, Technological advances in CO₂ conversion electro-biorefinery: a step toward commercialization, *Bioresour. Technol.* 215 (2016) 357–370.
- [209] K. Sekine, T. Yamada, Silver-catalyzed carboxylation, *Chem. Soc. Rev.* 45 (2016) 4524–4532.
- [210] H.B. Oladipo, E.A. Jaseer, A. Julián, F.J. Fernández-Alvarez, S. Al-Khattaf, L.A. Oro, Effect of the CO₂-pressure on the hydrosilylation of CO₂ catalyzed by [Ir (NSiN)] species, *J. CO₂ Util.* 12 (2015) 21–26.
- [211] E. Korovin, D. Selishchev, D. Kozlov, Photocatalytic CO₂ reduction on the TiO₂ P25 under the high power UV-LED irradiation, *Top. Catal.* 59 (2016) 1292–1296.
- [212] X. Li, J. Wen, J. Low, Y. Fang, J. Yu, Design and fabrication of semiconductor photocatalyst for photocatalytic reduction of CO₂ to solar fuel, *Sci. China Mater.* 57 (2014) 70–100.
- [213] W.-J. Ong, L.-L. Tan, S.-P. Chai, S.-T. Yong, A.R. Mohamed, Self-assembly of nitrogen-doped TiO₂ with exposed {001} facets on a graphene scaffold as photo-active hybrid nanostructures for reduction of carbon dioxide to methane, *Nano Res.* 7 (2014) 1528–1547.
- [214] J.E. Benedetti, D.R. Bernardo, A. Morais, J. Bettini, A.F. Nogueira, Synthesis and characterization of a quaternary nanocomposite based on TiO₂/Cds/rGO/Pt and its application in the photoreduction of CO₂ to methane under visible light, *RSC Adv.* 5 (2015) 33914–33922.
- [215] C. Zhao, L. Liu, Q. Zhang, J. Wang, Y. Li, Photocatalytic conversion of CO₂ and H₂O to fuels by nanostructured Ce-TiO₂/SBA-15 composites, *Catal. Sci. Technol.* 2 (2012) 2558–2568.
- [216] X.-J. Lv, W.-F. Fu, C.-Y. Hu, Y. Chen, W.-B. Zhou, Photocatalytic reduction of CO₂ with H₂O over a graphene-modified NiO_x-Ta₂O₅ composite photocatalyst: coupling yields of methanol and hydrogen, *RSC Adv.* 3 (2013) 1753–1757.
- [217] A. Wang, X. Li, Y. Zhao, W. Wu, J. Chen, H. Meng, Preparation and characterizations of Cu₂O/reduced graphene oxide nanocomposites with high photo-catalytic performances, *Powder Technol.* 261 (2014) 42–48.
- [218] L.-H. Tseng, W.-C. Chang, J.C.S. Wu, Photoreduction of CO₂ using sol-gel derived titania and titania-supported copper catalysts, *Appl. Catal. B* 37 (2002) 37–48.
- [219] W. Tu, Y. Zhou, Q. Liu, S. Yan, S. Bao, X. Wang, M. Xiao, Z. Zou, An in situ simultaneous reduction-hydrolysis technique for fabrication of TiO₂-graphene 2D sandwich-like hybrid nanosheets: graphene-promoted selectivity of photocatalytic-driven hydrogenation and coupling of CO₂ into methane and ethane, *Adv. Funct. Mater.* 23 (2013) 1743–1749.
- [220] W. Tu, Y. Zhou, Q. Liu, Z. Tian, J. Gao, X. Chen, H. Zhang, J. Liu, Z. Zou, Robust hollow spheres consisting of alternating titania nanosheets and graphene nanosheets with high photocatalytic activity for CO₂ conversion into renewable fuels, *Adv. Funct. Mater.* 22 (2012) 1215–1221.
- [221] J. Bonin, M. Robert, M. Routier, Selective and efficient photocatalytic CO₂ reduction to CO using visible light and an iron-based homogeneous catalyst, *J. Am. Chem. Soc.* 136 (2014) 16768–16771.
- [222] Y. Tamaki, K. Koike, O. Ishitani, Highly efficient selective, and durable photocatalytic system for CO₂ reduction to formic acid, *Chem. Sci.* 6 (2015) 7213–7221.
- [223] M.M. Taqui Khan, N. Nageswara Rao, D. Chatterjee, A novel photosynthetic mimic reaction catalysed by K[Ru(H-EDTA)Cl]₂·2H₂O; reduction of carbon dioxide to formate and formaldehyde in the presence of an aqueous suspension of Pt-Cds-RuO₂, *J. Photochem. Photobiol. A* 60 (1991) 311–318.
- [224] T. Inoue, A. Fujishima, S. Konishi, K. Honda, Photoelectrocatalytic reduction of carbon dioxide in aqueous suspensions of semiconductor powders, *Nature* 277 (1979) 637–638, <http://dx.doi.org/10.1038/277637a0>.
- [225] Y.T. Liang, B.K. Vijayan, O. Lyandres, K.A. Gray, M.C. Hersam, Effect of dimensionality on the photocatalytic behavior of carbon-titania nanosheet composites: charge transfer at nanomaterial interfaces, *J. Phys. Chem. Lett.* 3 (2012) 1760–1765, <http://dx.doi.org/10.1021/jz300491s>.
- [226] (a) E.S. Baeissa, Green synthesis of methanol by photocatalytic reduction of CO₂ under visible light using a graphene and tourmaline co-doped titania nanocomposites, *Ceram. Int.* 40 (2014) 12431–12438;
- (b) A.A. White, Food for thought, *Spine (Phila. Pa. 1976)* 27 (2002) 1965–1970, <http://dx.doi.org/10.1097/00007632-200209150-00003>;
- (c) P.M. Vitousek, Human domination of earth's ecosystems, *Science* 277 (1997) 494–499, <http://dx.doi.org/10.1126/science.277.5325.494>;
- (d) R.S. Haszeldine, Carbon capture and storage: How green can black be? *Science* 325 (2009) 1647–1652, <http://dx.doi.org/10.1126/science.1172246>.
- [227] X. Li, Q. Wang, Y. Zhao, W. Wu, J. Chen, H. Meng, Green synthesis and photo-catalytic performances for ZnO-reduced graphene oxide nanocomposites, *J. Colloid Interface Sci.* 411 (2013) 69–75.

- [228] L. Zhang, N. Li, H. Jiu, G. Qi, Y. Huang, ZnO-reduced graphene oxide nanocomposites as efficient photocatalysts for photocatalytic reduction of CO₂, *Ceram. Int.* 41 (2015) 6256–6262.
- [229] M.R. Hasan, S.B. Abd Hamid, W.J. Basirun, S.H. Meriam Suhaimy, A.N. Che Mat, A sol-gel derived, copper-doped, titanium dioxide-reduced graphene oxide nanocomposite electrode for the photoelectrocatalytic reduction of CO₂ to methanol and formic acid, *RSC Adv.* 5 (2015) 77803–77813, <http://dx.doi.org/10.1039/c5ra12525a>.
- [230] Q. Li, W. Zhu, J. Fu, H. Zhang, G. Wu, S. Sun, Controlled assembly of Cu nanoparticles on pyridinic-N rich graphene for electrochemical reduction of CO₂ to ethylene, *Nano Energy* 24 (2016) 1–9, <http://dx.doi.org/10.1016/j.nanoen.2016.03.024>.
- [231] M.R. Hasan, S.B. Abd Hamid, W.J. Basirun, Charge transfer behavior of graphene-titania photoanode in CO₂ photoelectrocatalysis process, *Appl. Surf. Sci.* 339 (2015) 22–27, <http://dx.doi.org/10.1016/j.apsusc.2015.02.162>.
- [232] K.S. Novoselov, V.I. Fal'ko, L. Colombo, P.R. Gellert, M.G. Schwab, K. Kim, A roadmap for graphene, *Nature* 490 (2012) 192–200, <http://dx.doi.org/10.1038/nature11458>.
- [233] Z.Y. Xia, S. Pezzini, E. Treossi, G. Giambastiani, F. Corticelli, V. Morandi, A. Zanelli, V. Bellani, V. Palermo, The exfoliation of graphene in liquids by electrochemical, chemical, and sonication-assisted techniques: a nanoscale study, *Adv. Funct. Mater.* 23 (2013) 4684–4693, <http://dx.doi.org/10.1002/adfm.201203686>.